Quantitative analysis of neural stem cell growth and differentiation

Shvetha Sankaran

2014

Shvetha Sankaran. (2014). Quantitative analysis of neural stem cell growth and differentiation. Doctoral thesis, Nanyang Technological University, Singapore.

https://hdl.handle.net/10356/55362

https://doi.org/10.32657/10356/55362

NANYANG TECHNOLOGICAL UNIVERSITY

QUANTITTATIVE ANALYSIS OF NEURAL STEM CELL GROWTH AND DIFFERENTIATION

SHVETHA SANKARAN

SCHOOL OF BIOLOGICAL SCIENCES

2014

QUANTITTATIVE ANALYSIS OF NEURAL STEM CELL GROWTH AND DIFFERENTIATION

SHVETHA SANKARAN

SCHOOL OF BIOLOGICAL SCIENCES

A thesis submitted to the Nanyang Technological University
in partial fulfilment of the requirement for the degree of
Doctor of Philosophy

2014

ACKNOWLEDGEMENTS

I will be forever grateful to Dr. Sohail Ahmed for giving me the opportunity to work in his lab. His patient guidance and encouragement have helped me immensely through this journey. I thank Dr. Cheng Gee Koh for supporting my candidature.

Thank you to my wonderful collaborators Weimiao Yu, Chaohui Huang, Shue Ching Chia, and Hwee Kuan Lee, without whom much of the work described here would not have been possible. I would also like to thank Guna for helping with the mRNA profiling and drug screen, and Francesco Pampaloni, Philippe Girard, and Ernst Stelzer for their help with imaging on the DSLM system.

Special thanks to Muly Tham and Graham Wright for proof-reading this thesis and for providing invaluable comments and suggestions. I would also like to thank Ivy Low and Seri Mustafah for their expert technical assistance with FACS, and Srivats Hariharan for help with microscopy.

A special note of gratitude to Srinivas, Guna, and Mike for always lending a helping hand, and to Srinivas for the many stimulating discussions. Thank you to Sudha, Kai Ping, Amy, Muly, Hui Ting, and Helen for their help and feedback over the years.

I thank my husband and parents for always standing by me and extending their support, and for motivating and inspiring me everyday.

TABLE OF CONTENTS

ACKNOWLEDGEMENTS ..... **i**

TABLE OF CONTENTS ..... **ii**

LIST OF FIGURES ..... **vii**

LIST OF TABLES ..... **ix**

ABBREVIATIONS ..... **x**

SUMMARY .... **xiii**

1. INTRODUCTION **1**

1.1. Development- from zygote to embryo 1

1.2. Stem cells 4

1.2.1. The stem cell niche 5

1.2.2. Embryonic NSCs (eNSCs) 8

1.2.3. Adult NSCs (aNSCs) 10

1.3. The study of NSCs 11

1.3.1. *In vivo* 11

1.3.2. *In vitro*: the culture of NSCs 13

1.3.2.1. The neurosphere assay (NSA) 13

1.3.2.2. Neurospheres are natural 3-D cultures 14

1.3.2.3. Clonal assays 15

1.3.2.4. Estimation of NSC frequency 16

1.4. Imaging of 3-D cultures 17

1.5. Microscopy and imaging 19

1.5.1. Labels 19

1.5.2. Fixed samples 20

1.5.3. Live samples 21

1.5.4. Widefield and confocal microscopy 23

1.5.4.1. Point spread function 23

1.5.4.2. Widefield versus LSCM for 3-D imaging 24

1.5.5. Selective plane illumination microscopy (SPIM) and digital scanned laser light sheet microscopy (DSLM) 26

1.5.6. Confocal versus light sheet based microscopy 29

1.6. Image analysis 31

1.6.1. Evolving generalised Voronoi diagram (EGVD) 31

1.7. High content and high throughput screening (HCS and HTS) assays 32
1.7.1. Implication for the study of diseases 35
1.7.1.1. Neurodegenerative diseases 35
1.7.1.2. Brain tumours 36
1.8. AIMS OF CURRENT WORK 39
2. MATERIALS AND METHODS 40
2.1. Isolation of NSCs/NPs and cell culture 40
2.2. Seeding densities of NSCs/NPs 40
2.3. Freezing NSCs/NPs 41
2.4. Single neurosphere differentiation 41
2.5. Transfection 42
2.6. Immunocytochemistry 42
2.6.1. Labelling of live cells 42
2.6.2. Lineage labelling of differentiated cells 43
2.7. Use of hydrogel for immobilisation 44
2.7.1. Preparation of Gtn-HPA polymer 44
2.7.2. Suspending cells in polymer 44
2.8. Fluorescent Activated Cell Sorting (FACS) 45
2.9. Single cell mRNA profiling and data processing 45
2.9.1. FACS-sorting and cell lysis 45
2.9.2. Single cell PCR 46
2.10. 3-D imaging of neurospheres 47
2.10.1. LSCM 47
2.10.2. SDC microscope 48
2.10.3. DSLM 48
2.10.3.1. Sample preparation 48
2.10.3.2. Acquisition parameters 49
2.11. EGVD 49
2.12. Time-lapse imaging 49
2.13. Imaging of single cells and measurement of phase intensity 50
2.14. Measurement of single cell size 50
2.15. Time-point analysis of NSCs/NPs expressing eYFP-PMT 51
2.16. Drug treatment 51

2.17. HTS assay 51
2.18. Statistical analysis 52

3. RESULTS 53
3.1. Imaging of live neurospheres in 3-D 53
3.1.1. Comparison of microscopes for 3-D neurosphere imaging 53
3.1.2. Dyes used to label intracellular structures 56
3.1.2.1. Membrane and cytoplasmic dyes 56
3.1.2.2. Nuclear dyes 57
3.2. Quantitative measurements of neurosphere features 59
3.2.1. EGVD 60
3.2.2. Estimation of cell number 62
3.2.3. Cell, nuclear volumes and cell number 64
3.2.4. Nuclear/cell volume ratio and cell number 64
3.2.5. Sphericity 65
3.2.6. Positional information 66
3.2.7. ECS and neurosphere volume 68
3.3. Identification and characterisation of the NFC 70
3.3.1. Online 3-D tracking of neurosphere formation 70
3.3.2. FACS-based enrichment of NFCs 74
3.3.3. Time-lapse analysis of neurosphere formation 76
3.3.4. Cell size predicts neurosphere formation 78
3.3.5. Single cell dynamics are indicative of neurosphere formation 79
3.3.6. NFCs have a shorter doubling time 81
3.4. Correlation between mechanism of cell division and potency 82
3.4.1. Time point analysis of cell division using eYFP-PMT 83
3.4.2. Surface marker distribution reflects potency 84
3.5. Use of surface markers to study NSC/NP behaviour 86
3.5.1. Marker distributions in doublets 86
3.5.2. Marker distributions in neurospheres 88
3.6. Purification of NSCs 91
3.6.1. Phase intensity predicts neurosphere formation 91
3.6.2. Phase bright cells are enriched for NSCs 93
3.7. mRNA profile of CD15+/C1qR1+/Phbrt+ cells 95

3.8. A HTS assay to study changes in neurosphere growth and gene expression 97
3.8.1. Design of the HTS assay..... 98
3.8.2. Proof-of-principle test: effects of Ifenprodil on NSCs/NPs... 100
3.8.3. Effects of neuromodulators on NFU, neurosphere diameter, and *Sox2* promoter activity 101
3.8.4. Use of brightfield and phase imaging modalities in a HTS assay 107
4. DISCUSSION 109
4.1. 3-D imaging of neurospheres..... 109
4.1.1. Comparison of microscopes for 3-D neurosphere imaging ... 110
4.1.2. Labelling of live cells. 110
4.2. Segmentation by EGVD 111
4.3. Quantitative analysis of the neurosphere structure 112
4.4. Salient features of NFCs and NSCs 114
4.4.1. Time-lapse analysis of neurosphere formation
4.4.1.1. Challenges of imaging live NSCs/NPs 115
4.4.1.2. Automated tracking of NSCs/NPs over time 117
4.4.2. Enriching for NFCs..... 118
4.4.2.1. Big cells form more neurospheres 118
4.4.2.2. Cell dynamics as a predictor of neurosphere formation..... 119
4.4.2.3. NFCs have a shorter doubling time 119
4.4.2.4. NFCs are phase bright..... 120
4.4.3. Evaluation of multipotency.....120
4.4.3.1. Relevance of marker distributions to multipotency .. 120
4.4.3.2. Features of the single cell and multipotency 121
4.4.4. Purification of NSCs 122
4.4.5. NSC purification by imaging- implications for future work . 123

4.4.6. mRNA profile 124

4.5. HTS..... 126

4.5.1. Design of the HTS assay..... 126

4.5.2. Testing the HTS assay on neurospheres 127

4.5.3. Effects of neuromodulatory drugs on E14.5 NSCs/NPs..... 128

4.5.4. Label-free assay 129

4.6. Conclusions and future work..... 130

PUBLICATIONS 132

REFERENCES.. 133

LIST OF FIGURES

Introduction

Figure 1.1. Stages of mammalian development 3

Figure 1.2. Constituents of the stem cell niche 6

Figure 1.3. Symmetric versus asymmetric stem cell divisions in homeostasis and development 7

Figure 1.4. NSCs and their lineage in the developing forebrain..... 9

Figure 1.5. Configuration of a DSLM microscope 28

Figure 1.6. Sample holders for SPIM/DSLM 29

Figure 1.7. Comparison of LSCM, SPIM, and DSLM 30

Figure 1.8. Comparison of HTS and HCS systems 35

Figure 1.9. Overview of the preclinical validation of antitumor agents 37

Results

Figure 2.1. Comparison of imaging modalities for 3-D imaging of neurospheres 54

Figure 2.2. Imaging of cellular structures in neurospheres with a laser scanning confocal microscope (LSCM) 55

Figure 2.3. 3-D neurosphere imaging on the digital scanned laser light sheet microscope (DSLM) 56

Figure 3.1. Enumeration of cell number by manual counting 59

Figure 3.2. Segmentation of 3-D images using Evolving Generalised Voronoi Diagram (EGVD) 61

Figure 3.3. Estimation of cell number by EGVD 63

Figure 3.4. Estimation of cellular and nuclear volumes by EGVD 65

Figure 3.5. Changes in sphericity relative to size of the neurosphere 66

Figure 3.6. Positional information of cells 67

Figure 3.7. Extracellular space (ECS) within neurospheres 69

Figure 4.1. Automated online tracking of cells over time 73

Figure 4.2. FACS enrichment of NFCs 75

Figure 4.3. Imaging neurosphere formation 77

Figure 4.4. Cell size predicts neurosphere formation 78

Figure 4.5. Cellular dynamics during the first 24h 80

Figure 4.6. NFCs have a shorter doubling time 82

Figure 4.7. Cell division patterns in NSCs/NPs.....84

Figure 4.8. Non-uniform marker distribution indicates multipotency.....85

Figure 4.9. Distribution of CD15 and C1qR1 in FACS-sorted doublets...87

Figure 4.10. Non-uniform surface marker distribution in neurospheres ...89

Figure 4.11. Distribution of CDy5 in FACS-sorted neurospheres 90

Figure 4.12. Phase intensity predicts neurosphere formation.....92

Figure 4.13. Analysis of CD15+/C1qR1+/Phbrt+ cells.....94

Figure 4.14. mRNA signature of CD15+/C1qR1+/Phbrt+ cells.....96

Figure 5.1. Design of the HTS assay 99

Figure 5.2. Effects of Ifenprodil on E14.5 NSCs/NPs.....101

Figure 5.3. Effects of neuromodulatory drugs on NFU, size, and *Sox2* promoter activity 103

Figure 5.4. Development of label-free segmentation methods for HTS..108

LIST OF TABLES

Table 1. Summary of dyes used to label neurospheres.....58

Table 2. Summary of the effects of neuromodulatory drugs tested on E14.5 NSCs/NPs.....102

ABBREVIATIONS

3-D	Three-dimensional
AD	Alzheimer's disease
ALDH	Aldehyde dehydrogenase
ALS	Amyotrophic lateral sclerosis
aNSC	Adult neural stem cell
eNSC	Embryonic neural stem cell
bFGF	Basic fibroblast growth factor
bHLH	Basic helix loop helix
BrdU	Bromodeoxyuridine
BMP	Bone morphogenetic protein
BTSC	Brain tumour stem cell
CCD	Charge-coupled device
CNS	Central nervous system
CSC	Cancer stem cell
CSPG	Chondroitin sulphate proteoglycans
DAPI	4',6'-diamidino-2-phenylindole
DG	Dentate gyrus
DMSO	Dimethyl-sulfoxide
DNA	Deoxyribonucleic acid
DSLM	Digital scanned laser light sheet microscopy
ECM	Extracellular matrix
ECS	Extracellular space
EGF	Epidermal growth factor
EGFR	Epidermal growth factor receptor
EGVD	Evolving generalised Voronoi diagram
ESC	Embryonic stem cell
eYFP	Enhanced yellow fluorescent protein
FACS	Fluorescence activated cell sorting
FGF	Fibroblast growth factor
FSC/SSC	Forward scatter channel/side scatter channel
GBM	Glioblastoma multiforme

GDNF	Glial cell-line derived neurotrophic factor
GFAP	Glial fibrillary acid protein
GFP	Green fluorescent protein
GLAST	Glutamate-aspartate transporter
GM	Growth medium
GPCR	G protein-coupled receptor
HCS	High content screen
hESCs	Human embryonic stem cells
Hes	Hairy and enhancer of split proteins
HCS	High content screen
HTS	High throughput screen
HRP	Horseradish peroxidase
HSE	Human skin equivalent
HSC	Haematopoietic stem cell
HTS	High throughput screen
ICM	Inner cell mass
iPS cells	Inducible pluripotent stem cells
MSC	Mesenchymal stem cell
N-CFCA	Neural-colony forming cell assay
NFC	Neurosphere forming cell
NFU	Neurosphere forming unit
NGF	Nerve growth factor
NP	Neural progenitor
NSA	Neurosphere assay
NSC	Neural stem cells
PAO	Phenylarsineoxide
PBS	Phosphate-buffered saline
PCR	Polymerase chain reaction
PD	Parkinson's disease
PE	Phycoerythrin
PFA	Paraformaldehyde
PI	Propidium iodide
PLL	Poly-L-lysine
PMT	Photo multiplier tube

PMT	Plasma membrane targeted
PNA	Peanut agglutinin
PSF	Point spread function
PTEN	Phosphatase and tensin homolog
RGC	Radial glia cell
RNA	Ribonucleic acid
RP2	Retinitis pigmentosa
Sox2	SRY (sex determining region Y)-box 2
SGZ	Subgranular zone
Shh	Sonic hedgehog
SPIM	Selective plane illumination microscopy
SSEA-1	Stage-specific embryonic antigen 1
SVZ	Subventricular zone
VEGF	Vascular endothelial growth factor
VZ	Ventricular zone

SUMMARY

Neural stem cells (NSCs) are self-renewing, multipotent cells in the embryonic or adult brain that can give rise to neurons and glia. NSCs and neural progenitors (NPs) can be propagated *in vitro* through a natural 3-D culture system known as neurospheres. Here, I report the use of non-invasive image acquisition and processing techniques to gain insight into the 3-D architecture of the neurosphere, characterise neurosphere forming cells (NFCs), develop an imaging-based method to enrich for NSCs, and a high throughput screening (HTS) strategy to study the effects of drugs on NSCs/NPs.

For 3-D imaging of live neurospheres, different imaging modalities were compared and the laser scanning confocal microscope (LSCM) was found to produce images with clearly delineated cell boundaries. GFP-targeted to the plasma membrane and Hoechst 33342 were found to be the labels most suitable for 3-D imaging and segmentation analysis. Segmentation of 3-D neurosphere images was performed by using a novel algorithm called evolving generalised Voronoi diagram (EGVD). EGVD was found to be reliable for segmenting nuclei as well as cells that are in contact with one another. Segmentation of 3-D images of live neurospheres by EGVD yielded quantitative information on cell number, neurosphere size, cell and nuclear volumes, extracellular space (ECS), sphericity, and the positional impact of these parameters.

Given that there are as yet no definitive markers for NSCs *in vitro*, it is important to investigate and identify new markers that would enable NSC selection and

purification. The study of NSCs/NPs *in vitro* was carried out by the neurosphere and multipotency assays. Analysis of single cell features revealed a positive correlation between cell size, phase intensity, and motility with neurosphere formation and multipotency. Asymmetric distribution of surface markers such as CD15 and C1qR1 correlated highly with multipotency.

Lastly, a HTS assay to evaluate the response of large numbers of neurospheres in drug screens was developed and tested on E14.5 NSCs/NPs. The HTS assay was used for the quantitative analysis of changes in neurosphere growth as well as *Sox2* promoter activity and is relevant to drug development.

1. INTRODUCTION

1.1. Development- from zygote to embryo

The development of a multicellular organism begins when a zygote is formed upon fertilisation of the egg. Following fertilisation the mammalian zygote undergoes a series of mitotic divisions referred to as cleavage, to give rise to numerous smaller cells called blastomeres. The mammalian zygote is unique in that it has asynchronous cell divisions. At the 8-cell stage the blastomeres are compacted into a tight ball of cells called the blastula. A further round of division leads to the formation of the 16-cell morula. The morula is composed of two groups of cells- the internal cells, which are precursors to the inner cell mass s that eventually forms the embryo and the external cells, the trophoblast that will form the embryonic portion of the placenta. At the 64-cell stage the ICM and trophoblast separate into two distinct layers, an event that enables the attachment of the embryo to the uterus. The next developmental stage is the formation of the blastocyst which is characterised by the formation of a cavity (blastocoel) by the secretion of fluids by trophoblast cells. The blastocyst expands by drawing in water to the blastocoel and leaves the zona pellucida to be implanted in the uterus. Before implantation the blastocyst emerges from the zona and attaches to the uterine wall.

Following implantation to the uterus a process called gastrulation occurs during which the cells are rearranged in the blastocyst to form the three germ layers, the ectoderm, endoderm, and mesoderm. The three layers are responsible for producing all the tissues and organs constituting the organism. Cells of the ICM are segregated into the hypoblast and epiblast. The hypoblast gives rise to the yolk

sac while the epiblast undergoes gastrulation. Meanwhile, the developing embryo is filled with amniotic fluid to protect it from external stress. Further development is characterised by a series of events specifying the anterior-posterior, dorso-ventral, and left-right axes.

Cells of the epiblast migrate inwards to the blastocoel forming the primitive streak resulting in the endoderm and mesoderm while cells at the surface constitute the ectoderm. The migration of cells and their subsequent organisation into the three distinct germ layers sets the stage for the formation of future tissues and organs. The endoderm or the innermost layer gives rise to the lining of the digestive tubes and the respiratory system. Blood cells, gonads, kidneys, bones, and heart arise from the middle layer or mesoderm. The ectoderm is precursor to the epidermis, nervous system, as well as pigment cells. This series of events characterises early embryonic development in mammals (Gilbert, 2000) (figure 1.1).

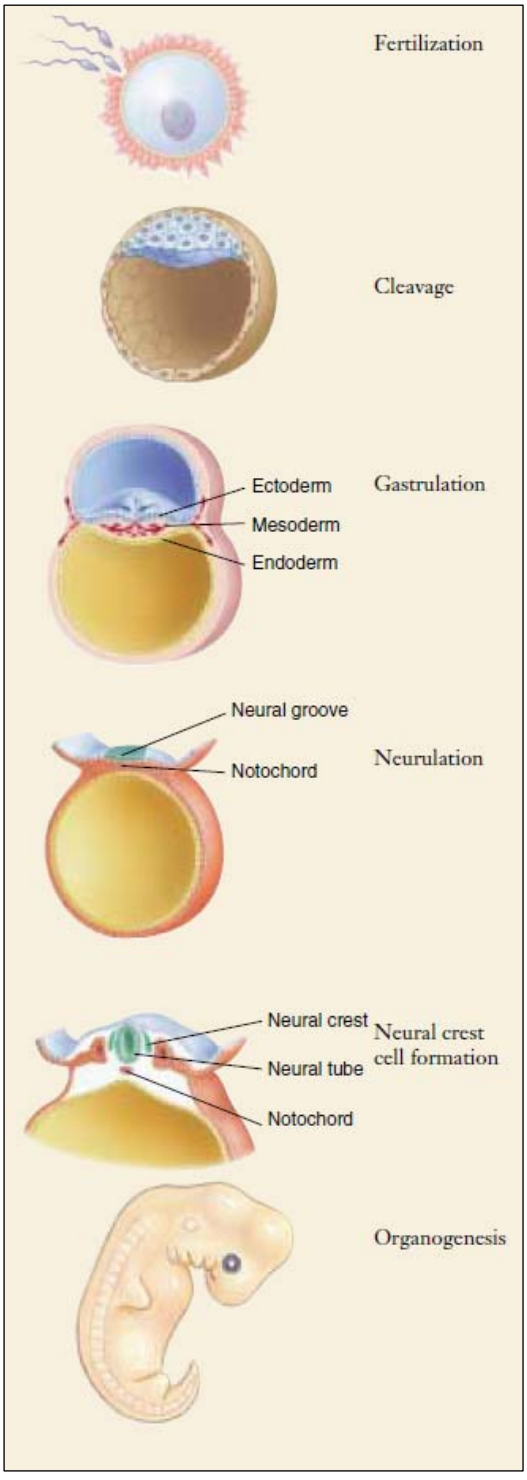

Figure 1.1. Stages of mammalian development.
The various stages of vertebrate development are depicted, beginning from fertilisation to organogenesis (adapted from (Raven, 2007).

1.2. Stem cells

Stem cells are defined by their ability to self-renew and generate the various cell lineages constituting an organism. Stem cells can be derived from both the embryo and the adult. More recently it has been shown that terminally differentiated cells from mouse and humans can be reprogrammed to yield induced pluripotent stem cells (iPSCs) (Takahashi and Yamanaka, 2006; Takahashi et al., 2007). Stem cells are unique in being unspecialised cells that can give rise to different cell types and this property is termed as potency. Blastomeres at the 8-cell stage are totipotent; this means that a single cell is capable of dividing and differentiating to give rise to an entire organism. Cells of the ICM on the other hand are pluripotent and can generate all the tissues and organs except the extraembryonic tissues such as the placenta. As the embryo develops cells become more committed to certain lineages. For instance, groups of cells such as the haematopoietic stem cells (HSCs) or NSCs are multipotent because they give rise to a certain number of specific cell lineages (Gilbert, 2000).

Stem cells play important roles in both the embryonic and adult stages of an organism. Soon after fertilisation the proliferating cells of the ICM are involved in organogenesis and development of the organism. In the adult a pool of stem cells is maintained to aid in recovery following injury or disease (Evans and Potten, 1991). However, the stem cells are defined by their functional characteristics since there is still a lack of definitive markers to identify and purify them (Ahmed, 2009).

1.2.1. The stem cell niche

The microenvironment in which stem cells reside is referred to as a niche (Potten and Loeffler, 1990; Evans and Potten, 1991; Somorjai et al., 2012; Wagers, 2012). The niche is a specialised domain that provides stem cells with physiological and biochemical cues that enable them to function correctly in space and time (Schofield, 1978). This is particularly relevant in the context of studying stem cell biology and developing therapies for use in the clinical setting. The niche is involved in the regulation of the proliferation, survival, and differentiation of stem cells. It is a combination of specific cell types, soluble and membrane-associated cell signalling factors, and physical parameters such as rigidity, O_2 availability, and temperature (Wagers, 2012). Interplay between stem cells and the niche-mediated interactions with the surrounding environment influence stem cell behaviour and the decisions to proliferate, differentiate, migrate, or remain quiescent (figure 1.2).

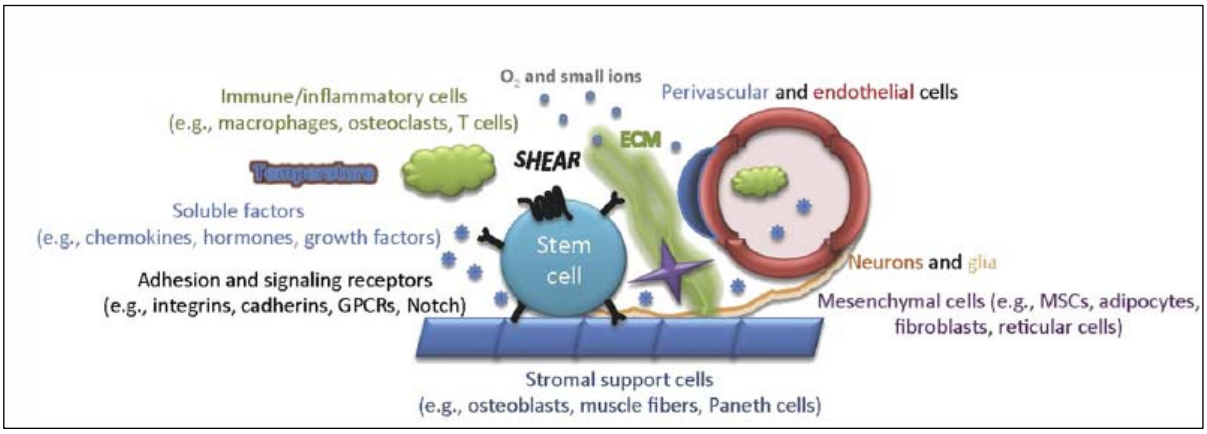

Figure 1.2. Constituents of the stem cell niche.
The niche comprises of both cellular factors such as cell types, receptors, support cells, and acellular factors such as signalling molecules, temperature, and physical parameters (Wagers, 2012).

An important aspect of the regulation of the stem cell number relates to the type of division adopted by the cell (figure 1.3). When a stem cell divides symmetrically it produces two daughter cells with similar fates, while asymmetric divisions result in two cells destined for different fates. The balance between the two is critical for homeostasis and to prevent tumour formation. A number of cell signalling pathways are involved in the regulation of the mammalian stem cell niche with Wnt/β-catenin, bone morphogenetic protein (BMP), Notch, sonic hedgehog (Shh), glial cell-derived neurotrophic factor **(**GDNF), fibroblast growth factor (FGF), and vascular endothelial growth factor (VEGF) being key players in cell fate determination (Li and Xie, 2005; Morrison and Spradling, 2008; Plikus et al., 2008; Voog and Jones, 2010).

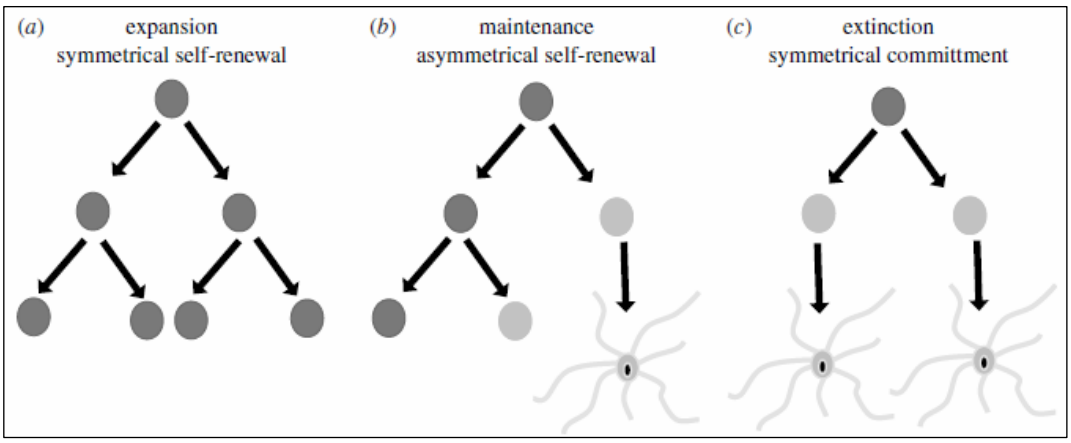

Figure 1.3. Symmetric versus asymmetric stem cell divisions in homeostasis and development.
Stem cells can choose to self-renew symmetrically (a) or asymmetrically (b). Symmetric division could also result in committed progenitors that deplete the stem cell pool (c) (Dirks 2007).

In recent years there have been tremendous advances in the study of mammalian stem cell niches. Lineage tracing, single cell transplantation and *in vitro* culture studies have helped in identifying niche factors and their effects on stem cell behaviour in diverse cell types such as HSCs (Weissman et al., 2001), intestinal stem cells (Barker et al., 2007), and the hair follicle (Blanpain and Fuchs, 2009). In the mouse neocortex integrin signalling has been shown to be important for adhesion, cell division, and cell fate of NSCs (Loulier et al., 2009). Given the importance of the niche in tissue homeostasis and repair it is not surprising that it is involved in ageing, tumour initiation, and metastasis (Voog and Jones, 2010). It is especially pertinent to the study of cancer stem cells (CSCs). For instance, bacterial or viral infection of haematopoietic and epithelial cells has been found to impact on the local microenvironments by altering signalling pathways that affect cancer cell proliferation (Coussens and Werb, 2002; Tlsty and Coussens, 2006). The role of non-malignant cells such as macrophages and bone marrow-derived progenitors in altering the niche to promote tumour invasion and metastasis has

also been described (Kaplan et al., 2005; Hiratsuka et al., 2006; Wels et al., 2008). Hence, a clear understanding of niche function and its role in regulating stem cells is a pre-requisite for the study and development of potential stem cell therapies.

1.2.2. Embryonic NSCs (eNSCs)

NSCs are undifferentiated cells of the brain that are multipotent and give rise to neurons and glia (astrocytes and oligodendrocytes). At the embryonic stage cells lining the ventricles called neuroepithelial cells initially divide symmetrically to increase the pool of NSCs. Subsequently asymmetric division occurs by which a pool of NSCs is maintained in the ventricular zone while the other daughter cells migrate radially outward to thicken the developing brain (Haubensak et al., 2004; Noctor et al., 2004; Merkle and Alvarez-Buylla, 2006). These neuroepithelial cells are believed to transform into radial glial cells, which then transform into astrocyte-like adult NSC (aNSC) (Merkle and Alvarez-Buylla, 2006). The lineage of the mammalian NSC is depicted in figure 1.4.

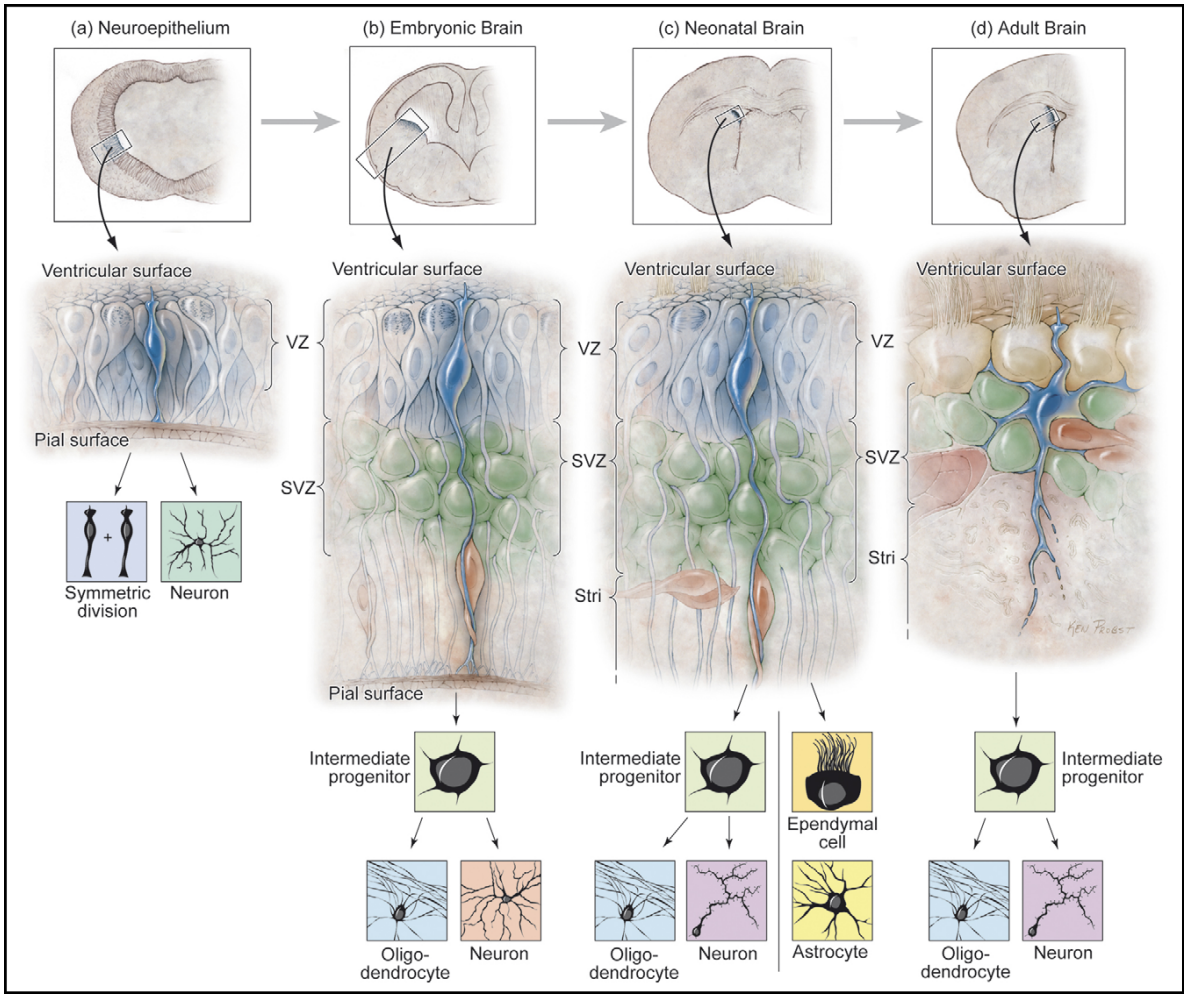

Figure 1.4. NSCs and their lineage in the developing forebrain.
The NSCs (shown in blue) begin as symmetrically dividing neuroepithelial cells (a) that expand the stem cell pool. These cells then transform into embryonic radial glial cells (b), which divide symmetrically or asymmetrically to produce neurons and oligodendrocytes via intermediate progenitors. In the neonatal brain, radial glial cells persist, giving rise to oligodendrocytes, olfactory bulb interneurons, ependymal cells, and astrocytic cells (c). The astrocytes are the stem cells of the adult brain (d) capable of generating olfactory bulb interneurons and oligodendrocytes (Merkle and Alvarez-Buylla, 2006).

The first study of the isolation and characterisation of eNSCs of the rat brain showed that a subset of isolated cells possessed stem cell-like properties (Temple, 1989). This was followed by the finding that Nestin+ cells could proliferate in the presence of basic fibroblast growth factor (bFGF) and nerve growth factor (NGF) (Cattaneo and McKay, 1990). The establishment of the neurosphere assay (NSA)

was critical in defining the nature of these cells and could be used to study the self-renewal and multipotency of NSCs in the presence of epidermal growth factor (EGF) *in vitro* (Reynolds and Weiss, 1992).

1.2.3. Adult NSCs (aNSCs)

The central dogma of neurobiology posited that neurogenesis did not occur in the adult brain. Although research in the 1960s and 70s had hinted at the presence of proliferative cells in the adult brain their identity was unclear (Altman and Das, 1965; Altman, 1969). The demonstration of the occurrence of neurogenesis in adult songbirds (Alvarez-Buylla et al., 1988; Nottebohm, 1989) and the subsequent isolation of NSCs from the adult mouse brain and their differentiation into neurons and glia *in vitro* (Reynolds and Weiss, 1992) helped break the dogma and established the presence of stem cells in the adult mammalian brain.

It is now known that the major neurogenic zones in the adult brain are the subventricular (SVZ) and subgranular zone (SGZ) of the dentate gyrus (DG) in the hippocampus. Besides their presence in the SVZ and SGZ NSCs are also thought to exist in the cortex (Palmer et al., 1999), spinal cord (Weiss et al., 1996), hypothalamus (Lie et al., 2002), and retina (Tropepe et al., 2000).

1.3. The study of NSCs

1.3.1. *In vivo*

NSCs in the mammalian brain have been identified based on the uptake of 5-Bromo-2′-deoxyuridine (BrdU) (Morshead et al., 1994). In this approach incorporation of BrdU was used to determine the time of origin of neurons, which

is coincident with the NSC's exit from the cell cycle. BrdU is taken up into the nuclei of rapidly dividing cells and the concentration of the label reflects the division status of the cell. On the other hand, use of transgenes such as β-galactosidase or green fluorescent protein (GFP) by means of retroviral-based vectors has been used to demonstrate the lineage commitment of the proliferating NSCs (Sanes, 1989). Expression of several proteins such as Nestin, Sox2, CD133 (Prominin-1), Lewis-X (LeX), Hes1, Hes5, Bmi1, and Musashi-1 is associated with NSCs.

Nestin is an intermediate filament protein expressed by the cells of the developing and mature CNS (Dahlstrand et al., 1995; Ernst and Christie, 2005) and was found to be downregulated in differentiated cells (Ernst and Christie, 2005; Ernst and Christie, 2006). However, cells in other tissues such as muscle (Lendahl et al., 1990) and skin (Medina et al., 2006) also express Nestin. Hence, presence of cells expressing Nestin cells is an indicator of the presence of neural precursors which include both NSCs and NPs.

Sox2 (sex determining region [SRY]Y-box 2) is a transcription factor involved in pluripotency of ESCs (Avilion et al., 2003). Expression of Sox2 has been shown in both e/aNSCs (Graham et al., 2003; Wang et al., 2006). Sox2 functions by inhibiting differentiation and maintaining the population of neural precursors (Bylund et al., 2003; Graham et al., 2003; Ferri et al., 2004). *Sox2* is one of the four genes required for generating iPS cells from fibroblasts (Takahashi et al., 2007); (Wernig et al., 2007).

CD133 is a glycoprotein that was originally identified as a HSC marker (Miraglia et al., 1997) and has since been routinely employed for the isolation of NSCs from tissues (Uchida et al., 2000). Stem cells expressing CD133 have been derived from the haematopoietic system and the CNS (Yin et al., 1997; Uchida et al., 2000). More recently CD133 expression has been found to be associated with brain tumours (Singh et al., 2004).

LeX is also referred to as CD15 or SSEA-1 (stage-specific embryonic antigen 1) and was found to be expressed by ESCs and stem cells from the bone marrow (Marani et al., 1986; Jiang et al., 2002). The identification of LeX+ cells in the subependymal cells of the adult mouse brain (Capela and Temple, 2002) was followed by the purification of eNSCs using LeX as a surface marker for FACS (Capela and Temple, 2006).

Hes1/5 are basic helix-loop-helix (bHLH) transcription factors that are important targets of the Notch signalling pathway (Ohtsuka et al., 1999). Similar to Sox2, Hes1/5 act by inhibiting neurogenesis and maintaining the progenitor pool (Kageyama and Ohtsuka, 1999; Kabos et al., 2002; Hatakeyama et al., 2004). Expression of Hes1 was recently found to oscillate and is important for the regulation of its activity (Shimojo et al., 2008).

Bmi1 is a polycomb ring finger oncogene that regulates NSC self-renewal (Zencak et al., 2005) by suppressing p16 and p19 which are cell cycle inhibitors (Bruggeman et al., 2005; Molofsky et al., 2005). It is expressed by several tissues

such as HSCs, ESCs, heart, testis, and thymus (van Lohuizen et al., 1991; Jacobs et al., 1999).

Musashi1, which is an RNA-binding protein was first identified in sensory organ development in *Drosophila* (Nakamura et al., 1994). It was subsequently found to be expressed in both embryonic and adult CNS (Sakakibara and Okano, 1997; Kaneko et al., 2000). Expression of Musashi-1/2 was found to be crucial for NSC self-renewal *in vitro* (Sakakibara et al., 2002). It is also expressed by stem cells of other tissues such as the intestine and breast (Potten et al., 2003; Clarke et al., 2005).

1.3.2. *In vitro*: the culture of NSCs

1.3.2.1. The neurosphere assay (NSA)

Reynolds and Weiss reported the isolation and culture of NSCs from the adult rat brain *in vitro* by culturing cells in the NSA (Reynolds and Weiss, 1992). This method allowed the culture of neural precursors as 3-D suspension cultures called neurospheres. Neurospheres are cultured in serum-free media supplemented with growth factors such as EGF, and bFGF to encourage the survival and expansion of stem cells as well as the more restricted progenitors (Reynolds and Weiss, 1992; Palmer et al., 1999). A combination of other supplements such as insulin, transferrin, and progesterone are also used to support growth.

The NSA has been used to detect the presence of stem cells and progenitors in isolates from embryonic and adult mammalian tissues and to study their characteristics *in vitro.* The central definition of an NSC is its: i) ability to self-

renew, ii) differentiate into the three neural lineages, and iii) regenerate tissue following injury. The NSA allows the direct assessment of self-renewal and differentiation. Regeneration of host tissue cannot be addressed by the NSA alone and involves transplantation of the cell population to test survival and differentiation.

One of the important read-outs of the NSA is the neurosphere forming unit (NFU). This refers to the number of neurospheres formed in culture per 100 cells plated. The NFU is an important output because not all cells will give rise to neurospheres. Apart from the NFU the NSA can be used to study cell survival and propagation over multiple passages, differentiation and multipotency.

1.3.2.2. Neurospheres are natural 3-D cultures

Neurospheres are a heterogeneous population of NSCs, NPs, and differentiated cells. They have been shown to express high amounts of EGF receptor (Lobo et al., 2003), cadherins (Campos et al., 2004), and β1 integrins (Jacques et al., 1998). An ECM rich in laminins, integrins, and chondroitin sulphate proteoglycans (CSPG) surrounds the cells in culture (Lobo et al., 2003). Hence, this naturally occurring 3-D culture system creates niches and is physiologically more relevant than 2-D culture systems. A recent study showed that brain tumour cells cultured in the NSA mirrored the phenotype and genotype of primary patient tumours in a more accurate manner than serum-derived lines obtained from the same patient (Lee et al., 2006). Moreover, the neurosphere can be used as an *in vitro* model of neural development and neurogenesis. For instance, neurosphere cells label positive for a variety of markers such as Nestin, LeX, Sox2, Olig2, S100β and GFAP (Brazel et

al., 2005; Parker et al., 2005). Upon differentiation they form astrocytes, neurons, and a small percentage of oligodendrocytes, which can be manipulated by the addition of different factors. These features mimic the behaviour of the neural precursor pool *in vivo*. Responsiveness to growth factors such as EGF and FGF2 also follows the developmental timeline (Tropepe et al., 1999) thus establishing the neurosphere as a model for the study of brain development. The study of brain development is essential for the development of therapies against neurodegenerative disorders and brain tumours (Lindvall et al., 2004; Kim, 2010).

1.3.2.3. Clonal assays

Since the development of the NSA and through most of the subsequent years cells were plated in bulk or high density conditions. Recent reports however have shown that under conditions of high cell density, cell aggregation is a common and significant event (Singec et al., 2006; Mori et al., 2007; Coles-Takabe et al., 2008). This could likely lead to misinterpretations of results such as the overestimation of NSC frequency in culture (Rietze et al., 2001). A clonal assay is particularly essential to ensure valid interpretation of the results of the NSA. Clonal assays can be carried out in suspension or gel-based formats such as the semi-solid collagen-based assay for neurosphere culture called the neural-colony forming cell assay (N-CFCA) (Louis et al., 2008).

Under clonal conditions (Gan et al., 2011) dissociated single cells are plated at single cell or 50-100 cells/well densities which ensures that the neurospheres that are formed arise from a single cell. Use of clonal suspension cultures allows for easy re-extraction of neurospheres for further analysis which is more challenging

in a gel-based assay. Similar to a clonal NSA a clonal multipotency assay can be carried out in a 50-well chambered coverslip sealed with a silicone gasket. Clonal neurospheres are individually placed in the chamber, differentiated, and scored for potency.

Cells that form neurospheres include NSCs and NPs (Seaberg and van der Kooy, 2002; Reynolds and Rietze, 2005) and may be collectively referred to as NFCs. It is important to distinguish between NSCs and NPs. Both NSCs and NPs can give rise to neurospheres. The difference lies in their potency. While NSCs can differentiate into all the three neural lineages namely astrocytes, neurons, and oligodendrocytes, NPs are either unipotent or bipotent. Hence, to conclusively identify NSCs in culture it is important to combine clonal assays evaluating neurosphere formation and multipotency.

1.3.2.4. Estimation of NSC frequency

A number of studies have used the NFU to calculate NSC frequency (Rietze et al., 2001; Capela and Temple, 2002; Kim and Morshead, 2003) based on the assumption that a one-to-one correlation exists between NSCs and neurospheres. This is flawed because not all neurospheres arise from NSCs leading to a gross overestimation of the presence of NSCs in culture. Moreover, it fails to take into account aggregation events in bulk density conditions and their impact on neurosphere formation. The NSC frequency derived independently by mathematical modelling of bulk-cultured E14 cells and from the N-CFCA are 0.16% and 0.07%, respectively (Reynolds and Rietze, 2005; Louis et al., 2008). However, it is unclear if these values reflect the true NSC frequencies in culture

since they are based on several assumptions such as 100% efficiency of NSC expansion or the emphasis on colony size as a reflection of NSC activity.

The NSA on its own does not reflect the true number of NSCs in culture. The actual NSC frequency can only be estimated from known values of clonal NFU and multipotency. When tested on E14.5 cultures this was found to be variable ranging from 0.6%-20% depending on the exact growth conditions used (Tham et al., 2010; Gan et al., 2011).

1.4. Imaging of 3-D cultures

3-D cell cultures such as neurospheres, skin organotypics, and intestinal crypts are powerful models for studying cell behaviour and function. Skin organotypic cultures or human skin equivalents (HSEs) were developed to study epidermal biology and to monitor processes such as repair following wounding (Egles et al., 2009). The behaviour of cells in HSEs and their morphology, growth and differentiation was found to mimic that of normal skin reinforcing their use as valuable models for the study of normal skin biology as well as diseases such as skin cancer (Carlson et al., 2008). Moreover, recent approaches of adopting 3-D cell culture systems for toxicity testing in epidermal cells (Gotz et al., 2012) or for the study of the development of organoid structures such as intestinal crypts *in vitro* (Sato et al., 2009) reinforce the invaluable insight provided by 3-D culture systems. It has also been shown that the elasticity of the matrix used to culture naïve mesenchymal stem cells (MSCs) influences cell fate (Engler et al., 2006). Similarly, upon differentiation in biodegradable 3-D matrices human embryonic stem cells (hESCs) were shown to form committed embryonic tissue-like

structures, providing a novel method of culturing viable tissues *in vitro* for potential applications in cell transplantation (Levenberg et al., 2003). The study of adipose tissue differentiation which is crucial for the development of treatment strategies for obesity and type 2 diabetes mellitus has been shown to require a 3-D culture system for the findings to be physiologically relevant (Kang et al., 2005). Although 2-D culture systems have led to the birth of several fundamental findings in the life sciences, it is important to recognize their limitations (Abbott, 2003; Keller et al., 2006). 3-D cultures are ideal systems for studying hitherto quiescent stem cells that cannot be successfully grown *in vitro* (Pastrana et al., 2011).

In vitro NSCs/NPs can be cultured as primary cell cultures or immortalised cell lines. A number of NSC lines such as C17.2 and ReN001 are being used for the study of NSC biology and potential applications in the treatment of neurodegenerative diseases such as stroke (Snyder et al., 1992; Choi, 2007). C17.2 was derived from cells of the cerebellar granule neurons of the postnatal brain that were immortalised with the *v-myc* oncogene (Ryder et al., 1990; Snyder et al., 1992) and shown to differentiate into astrocytes, neurons and oligodendrocytes *in vitro* as well as *in vivo* (Snyder et al., 1992; Taylor and Snyder, 1997; Vescovi and Snyder, 1999). C17.2 cells have been used in injury models wherein they have displayed favourable therapeutic outcome [reviewed in (Snyder et al., 2004)]. However, significant differences were identified on detailed examination of C17.2 cells and primary cortical cells (Mi et al., 2005). Firstly, although C17.2 cells expressed most NSC markers they glaringly failed to express Sox2. Expression patterns were also different from that of the cerebellar granule neurons which are the cells-of-origin of C17.2. Moreover, C17.2 cells were found to be aneuploid.

Hence, although invaluable for the study of NSC biological pathways such as directed migration and homing (Snyder et al., 1992; Liu et al., 1999) it is important to recognise the differences and utility of immortalised cell lines and primary cultures.

Primary NSCs/NPs are propagated as 3-D clusters called neurospheres. The presence of cell-to-cell contacts, cell-to-exterior contacts, and the ECM allows for a natural 3-D environment to exist that closely mimics tissue organization *in vivo*. It was recently shown that a sub-group of cytokines such as interleukin 1-β, BMP8b, FGF5, VEGFA are upregulated in both neurospheres and cells grown in 3-D matrices (Lai et al., 2011). 3-D culture systems are also relevant in high content assays (Justice et al., 2009). Given the links between stem cells and brain tumours (Dirks, 2008) the establishment of 3-D model systems would enable a more physiologically relevant approach to drug design.

1.5. Microscopy and imaging

1.5.1. Labels

Labelling cells with fluorescent tags was revolutionised with the discovery of the green fluorescent protein (GFP) as a marker for *in vivo* imaging studies (Chalfie et al., 1994). In the years following the initial use of GFP several variants have been cloned providing a diverse array of multicolour labelling possibilities (Chudakov et al., 2010). Advances have also been made in the development and application of chemical dyes for labelling various intracellular components of the cell. Fluorescent proteins such as GFP are used to study the localisation, dynamics, interaction with other proteins, and functions of genes of interest. Similarly, use of

chemical dyes to monitor intracellular processes such as calcium signalling has enabled the detailed study of the importance of such processes in homeostasis and development.

1.5.2. Fixed samples

Cells are immobilised by chemical fixatives such as paraformaldehyde. Fixation with aldehydes results in the formation of covalent bonds between the intracellular components and helps preserve cellular organisation. Following fixation cells are permeabilised to allow the fluorescent markers in the form of antibodies or chemical dyes to access intracellular compartments.

Examples of dyes commonly used in cellular labelling include calcein, phalloidin to label actin, DAPI to label nuclei, and FM1-43, FM4-64 to study endocytosis among others. In procedures involving the use of antibodies for labelling the primary antibody against the protein of interest is usually unlabelled. The primary antibody is detected by means of a fluorescently tagged secondary antibody. In studies using NSCs/NPs one of the common applications of fixation and labelling is in the differentiation assay. NSCs/NPs are allowed to differentiate into astrocytes, neurons, and oligodendrocytes which are then identified by lineage-specific antibodies. Recent advances in labelling techniques have seen the advent of quantum dots and their use in a wide variety of applications (Pinaud et al., 2006).

Although fixation of cell samples should optimally immobilise and expose the antigen while simultaneously preserving cellular structure, the procedure has

several disadvantages. Different fixatives preserve cellular structure to varying degrees and hence the fixative has to be carefully chosen depending on the type of cell structure or protein being studied. Instances of cells and intracellular structures appearing shrunken and distorted owing to dehydration from methanol fixation have been reported (Becker and Gard, 2006). Additionally, fixation may result in the denaturation of the antigen which is a potential problem when the antibody is not raised against the denatured form of the protein. Moreover, each fixation method is sensitive to temperature, pH of the buffers, concentration and penetration of fixatives, size of specimen and duration of fixation and can produce artifacts and background fluorescence.

1.5.3. Live samples

The study of live cells is a powerful tool for a number of reasons. First, it offers insight into the process being studied in a physiological context. Phenomena such as fluctuations in gene expression or changes in protein localisation are easy to measure with appropriate markers and techniques. Secondly, there are no artifacts such as those arising from cell fixation (Schnell et al., 2012). Lastly, studying changes in environmental conditions and their impact on cellular mechanisms is more relevant when live samples are used.

For dyes and markers to be used on live samples they must be cell permeable. There are a number of labelled organelle-specific dyes and lipid molecules that are added to the cell culture medium for uptake. Examples include the DNA binding benzimide Hoechst 33342 (Darzynkiewicz and Huang, 2004), the cytoplasmic marker Cell Tracker Green CMFDA (Poole et al., 1996), lectins such as wheat

germ agglutin (Kanazawa et al., 2008), and mitochondrial markers such as Mito tracker (Miyake et al., 2011). Alternatively, cell impermeable dyes and proteins may be microinjected into the cell of interest (Mohanty et al., 2003).

There are several important factors to bear in mind while imaging live samples labelled with fluorophores. Upon illumination by a light source fluorophores release free radicals that can cause damage to cells, a phenomenon referred to as phototoxicity. Bleaching of the fluorescent signal is another problem that could affect data acquisition. Environmental conditions play a crucial role in the outcome of imaging living cells. Live cells require the maintenance of optimal growth conditions involving temperature, pH, and atmosphere (Stephens and Allan, 2003). Adverse environmental conditions could result in abnormal membrane structures, vacuole formation, cell rounding, and membrane blebbing. Hence, rapid image scanning and acquisition speeds are desired. Imaging modalities such as the digital scanned laser light sheet microscopy (DSLM) help in significantly reducing both photodamage and bleaching by using a novel illumination method coupled with rapid acquisition (Verveer et al., 2007). This enables imaging of live, whole specimens such as embryos (Keller et al., 2008).

1.5.4. Widefield and confocal microscopy

1.5.4.1. Point spread function

The point spread function (PSF) can be defined as the 3-D diffraction pattern of a point source of light collected by a lens. The diffraction pattern takes the forms of an Airy disc characterised by concentric rings of light in the lateral, or *xy* plane,

and elongated cones of light in the axial, or *z* plane. The numerical aperture (NA) of the lens determines the size of the Airy disk for a given wavelength of light.

The shortest distance between two points in an image from an optical microscope at which they can be distinguished as two individual entities is referred to as the limit of resolution for that system. Since the diameter of the Airy disc determines resolution, it is said to be diffraction limited. The lateral resolution in a widefield (eqn. 1) and confocal microscope (eqn. 2) is determined by the following formulae, respectively:

Eqn. 1 $$d_{wf} = \frac{0.61\lambda}{NA}$$

Eqn. 2 $$d_{conf} = \frac{0.37\lambda}{NA}$$

where, d is the distance between two points in the image and λ is the wavelength of light. A confocal microscope provides a 1.4-fold gain in lateral resolution compared to a widefield system through the use of a pinhole that also offers optical sectioning and improved contrast.

Spatial resolution is a major limitation in fluorescence microscopy. As shown in eqn. 1 lateral resolution is determined by the wavelength of the light used and the NA of the objective lens. Resolution in the axial direction, which is related to the depth of field is another major consideration when considering biological samples which are inherently 3-D. Thin or fine structures have a small depth of field whereas large structures have relatively larger depths of field. With the latter, because relatively distant focal planes can contribute to the final detected image out-of-focus light and loss of contrast are significant issues.

Different methods can be used to address the issue of out-of-focus light. Widefield fluorescence microscopy can be used to generate 3-D images, which can then be restored using deconvolution methods. The resulting images are significantly improved for signal-to-noise ratio, optical sectioning and contrast by using the knowledge of the PSF of the microscope and computationally processing the image with one of a variety of deconvolution algorithms (Stuurman and Swedlow, 2012). Another common method to remove out-of-focus light is to use a confocal microscope [LSCM or spinning disk (SDC)]. It should be noted that deconvolution can be applied on images obtained from widefield and confocal systems to improve the quality of the image.

1.5.4.2. Widefield versus LSCM for 3-D imaging

In a conventional widefield fluorescence microscope the entire sample in the field of view is uniformly illuminated by an incoherent source of a wavelength-band of intense light, usually from a mercury arc or xenon lamp source. The light emitted by the specimen can be viewed either directly by the eye or projected to an image capturing device. Acquisition is relatively fast compared to LSCM, since the entire field of view is illuminated at once and the emitted photons are collected by an array high sensitive charge-coupled device (CCD) cameras. However, there is a significant issue that can degrade the quality of the image collected; in a widefield system light fluorophores in out-of-focus planes are also excited and the emitted light collected at the same time results in poor signal-to-background ratio. The problem is particularly compounded in specimens >2 μm in thickness since emission from the planes above and below the plane of focus cause loss of finer

details that are lost in the blurry image. Hence, unless combined with efficient deconvolution methods, widefield imaging is difficult to apply in 3-D imaging of thicker samples (Wallace et al., 2001).

Confocal imaging is better suited for 3-D imaging of relatively thick samples and offers several advantages over the widefield system. First, only light emitted from the focal plane of the sample is detected; the out-of-focus light is eliminated resulting in sharper images with a higher signal-to-noise ratio. This is achieved by means of a pinhole positioned in a plane conjugate to the focus plane in the sample, which prevents the out-of-focus light from ever reaching the detector. Secondly, it results in an increase in lateral as well as axial resolution. LSCM also allows very thin optical sectioning (<1 μm), which generates details about sub-cellular structures that can be very difficult to obtain with a widefield system. Sensitive and fast detectors called photon multiplier tubes (PMT) are used in which the incoming photons are converted to electrons and electronically multiplied several-fold to increase the signal received from the sample.

The main advantages of a confocal microscope for 3-D imaging lies in the configuration of optics that provides higher contrast by eliminating most of the out-of-focus light. However, elimination of a proportion of the emitted light from the sample also implies that a proportion of potentially useful light is excluded in the process. Additionally, use of a small aperture demands that high intensity excitation sources such as lasers, high NA objective lenses, and bright samples are used. These in turn, may increase the photobleaching of the sample, and phototoxicity to live cells. In a LSCM, the image is constructed by point-by-point

imaging of the sample. The point-by-point image acquisition allows for capture of optical sections but this occurs at the expense of speed– confocal is a relatively slow technique when compared to widefield imaging. Because of the time required to acquire an entire 3-D image stack, these systems are typically used with specimens that do not move during image acquisition and are typically not recommended for live-cell imaging. As an alternative, the SDC system was developed which overcomes these issues. The SDC systems have high speed imaging capabilities with slightly diminished confocality. These systems use a rotating disc with a pattern of slits or holes in a microscope plane conjugate to the sample focal plane. The opaque areas of the disk block out-of-focus light from the emission light path. This confocal method is faster as the sample is illuminated in parallel at multiple points at the same time and collected with an array detector (like a CCD) as the disk spins as opposed to the LSCM, where the sample is imaged point-by-point. Compared to the LSCM, the SDC offers the benefit of speed and reduced phototoxicity for live-cell imaging experiments. However, the SDC cannot deliver such high quality optical sections as the LSCM, cannot penetrate as deep into the sample effectively and is much less versatile in terms of objective lens.

1.5.5. Selective plane illumination microscopy (SPIM) and digital scanned laser light sheet microscopy (DSLM)

The use of light sheets to optically section samples has been in use for several years now. In 1903, an instrument called the Ultramikroskop was invented for investigating gold particles (reviewed in Keller et al., 2006). Subsequently, the technology has been used to study cochlea (Voie et al., 1993) and observe

microbes (Fuchs et al., 2002). More recently, Stelzer and colleagues have developed a novel imaging technology using light sheets called selective plane illumination microscopy (SPIM) (Huisken et al., 2004) and DSLM (Keller et al., 2008). In these systems, a focussed sheet of light is used as the illumination source in a perpendicular orientation to that of the imaging objective lens that only excites fluorophores illuminated by the light sheet. Since only the plane being observed is illuminated, out-of-focus fluorescence is not generated. Hence, it allows the acquisition of several planes in thick samples by limiting phototoxicity and bleaching. Two separate lenses are used, one for illumination and a second one for detection. In addition, 3-D imaging is performed by rotating the sample through the optical axis of the detection system. This enables multi-angle imaging, which refers to the acquisition of multiple 3-D stacks of the object from different angles. In a further post-processing step, the data sets that are generated along different angles are computationally combined into a single stack with a much more isotropic point spread function.

While SPIM uses a cylindrical lens to produce the laser sheet, in DSLM a laser scanner generates a beam of light that can be moved vertically and horizontally through the specimen (Keller et al., 2008) (figure 1.5). DSLM uses an illuminating lens with much lower NA relative to the detection lens. Using DSLM results in several advantages for 3-D imaging of thick samples; (1) imaging speeds are rapid, with high signal-to-noise ratio and fine axial resolution, (2) since the same intensity is used for illumination, quantitative imaging is more accurate, and (3) optical aberrations are minimal since apertures are not used to form the laser profile. Lastly, the illumination efficiency is dramatically increased since the total

illumination is focussed into a single line (Keller et al., 2008). Hence, this approach is particularly useful for rapid 3-D imaging, with minimal photodamage to the specimen.

Samples for SPIM/DSLM require special holders as illustrated in figure 1.6.

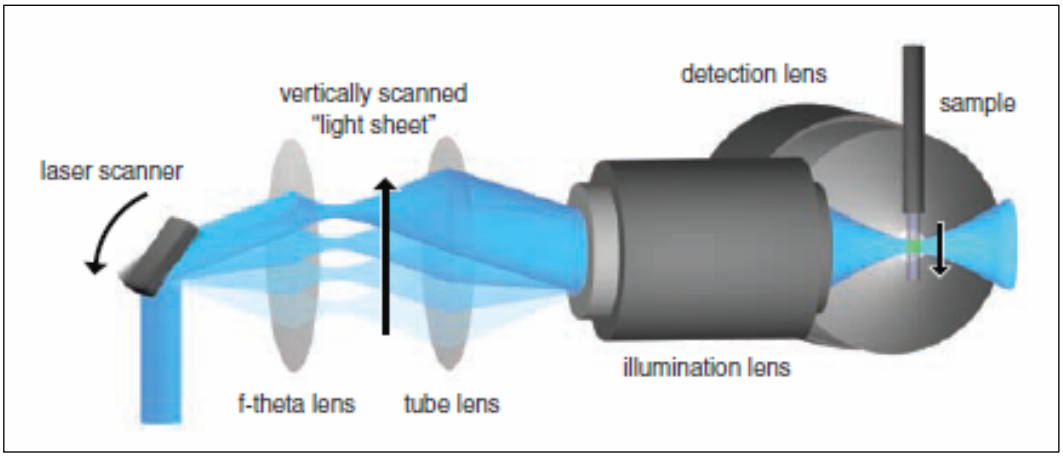

Figure 1.5. Configuration of a DSLM microscope.
The specimen is illuminated by an illumination lens and the excited fluorophores are scanned in a single line. A separate lens is used for detection.

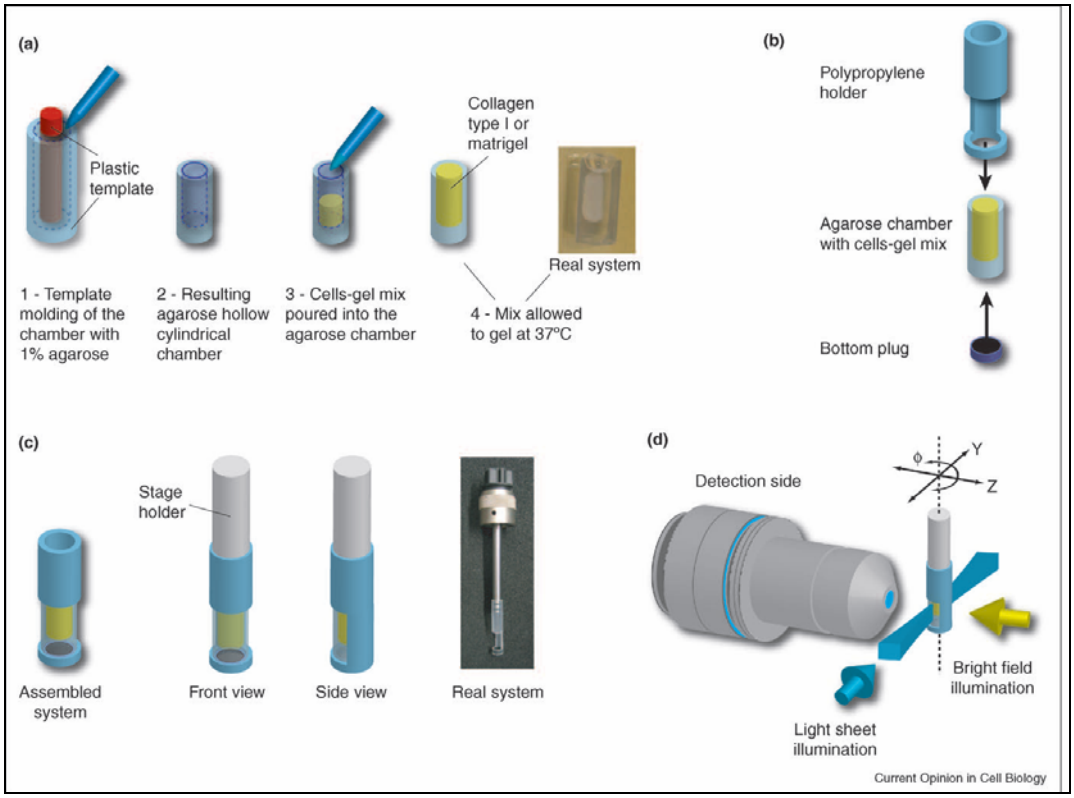

Figure 1.6. Sample holders for SPIM/DSLM.
Custom-designed sample holders with the matrix (a-c) and the configuration of the optics are shown (Keller et al., 2006).

1.5.6. Confocal versus light sheet based microscopy

High resolution imaging with a LSCM requires the use of high NA lenses, which have a limited working distance that greatly limits the penetration depth. Furthermore, illumination of the entire volume of the sample in a LSCM means that during 3-D imaging, repeated illumination of the sample can result in photobleaching and photodamage. By contrast, in light sheet microscopy such as SPIM or DSLM, limiting the illumination to the plane being observed reduces photobleaching of the out of focus planes of the specimen and hence, reduces the photodamage. For these reasons it can be considered a superior imaging modality to use for 3-D imaging of live cells or embryos. Moreover, no out-of-focus light is

generated in the SPIM/DSLM and the use of low NA illumination lenses causes minimal spherical aberrations. Imaging of *Drosophila* and zebrafish embryonic development on LSCM and the DSLM revealed that the latter used three orders of magnitude less light energy to illuminate the sample and provided 50 times faster imaging speeds and a 10–100-fold higher signal-to-noise ratio. Multiview imaging and improved penetration depth make the DSLM/SPIM the best suited imaging modalities to study fine details of cellular structures within entire biological samples without compromising sample integrity and viability (figure 1.7).

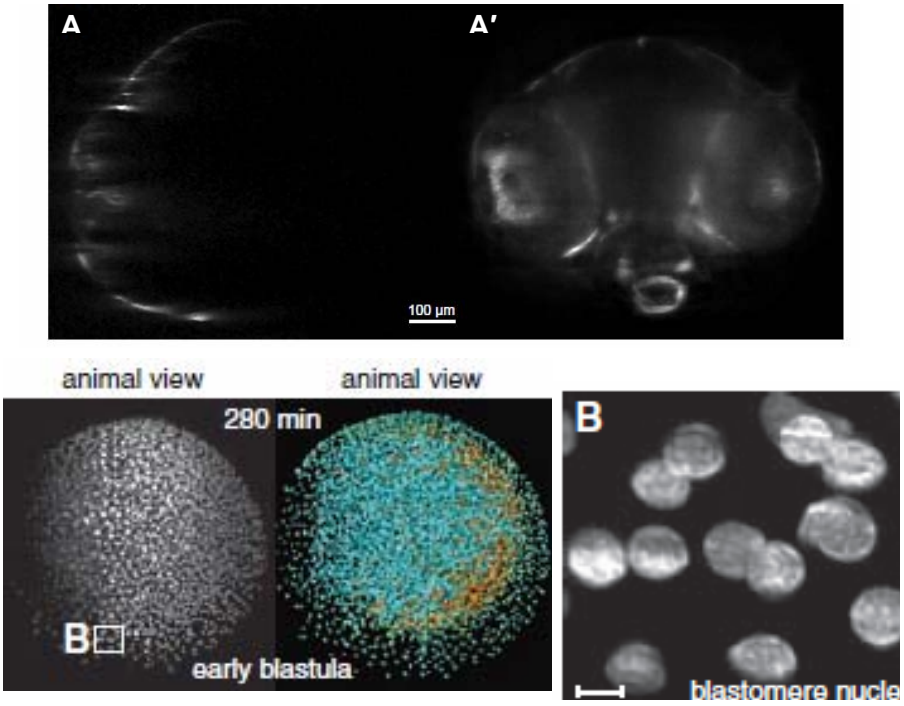

Figure 1.7. Comparison of LSCM, SPIM and DSLM.
Slices from 3-D images of a Medaka embryo imaged on a LSCM (A) and SPIM (A') are shown. Although the LSCM provides surface resolution, lack of penetration depth results in lack of information from the centre-outward regions of the embryo (adapted from Huisken et al., 2004). B, Imaging of zebrafish embryos on the DSLM provides sub-cellular resolution of the nuclei of the early blastula. Maximum intensity projection and digital reconstruction of the nuclear-labelled zebrafish embryo are shown on the left (Keller et al., 2008).

1.6. Image analysis

Digital images are recorded as pixels which are manifestations of photon flux (Stuurman and Swedlow, 2012). 3-D image processing can be broken down into steps involving segmentation of the image, feature extraction and validation, followed by statistical quantification.

1.6.1. Evolving generalised Voronoi diagram (EGVD)

The derivation of meaningful information from 3-D images is based on several basic requirements: clear markers for cellular organelles such as nuclei or cell membrane to facilitate accurate segmentation, efficient segmentation approaches, and sensitive detection and reproducibility.

Image segmentation is the process by which the boundaries of an object are delineated. A number of different methods such as simple thresholding (Lerner et al., 2001), level set function (Yan et al., 2008), and watershed algorithm (Lockett and Herman, 1994; Malpica et al., 1997) are often used to segment nuclei and cells. However, segmentation of neurosphere images requires specific methods that can tackle the issue of cells in contact with one another. EGVD is a method that was initially developed for the segmentation of 2-D neurite images (Yu 2010). This method allows the segmentation of both nuclei and cells that are in contact with one another by preserving the topological dependence.

Segmentation by EGVD consists of the following steps: 1) nuclear segmentation, 2) GVD to demarcate boundaries, and 3) cell segmentation. Validation of the algorithm is performed by comparison with manual ground truth. EGVD was also

compared with commercially available image analysis packages and found to have a mean accuracy of 8% and 12% higher than MetaMorph and CellProfiler, respectively (Yu et al., 2010). EGVD was subsequently modified and applied for the segmentation and analysis of 3-D neurosphere images (Yu and Sankaran, unpublished data) discussed in section 3.2.

1.7. High content and high throughput screening (HCS and HTS) assays

HCS and HTS are cell-based or biochemical assays that combine automated testing and post-processing technologies and applied in basic biomedical research and pharmaceutical and biotechnological industries. HCS and HTS are efficient methods to evaluate diverse questions such as gene function, disease research, and drug discovery. A range of commercial systems are available that allows one to custom-design screens. Automation of the acquisition process has translated into rapidity in the screening process.

HCS/HTS consist of four major components: sample preparation, automated image acquisition, image storage, processing, and analysis, data mining, and image archiving (Dragunow, 2008). Each individual component is crucial to the ultimate outcome thereby requiring careful consideration of the design and implementation of each step is required.

Sample preparation entails testing and optimisation of the cells of interest in the assay format to ensure reproducible results. Several parameters such as i) cell density, ii) time of addition of chemical compound or drug, iii) growth or differentiation conditions, iv) duration of assay, v) use of live or fixed cells at the

time of imaging, and vi) addition of markers for visualisation have to be duly taken into account.

Image acquisition can be performed on widefield or confocal microscopes with the type of assay determining the choice of the system. Some of the major parameters to bear in mind while deciding the optimal imaging platform for a HCS/HTS assay are the following: i) speed of image acquisition, ii) sensitivity of detection, and iii) viability of the specimen during, and post-imaging.

Image acquisition is followed by analysis. There are several commercial packages available that are equipped with tools to carry out qualitative and quantitative analysis. Information is thus mined from the initial 'raw' images and cell number or GFP intensity is then quantified. This can be applied on individual images to generate cell-to-cell or well-by-well results. Some of the packages allow access to the code such that they can be modified by the end-user or third party software developers to create new algorithms that can be custom designed for specific applications.

Data management is a crucial component of the assay since data in the order of a few gigabytes (GB) to terabytes (TB) is generated. The data needs to be analysed, stored and maintained in a way that links raw data to that resulting from analysis. Hence, an ideal data management solution is critical to ensuring the success of a screen.

A typical HTS works by using robotics and computers integrated with automated testing techniques. This allows as many as >100,000 assays per day to be tackled (Hertzberg and Pope, 2000). HCS on the other hand refers to a technique used to assess events at a single-cell level where quantitative observation of cellular response can be performed. In HCS microscopic images are commonly used as the assay read-out and it offers heterogeneity of findings related to cellular response (Xia and Wong, 2012). While vast numbers of reagents can be arrayed and tested automatically by using purified biochemical compounds or cell cultures, recording of individual cell response is the hallmark of HCS (figure 1.8). Owing to the differences in the design of HCS and HTS assays the computing power required for the former is significantly higher.

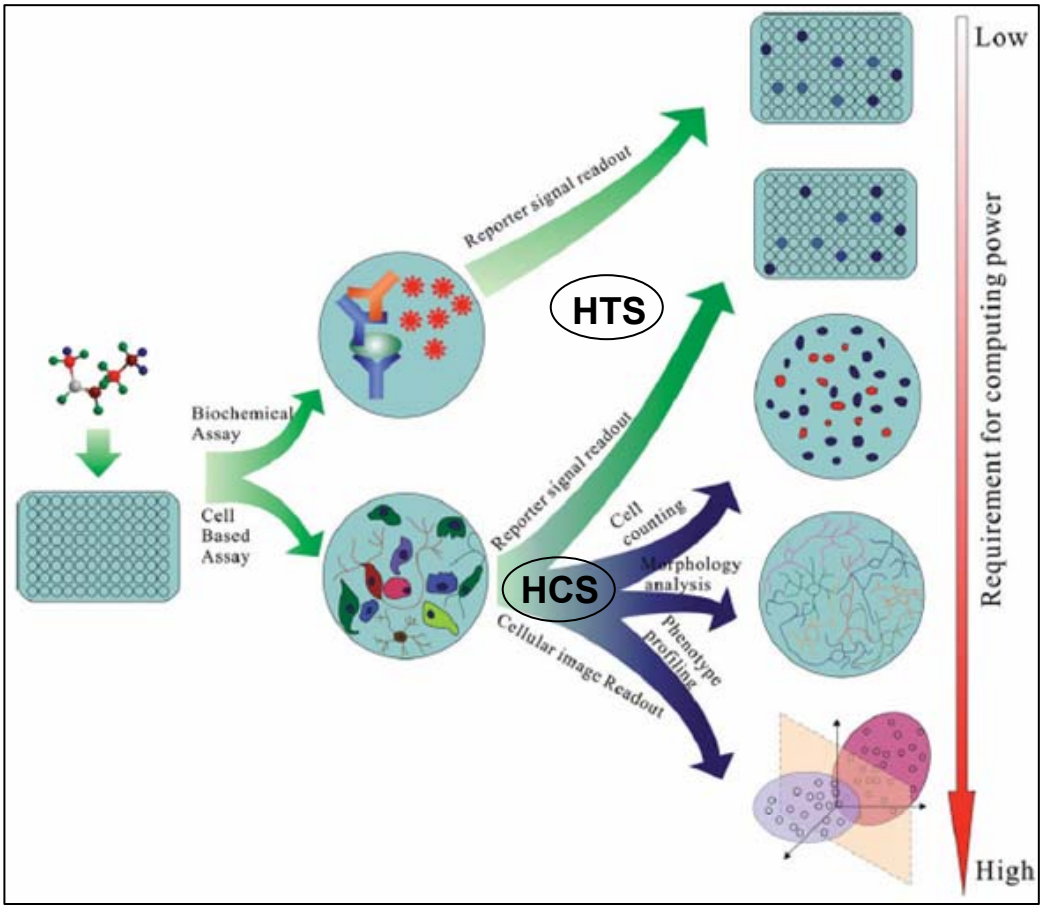

Figure 1.8. Comparison of HTS and HCS screening systems.
HTS assays are depicted by the green branches; HCS by the blue branches reflecting the different requirements and read-outs of the two screening formats.

1.7.1. Implication for the study of diseases

1.7.1.1. Neurodegenerative diseases

A number of neurodegenerative disorders such as Parkinson's disease (PD), stroke, amyotrophic lateral sclerosis (ALS), Huntington's disease manifest as damage to various types of neurons (Lindvall et al., 2004). Some of them such as Huntington's disease, Alzheimer's disease (AD), ALS and PD are characterised by protein misfolding and aggregation. PD is also characterized by loss of dopaminergic neurons in the substantia nigra; stroke, by the degeneration of different types of neurons and glia; and Huntington's, by the loss of medium spiny

neurons. AD is characterised by the accumulation of amyloid-β in the brain (Neve et al., 1990). Studies of the mechanisms of neurite morphology and numbers and inclusion formation are undertaken to better understand the biology of these diseases.

HTS and HCS-based analysis can be used to quantitatively study neurons and dendrites. For instance, a recent study found that rat cortical cultures responded to amyloid-β by having reduced neurite outgrowth although neurite number was not affected (Hu et al., 2007). Another study used a HCS assay to identify compounds that affected neuronal differentiation (Richards et al., 2006).

Apart from observing neurite outgrowth HTS methods have been developed to automatically quantify cell numbers in primary cultures and tissue sections (Narayan et al., 2007). Cell proliferation in C6 glioma cells was analysed by quantifying the number of BrdU+ cells (Lind et al., 2006). HTS assays have also been developed to study inclusion formation in Huntington's disease (Scotter et al., 2008) and amyloid plaques in AD brain tissue slices (Chubb et al., 2006). While most platforms for HCS/HTS have used adherent cells, a novel technology for the analysis of suspension cells is now available (George et al., 2004; George et al., 2006) and is a potentially useful application in the study of suspension cells such as the neurospheres.

1.7.1.2. Brain tumours

The success rate of anti-tumour drugs is very low despite the progress in the understanding of the biology of the disease (Rubin and Gilliland, 2012). Resistance

of tumours to chemotherapy or radiation was known and the discovery of the CSCs has contributed significantly to better appreciate this phenomenon (Dirks, 2008). While treatment may be effective in killing the bulk of the tumour it fails in targeting the CSCs resulting in resistance and relapse (Bao et al., 2006; Diehn and Clarke, 2006; Eyler and Rich, 2008). Although HTS-based technology can be used to uncover drugs that specifically target CSCs, it is a challenging task given the rare occurrence of CSCs within the tumour (Gupta et al., 2009). Assays targeting the bulk population of tumour cells would likely fail in identifying CSC-targeted agents. Hence, existing screening formats should be modified to allow testing against CSCs. Furthermore, assays should include 3-D culture models to enable accurate prediction of the clinical effectiveness of the drugs since 2-D cultures will not mimic the microenvironment of an *in vivo* tumour (Kunz-Schughart et al., 2004). The added usefulness of 3-D cultures lies in their potential to be used in lieu of animal models as described in figure 1.9.

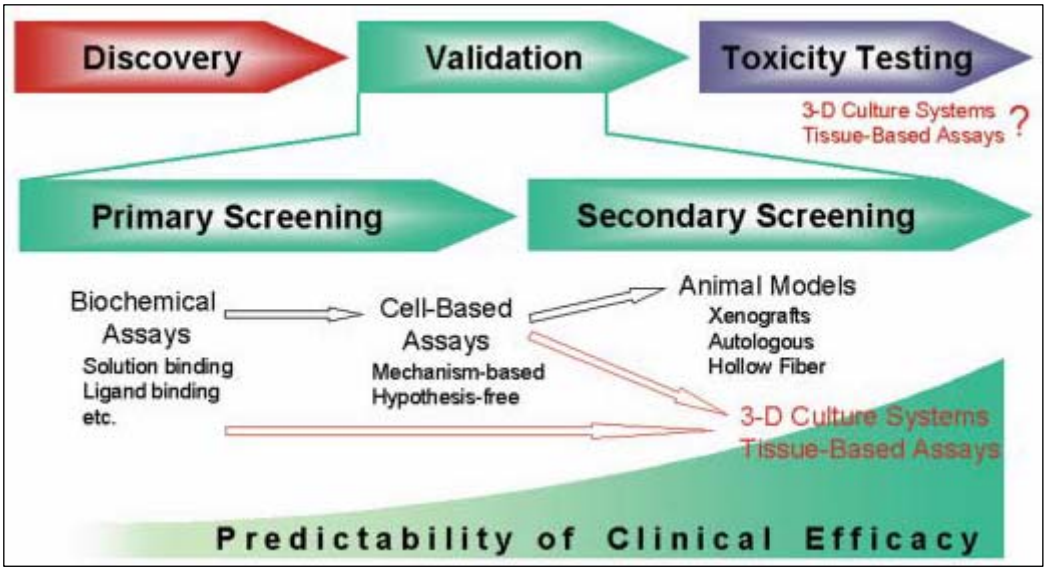

Figure 1.9. Overview of the preclinical validation of antitumor agents.
3-D culture systems could potentially be used to enhance the predictability of clinical efficacy of new candidates and minimise, or replace animal test models. This could significantly result in cost- and time-savings (Kunz-Schughart, 2004).

Recently a HTS assay was used to identify kinase inhibitors as potential treatment for ependymoma, which is a chemoresistant brain tumour (Atkinson et al., 2011). Another study found that GBM can be sensitised to tumour necrosis factor apoptosis-inducing ligand (TRAIL) by using cardiac glycosides (Badr et al., 2011). Similar approaches have been used to identify small molecule inhibitors of Wnt signalling for the treatment of pancreatic cancer (Chen et al., 2010) and agents that specifically target CSCs in breast cancers (Gupta et al., 2009). Besides, HTS-based toxicity assays are invaluable in the assessment of the safety of novel chemical compounds (Breier et al., 2009).

Although significant progress has been made in the areas of cancer biology and the development of novel therapies, results indicate that the efficacy and the specificity of drugs need to be constantly evaluated and approaches modified to enable successful therapy. In this regard, HCS and HTS-based are here to stay as they are an integral component of development of new strategies to combat disease.

1.8. Aims of current work

The *in vitro* propagation of NSCs/NPs occurs through 3-D clusters called neurospheres. However, very little is known about the architecture of the neurosphere. Although the neurosphere is known to be heterogeneous in composition consisting of NSCs, NPs, and differentiated cell types the lack of specific NSC markers makes selection and purification of NSC populations very challenging. This necessitates the identification of markers that exclusively label the NSCs. Methods to study NSC populations and analyse growth, gene expression, and response to drugs are crucial to the identification, development and testing of drugs for diseases such as brain tumours.

Therefore, the three main aims of this thesis are:

i) 3-D architecture of the neurosphere.

ii) Identification and characterization of the NFC.

iii) Development of a HTS assay and its applications in drug screening.

2. MATERIALS AND METHODS

2.1. Isolation of NSCs/NPs and cell culture

NSCs from the forebrain of embryonic (E14) C57BL/6 mice were isolated as described previously with some modifications (Jurvansuu et al., 2008). Pregnant C57BL/6 mice were sacrificed by cervical dislocation and the embryos were aseptically removed and transferred to a Petri dish containing ice-cold Hanks' balanced salt solution. The cerebral cortices were then rapidly excised from the embryos and triturated into a single cell suspension. Dissociated single cells were seeded at a density of 2 x 10^5 cells/mL in 10 cm culture dishes (Nunc) in growth medium (GM) consisting of Dulbecco's Modified Eagle's Medium (DMEM)/nutrient mixture F-12 medium (1:1) (Invitrogen), B27 supplement (Invitrogen), 20 ng/mL EGF (Peprotech), 10 ng/mL bFGF (Peprotech) and 1% penicillin/streptomycin (Invitrogen). Neurospheres were propagated for 5-7 days at 37°C and 5% CO_2 in a humidified incubator. Neurospheres were passaged between days 5-7 by dissociating with 0.05N sodium hydroxide and neutralizing with 0.05N hydrochloric acid (both from Sigma).

2.2. Seeding densities of NSCs/NPs

Single cells were plated at a density of 2 x 10^4 cells/mL (bulk density), or 2 x 10^3 cells/mL (low density) at each passage. For clonal density cultures a seeding density of 100 cells/mL was used. Neurospheres before passage 8 were used for all experiments.

2.3. Freezing NSCs/NPs

Dissociated cells from passage 2 were grown as small neurospheres for two days. On day 2 the neurospheres were collected by centrifugation and resuspended in fresh GM supplemented with 10% DMSO. The resulting cell suspension was then aliquoted into polypropylene cryovials (Nunc). The vials were placed in a freezing chamber (Nalgene) at −80°C overnight followed by transfer to the liquid nitrogen tank for long term storage.

2.4. Single neurosphere differentiation

50-well glass coverslips (Sigma) were coated with 0.01% poly-L-lysine (PLL, Sigma) and 10 μg/mL laminin (Invitrogen) and incubated at 37°C for 2-4 h. This was followed by removal of PLL/laminin by washing three times with phosphate buffered saline (PBS). Cells were plated after the glass was air-dried.

Cells were cultured in differentiation medium consisting of DMEM/F-12 medium (1:1) (Invitrogen), B27 supplement (Invitrogen), 1% penicillin/streptomycin (Invitrogen), and 0.5% foetal bovine serum (Invitrogen) for 7 days with half medium changes every 2 days.

For single neurosphere differentiation, individual neurospheres were transferred under a microscope to a single well of the 50-well chamber filled with differentiation medium. The neurospheres were allowed to settle over night at 37ºC in a humidified CO_2 incubator. In parallel, a master plate using bulk culture neurospheres was prepared. 5 mL of bulk density neurospheres between days 5-7 were plated in a 10 cm culture dish (NUNC) coated with PLL and laminin. This

was topped up with 5 mL of differentiation medium and cells were allowed to differentiate at 37ºC in a humidified CO_2 incubator overnight.

The following day, the 50-well chamber containing the attached single neurospheres was inverted onto the 10 cm master plate allowing the neurospheres to come in contact with the differentiation medium. Differentiating neurospheres from the master plate condition the medium with neurotrophic factors that support differentiation of the individually plated neurospheres, which would otherwise die without the supporting cells or only generate astrocytes.

2.5. Transfection

Transfection was carried out using Amaxa Nucleofector® (Lonza) and Mouse Neural Stem Cell Nucleofector® Kit according to the manufacturer's instructions. Plasma membrane targeted eYFP (eYFP-PMT) was used to label the cell membrane (Chapple et al., 2002). Briefly, neurospheres were passaged and 0.5 x 10^6 single cells were transfected with 2 μg eYFP-PMT plasmid DNA. Transfected cells were allowed to grow and proliferate in GM and the resulting neurospheres were imaged between days 3 and 5.

2.6. Immunocytochemistry

2.6.1. Labelling of live cells

Neurospheres were labelled with 5 μM CellTracker Green CMFDA (Invitrogen) for 15-30 min. SSEA-1 antibody (Stemgent) was used at 1:100 for 30 min. Anti-CD15 antibody conjugated to FITC was used at 1:10 dilution (R&D Systems); anti-C1qR1 conjugated to PE (R&D Systems) was used at 1:10 dilution. Hoechst

33342 (Invitrogen) was used at 2 μg/mL for 15-30 min. Dextran (MW 70,000, Invitrogen) was used at 100 μg/mL for 10 min. The concentration and incubation time for other dyes used are as follows: wheat germ agglutinin (5 μg/mL; 2-5 min; Invitrogen); Vybrant DiI/DiO (5 μL/mL; 5 min; Invitrogen); calcein AM (1:100; 5 min; Invitrogen); di-4-ANEPPDHQ (15 μM; 10-30 min; Invitrogen); FM 1-43 (5 μg/mL, 2-5 min; Invitrogen); SYTO 62/84 (2-5 μg/mL; 30 min; Invitrogen); Draq5 (2 μM, 30 min; Cell Signalling Technology). CDy5 was provided by Young-Tae Chang (Singapore Bioimaging Consortium) and was used at a final concentration of 4 μM by adding the dye to the GM of live single cells. Cells were incubated with the dye for 1 h at 37ºC followed by washing out the dye. Cells were resuspended in fresh GM prior to imaging.

Cells were incubated at 37ºC in a humidified CO_2 incubator for the stipulated time followed by rinsing with PBS or GM. To reduce intracellular and vesicle-like staining of the dyes being tested cells were incubated at 4°C or treated with 1 μM of phenylarsine oxide (PAO) for 15 min prior to the addition of the dyes.

2.6.2. Lineage labelling of differentiated cells

Following differentiation medium was removed and the cells were washed with PBS prior to fixation with 4% PFA (Sigma) for 20 min at room temperature. Cells were blocked with 3% BSA and permeabilised with 0.5% triton-X 100 in PBS and stained individually with the following antibodies: anti-βIII tubulin (1:500; Covance), anti-O4 (1:300; Chemicon) or anti-GFAP (1:1000; Dako). Anti-O4 antibody was added before the permeabilisation step since it is a surface antigen. The secondary antibodies (Invitrogen) used were Alexa Fluor 488 goat anti-mouse

IgM (1:500; O4), Alexa Fluor anti-mouse 594 IgG2a (1:500; βIII tubulin) and Alexa Fluor anti-rabbit 647 (1:500; GFAP). The nucleus was counter stained with 4', 6'-diamidino-2-phenylindole dihydrochloride (DAPI; Invitrogen). Coverslips were mounted with Hydromount (National Diagnostics) and dried prior to imaging.

2.7. Use of hydrogel for immobilisation

Hydrogel (Wang et al., 2010) was kindly provided by Dr. Motoichi Kurisawa (Institute of Bioengineering, Singapore).

2.7.1. Preparation of Gtn-HPA polymer

The polymer was weighed and dissolved in pre-warmed GM. A 2% polymer was used. It was then filtered through a 0.22 μm filter (Millipore). The prepared polymer may be stored at 4°C for up to a week. Since the polymer solidifies at 4°C it was gently warmed at 37°C before use.

2.7.2. Suspending cells in polymer

Neurospheres were suspended in the polymer-GM matrix. To this 1.5 μL/mL of horseradish peroxidase (HRP) was added and vortexed by hand for a few seconds. Then 1.5 μL/mL of 2% hydrogen peroxide (H_2O_2) was added and again vortexed by hand for a few seconds. This was quickly transferred to cell culture plates. The hydrogel was allowed to set for 30 minutes at 37ºC following which it was overlaid with 1-2 mL GM.

2.8. Fluorescence activated cell sorting (FACS)

Neurospheres were dissociated and single cells were resuspended in PBS and blocked with 3% bovine serum albumin (BSA, Sigma) for 15 min at room temperature. Surface antigens were then labelled with fluorescently-conjugated primary antibodies (FITC-CD15 and PE-C1qR1, R&D Systems) for 15-20 min at room temperature. Isotype-matched mouse immunoglobulin served as controls. Cells were washed with PBS and filtered (40 μm filter; BD Biosciences). Cell suspension was diluted to a final concentration of 0.5-2 x 10^6 cells/mL for sorting. Unstained cells were processed in parallel.

Cells were analysed and sorted on a fluorescence activated cell sorter FACSAria (Becton Dickinson) using FACSDiva software (Becton Dickinson). Data was analysed and presented using FlowJo software. Dead cells were excluded by propidium iodide (Sigma) staining. Debris and aggregated cells were excluded based on forward and side scatter of control samples. Gating for fluorescence was set by comparison with control samples. Unsorted live cells with no gating on any marker were used as control.

2.9. Single cell mRNA profiling and data processing

2.9.1. FACS-sorting and cell lysis

For single cell mRNA profiling of CD15+/C1qR1+/Phbrt+ cells, CD15+/C1qR1+ cells were FACS-sorted and allowed to recover at 37°C for at least two hours post-sorting. Single cells were then imaged in phase contrast mode using a 40× lens in the Olympus IX81 inverted motorised microscope and phase intensities were measured. Phbrt (>240 gray values) cells were identified and manually transferred

using a micropipette into PCR tubes. 6 µL of RT-PreAmp Master Mix was added to each cell prior to lysis. Cells were frozen at −80°C and thawed to induce lysis.

2.9.2. Single cell PCR

The RT-PreAmp Master Mix contained 5 µL CellsDirect 2x Reaction Mix (Invitrogen), 2.5 µL 0.2x Assay pool, 0.5 µL SuperScript® III RT/Platinum® *Taq* mix (Invitrogen) and 2 µL TE buffer (Qiagen). cDNAs of the 48 genes were generated by sequence-specific reverse transcription (50°C for 20 minutes), reverse transcriptase inactivation (95°C for 2 minutes) and sequence-specific pre-amplification (18 cycles at 95°C for 15 seconds; 60°C for 4 minutes). The reactions were carried out in a PCR thermal cycler (Biorad). The pre-amplified cDNA was diluted two-fold with nuclease-free water (Promega) and stored at −80°C.

A TaqMan assay pool was prepared by adding each of the 48 TaqMan assays (20×, Applied Biosystems) to a final concentration of 0.2× for each assay. 2.5 µL of each TaqMan assay (20x, Applied Biosystems) was added to 2.5 µL of 2x DA assay loading reagent (Fluidigm). 3.2µl of cDNA with 0.35µl of DA sample loading reagent and 3.5µl of TaqMan® Universal PCR Master Mix (Applied Biosystems) constituted the real-time sample mix. To begin the real-time PCR, control line fluid (Fluidigm) was introduced into the BioMark™ 48.48 dynamic array (Fluidigm) and primed in the integrated fluidic circuit controller (Fluidigm). 5 µL each of the real-time assay and sample mix was added into the array wells followed by loading into the reaction chambers using the integrated fluidic circuit

controller. The array was then transferred to the BioMark™ System (Fluidigm) and real-time PCR was performed.

Real-time PCR consisted of the following steps, i) amplification erase phase at 50°C for 2 minutes, ii) hot start phase at 95°C for 10 minutes to activate *Taq* polymerase, iii) cDNA denaturation at 95°C for 15 seconds followed by iv) annealing at 60°C for 1 minute. Denaturation and annealing were repeated for 40 cycles and Ct values were collected using the BioMark™ data collection software (Fluidigm) and exported to Microsoft Excel. Ct values between 9-16 for the endogenous control β-actin were considered. Ct values for a specific cell were normalised to the endogenous control by subtracting the Ct value of β-actin for that cell.

2.10. 3-D imaging of neurospheres

2.10.1. LSCM

3-D images of neurospheres were acquired using the Olympus FV1000 LSCM. Olympus Plan-Apochromat 60× water lens was used for 3-D imaging to reduce spherical aberration and minimize photobleaching. eYFP-PMT signal was imaged using the 488 nm laser and Hoechst 33342 was imaged using LD405 nm laser. Images were acquired with a XY resolution of 320 x 320 pixels and Z-slices were acquired every 0.2 μm. Appropriate laser power, gain and offset were used to maximise signal to noise ratio. To eliminate crosstalk, images were acquired in Sequential mode and emission bands were set at 505-550 nm for the eYFP-PMT and 420-460 nm for Hoechst33342. Similar conditions were applied to imaging performed on the Yokogawa CSU22 Spinning Disk Confocal attached to an

Olympus IX81 inverted microscope. Similar images were taken from a Zeiss confocal LSM 510 microscope. Labelled neurosphere samples were embedded in 2% hydrogel prior to imaging.

2.10.2. SDC microscope

3-D images of neurospheres were acquired using the Yokogawa CSU 22 spinning disk confocal microscope attached to an Olympus IX 81 microscope and a Photometrics QuantEM 512x512 EMCCD camera was used for detecting fluorescence emission signals. Olympus Plan-Apochromat 60× water lens was used for 3-D imaging to reduce spherical aberration and minimize photobleaching. An ASI XYZ piezo stage was used for high speed 3-D imaging. eYFP-PMT signal was imaged using the 488 nm laser from an Argon Krypton laser. Appropriate emission filters from Chroma were used for fluorescence imaging.

2.10.3. DSLM

2.10.3.1. Sample preparation

Neurospheres between days 5-7 were labelled with 2 µg/mL Hoechst 33342 to mark the nuclei. They were then centrifuged and the GM was discarded. Neurospheres were resuspended in 0.5-1 mL of 1% LMP agarose in a 1.5 mL Eppendorf tube. A glass capillary tube was inserted into the Eppendorf tube until it was filled half-way with the sample. At the time of imaging, a dissecting needle was used to push the agarose plug 1-2 mm out of the capillary tube to facilitate imaging.

2.10.3.2. Acquisition parameters

Images were acquired with a 63×/1.2NA water lens.

2.11. EGVD

EGVD as described in Yu et al (2010) was applied in 3-D. Briefly, phase congruency for edge detection was utilised to reveal edges irrespective of fluorescence intensity, following which seed detection and segmentation were carried out as reported.

2.12. Time-lapse imaging

Cells were imaged on a Zeiss Axiovert 200M or Olympus IX81 inverted motorized microscope. The system was fitted with a fully enclosed Pecon XL3 incubator to ensure focus stability. Pecon heating insert P was used to provide the cells with 37°C, 5% CO_2 and required level of humidification. An X-Cite 120 liquid light guided metal halide lamp provided fluorescence illumination. Appropriate bandpass fluorescence filters from Chroma were used for fluorescence imaging. A 40× phase lens was used to image cells in phase contrast mode. Marzhauser motorized XY stage and a CoolSnap HQ CCD camera was used for multi-point visiting and imaging respectively. The instrument was driven by Metamorph's multi-dimensional acquisition (MDA) feature. In most cases imaging was done at 2x2 binning to maximize signal-to-noise and to use low level of illumination to prolong cell survivability. To maximize the amount of data collected, multiple cells in the dish were identified, marked and revisited every 30 minutes or 4 hours over several days using the MDA feature in Metamorph. The data was reconstructed into Metamorph time-lapse stacks at the end of the experiment.

Cells were either seeded at clonal density in a 3 cm glass-bottom Mattek dish (Mattek Corporation) or in a plastic 96 well plate (Nunc).

2.13. Imaging of single cells and measurement of phase intensity

Cells were imaged with a 40× phase lens in phase contrast mode. The coordinates (*x*, *y*, *z*) for each cell were manually registered using the MDA feature of Metamorph. The focal plane where the cell membrane was apparent as a dark continuous circle was determined as the optimal *z* for each cell. Images were acquired at 2x2 binning. Subsequently images were analysed using Metamorph.

The phase contrast mode imparts a bright halo around the circumference of each cell. The intensity of this halo was measured and is referred to as phase intensity. Briefly, a circular region of interest was traced around each cell using the tools in Metamorph. A second region placed away from the cell was used as the background intensity. The phase intensity of each cell was thus calculated as the difference between the intensities of the cell and the background. The values were exported to Microsoft Excel.

2.14. Measurement of single cell size

Cells were plated under clonal conditions and imaged at the single cell stage followed by time-lapse imaging to determine neurosphere formation. Size of single cells was manually measured using Metamorph from images at t= 0 and reported in μm.

2.15. Time-point analysis of NSCs/NPs expressing eYFP-PMT

NSCs/NPs were nucleofected with 2 μg eYFP-PMT DNA and plated under clonal conditions. Five different samples were prepared to allow for imaging from days 1-5.

2.16. Drug treatment

Details of the drugs tested are as follows: ifenprodil tartarate, clozapine, paliperidone, ziprasidone hydrochloride, biperiden hydrochloride, fluoxetine (Prozac), imipramine, desipramine, temozolomide and L-3,4-dihdroxyphenylalanine methyl ester (all from Sigma). The drugs were solubilised in solvents recommended by the manufacturer, and added to the GM of cells immediately after passaging and cells were allowed to proliferate for 5-7 days. Cells from *Sox2*-GFP mice where GFP reports the promoter activity of *Sox2* were used for the HTS assay.

The potency of compounds was quantified by generating dose-response curves for cells plated at 1000 cells/mL. Starting from initial concentrations between 1nM to 300 μM, each compound was titrated across a series of ten half-log/log dilutions. Curve fitting was performed with GraphPad Prism software (GraphPad Software, Inc.).

2.17. HTS assay

Cells were plated at low or bulk density in a 96-well plate cultured for 5-7 days to form neurospheres. They were then imaged on Zeiss Axiovert 200M or Olympus IX81 inverted motorized microscope with a 4× lens. The Screen acquisition feature

in Metamorph software was used to image 15 regions per well and all the wells in the 96 well plate. Following imaging, neurosphere numbers, sizes, and GFP fluorescence were automatically determined using custom designed post-processing analysis tool attached to Metamorph.

The acquisition and analysis of the Screen acquisition features works like this: first, the coordinates of the borders of the first well (A1) were registered by using the feature, Set A1 centre. This was followed by specifying 15 regions per well to allow the entire well to be completely imaged. Then the *z* position for the plate was set by taking a sample image of well A1 followed by image acquisition in fluorescence mode of the entire 96 well plate.

Following imaging a custom designed Metamorph Journal was designed to stitch regions of individual wells together to generate a global image of each well. This was followed by segmentation of the neurospheres in wells using the fluorescence markers used to label the cells. Suitable filters for segmentation such as neurosphere size (30-200 μm) and object roundness (0.8-1) were included. Results of segmentation were designed to include neurosphere numbers, sizes, and GFP intensity and the data was exported and saved as Microsoft Excel worksheets. Data analysis to determine differences between control and drug treatments was then manually performed.

2.18. Statistical analysis

Statistical comparison of data was performed by using two-tailed paired Student's t test.

3. RESULTS

3.1. Imaging of live neurospheres in 3-D

The neurosphere is a naturally occurring 3-D cluster hence it is important to retain its structure if one is to derive meaningful information from it. To elucidate the 3-D architecture of the neurosphere I tested various dyes and imaging modalities on live neurospheres. This was done in an attempt to determine suitable labelling and imaging (widefield or confocal imaging modality) protocols and associated trouble-prone steps, if any. Neurospheres can be cultured in liquid medium, or embedded in matrices which support growth and proliferation such as Matrigel, collagen, and alginate- and gelatin-based hydrogels. In this work neurosphere samples were labelled with dyes and immobilised in a gelatin hydroxylphenylpropionic acid (Gtn-HPA) hydrogel (Wang et al., 2010) prior to imaging.

3.1.1. Comparison of microscopes for 3-D neurosphere imaging

To determine the optimal imaging system for 3-D imaging of neurospheres, three systems were compared: Zeiss LSM 510, Olympus FV1000, and Yokogawa CSU 22 spinning disk attached to an Olympus IX 81 microscope. Neurospheres can range in size from 50-100 μm or more. Day 5 neurospheres were labelled with Cell Tracker Green CMFDA or neurospheres from Actin-GFP transgenic mice were imaged on the three systems (figure 2.1A and B). In images obtained from the Olympus FV1000 LSCM individual cell contours were clearly visible. Hence, all subsequent 3-D imaging was performed on this system.

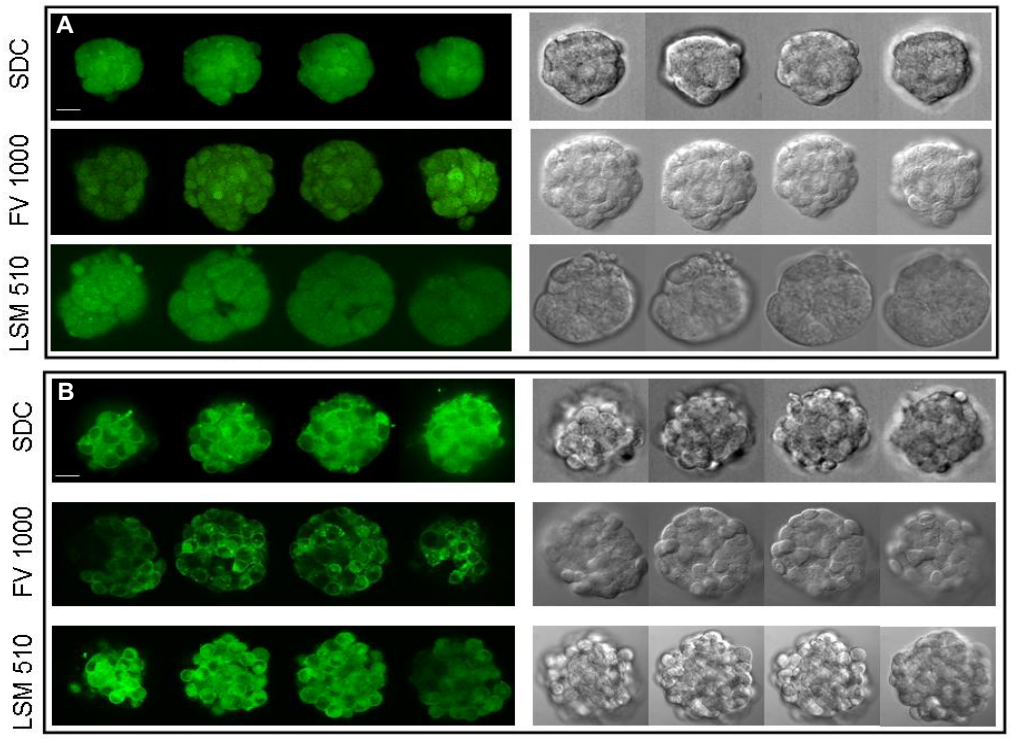

Figure 2.1. Comparison of imaging modalities for 3-D imaging of neurospheres. Day 5 neurospheres labelled with Cell Tracker Green CMFDA (A) or obtained from Actin-GFP transgenic mice were imaged on the spinning disk confocal (SDC), Olympus FV1000, and Zeiss LSM 510 confocal microscopes. DIC images are on the right panel. Single slices from 3-D stacks are shown. Images were acquired with 60×/1.2 NA water lens. Scale bar, 20 µm.

To enable segmentation of 3-D neurosphere images dyes to label the cell centre (nucleus) and edge (plasma membrane) were used. Hoechst 33342 was used for nuclear labelling of neurospheres. The plasma membrane-targeting domain (N-terminal Met-Gly-Cys-X-Phe-Ser-Lys motif) derived from the retinitis pigmentosa protein (RP2) (Chapple et al., 2002) tagged with YFP was found to be the best label for the plasma membrane of NSCs/NPs. Figure 2.2 shows an example of a neurosphere expressing eYFP-PMT imaged on the LSCM.

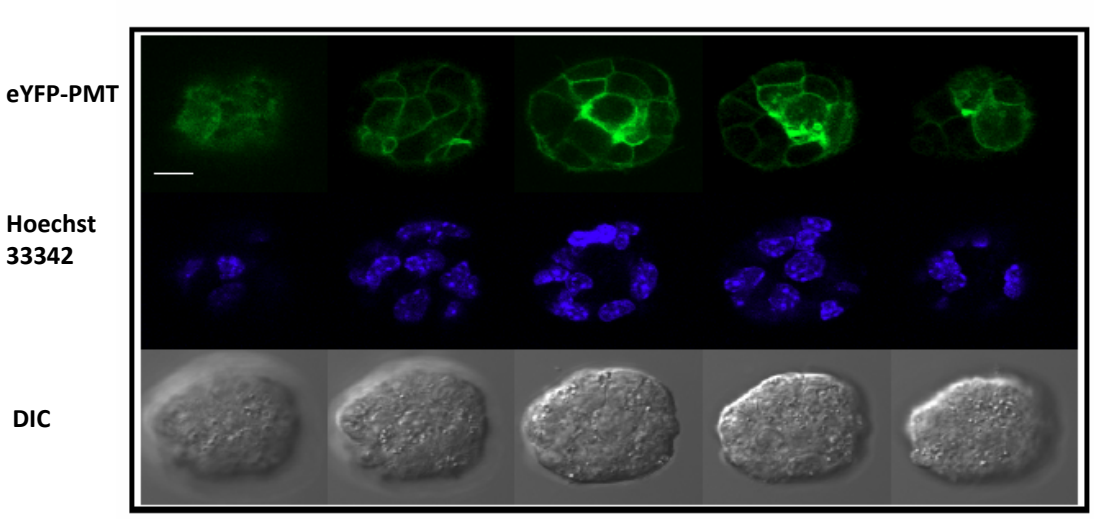

Figure 2.2. Imaging of cellular structures in neurospheres with a laser scanning confocal microscope (LSCM).
NSCs/NPs were transfected with eYFP-PMT and allowed to grow for five days. On day 5 neurospheres were labelled with Hoechst 33342. Single slices from 3-D stacks are shown. Images were acquired with a 60×/1.2 NA water lens on the Olympus FV1000 confocal microscope. Scale bar, 10 µm.

3-D neurosphere images were also generated on the DSLM (Keller et al., 2008). Neurospheres labelled with Hoechst 33342 (figure 2.3A, B) or Cytrak (figure 2.3C, D) to mark the nuclei and imaged on the DSLM. A raw image (figure 2.3A) and a deconvolved image stack (figure 2.3B) of a Hoechst 33342-labelled neurosphere are shown. The larger Cytrak-labelled neurosphere (figure 2.3C) was segmented and reconstructed (figure 2.3D) by the method described in (Khairy et al., 2008).

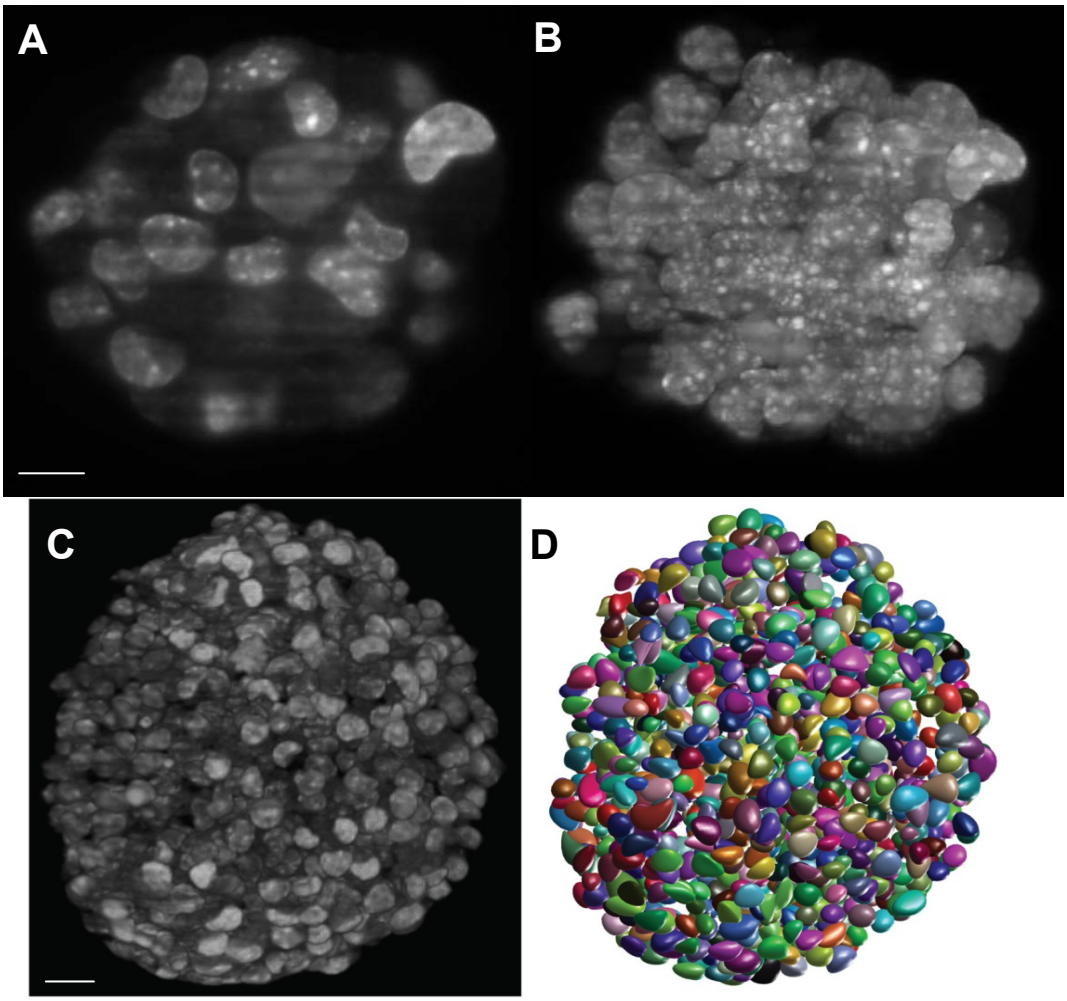

Figure 2.3. 3-D neurosphere imaging on the digital scanned laser light sheet microscope (DSLM).
Day 5 neurospheres were labelled with Hoechst 33342 and imaged with a 63×/1.0 NA objective lens. A single plane of the raw image (A, scale bar, 10 µm) and XY projection of deconvolved image stack (B) are shown. Neurosphere labelled with CyTRAK (C, Scale bar, 20 µm). A single plane from the reconstructed neurosphere structure generated by the segmentation algorithm described in Khairy, 2008 (D).

3.1.2. Dyes used to label intracellular structures

3.1.2.1. Membrane and cytoplasmic dyes

Table 1 summarises the results from testing various membrane markers for 3-D neurosphere imaging. This included commonly used membrane labelling dyes such as FM1-43, wheat germ agglutinin, Vybrant Di, di-4-ANEPPDHQ, and cytoplasmic dyes such as calcein and CellTracker Green CMFDA. Among the

dyes tested on neurospheres, with the exception of CellTracker Green CMFDA I found that all the membrane dyes resulted in the labelling of cytoplasm and vesicle-like structures within minutes of addition. Some of the dyes produced weak membrane labelling (Table 1). In addition, the dyes were highly sensitive to bleaching (Table 1).

To test if labelling of vesicle-like structures was a result of endocytosis, cells were either incubated with the dyes at 4ºC or treated with phenylarsineoxide (PAO) prior to the addition of dye to delay or inhibit endocytosis. However, neither treatment resulted in clear membrane labelling and the appearance of vesicle-like structures persisted (data not shown). It is unclear what causes the membrane dyes to label intracellular structures in neurospheres but it does not appear to be a result of rapid endocytosis. Hence, to generate clear labelling of the plasma membrane for 3-D neurosphere imaging, I have used eYFP-PMT (figure 2.2).

3.1.2.2. Nuclear dyes

SYTO62/84, Draq5, and Hoechst 33342 were the nuclear dyes tested for 3-D imaging (table 1). The former two were extremely sensitive to bleaching and were completely bleached before a *z* stack could be fully captured. Hoechst 33342 on the other hand was very stable against bleaching and was used with eYFP-PMT for high resolution 3-D imaging of neurospheres.

Membrane and cytoplasmic dyes

Dye	Labels	Vesicle formation	Sensitivity to bleaching	Image
Cell tracker green	Cytoplasm	No	Stable	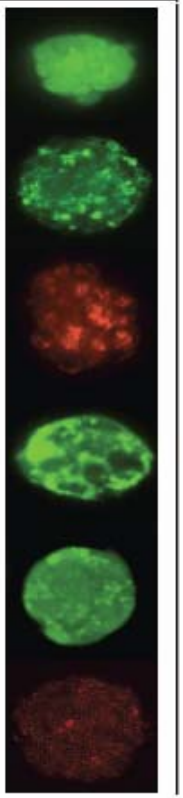
FM1-43	Membrane (vesicles)	Rapid	Stable	
Wheat Germ Agglutinin	Membrane (vesicles)	Rapid	Very sensitive	
Vybrant DiI/ DiO	Membrane (vesicles)	Rapid	Stable	
Calcein	Cytoplasm	Yes	Very sensitive	
di-4-ANEPPDHQ	Weak cytoplasmic staining	Yes	Very sensitive	

Nuclear dyes

Dye	Bleaching	Live imaging
SYTO62/ 84	Very sensitive	Unsuitable
Draq5	Sensitive	Unsuitable
Hoechst 33342	Stable	Suitable

Table 1. Summary of dyes used to label neurospheres.
The dyes that were tested for membrane and cytoplasmic labelling (left) and nuclear labelling (right) are shown

3.2. Quantitative measurements of neurosphere features

Once neurospheres were imaged in 3-D an essential step to deriving quantitative measurements from the 3-D images required segmenting individual cells within a neurosphere. This was a challenging task given the close proximity of the cells constituting a neurosphere. For instance, the number of cells per neurosphere was first estimated by manual enumeration as shown in figure 3.1. Neurospheres labelled with eYFP-PMT and Hoechst 33342 (figure 3.1A) were imaged once as a 3-D stack. 3-D images were then analysed manually by tracing a grid on the 3-D image stack (figure 3.1B) using Olympus Fluoview software. Then individual cells were counted slice-by-slice by using the membrane and nuclear labels. The disadvantages of this approach are that it is tedious and intensity measurements cannot be quantified. Moreover, relying on membrane and nuclear labels to qualitatively delineate boundaries in 3-D image stacks can be inaccurate.

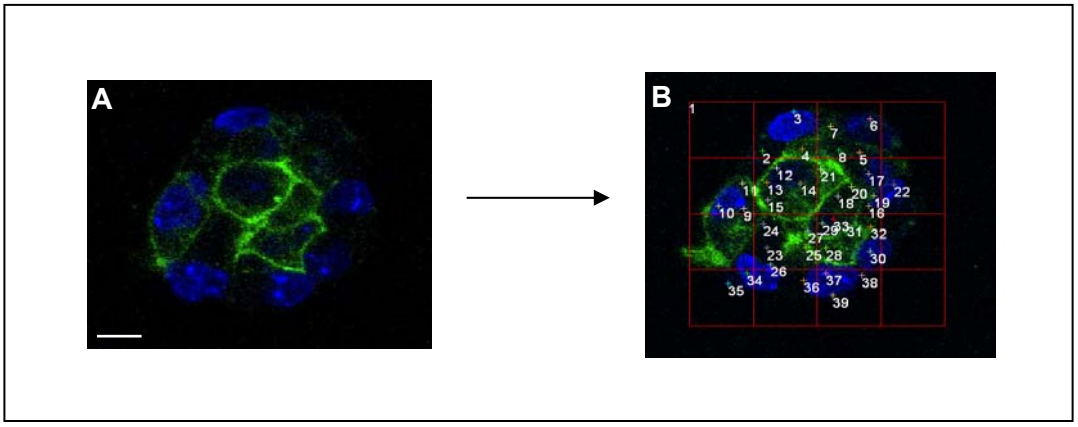

Figure 3.1. Enumeration of cell number by manual counting.
3-D images of neurospheres labelled with eYFP-PMT and Hoechst 33342 were analysed manually. A slice of a 3-D stack is shown in (A). Using Olympus Fluoview image processing tools a grid was traced on the 3-D image stack (B) and cells were manually enumerated as indicated by the numbers in the grid. Scale bar, 10 µm.

Hence, there was a need for automated segmentation algorithms with high accuracies that did not result in under- or over-segmentation. A novel algorithm called EGVD (Yu et al., 2010) adapted to 3-D was applied to segment individual cells within 3-D neurosphere images.

3.2.1. EGVD

As discussed in section 1.6.1 EGVD works in the following manner (figure 3.2): seed finding is performed by using the nuclear label followed by nuclear segmentation. The membrane label enables segmentation of cells; an outer loop for level set evolution and an inner loop for EGVD prevents splitting and merging of objects. Use of an edge detector referred to as phase congruency aids in detection and segmentation of the non-uniform membrane signal.

The use of eYFP-PMT and Hoechst 33342 to label the membrane and nuclei allowed segmentation by EGVD and extraction of several neurosphere features were extracted. These include cell number per neurosphere, cell and nuclear volumes, sphericity, ECS, and the positional impact of these parameters.

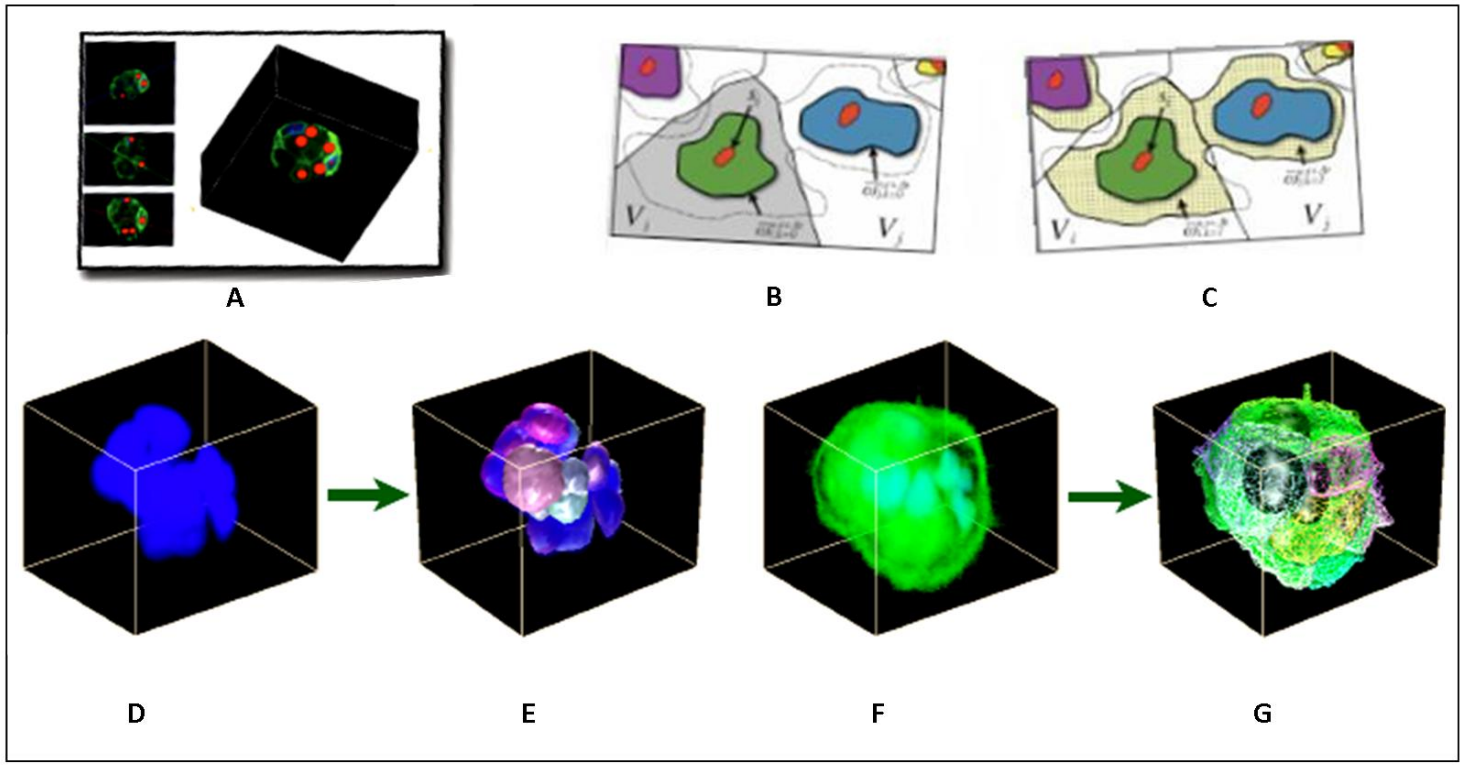

Figure 3.2. Segmentation of 3-D images using Evolving Generalized Voronoi Diagram (EGVD).
Segmentation by EGVD begins with seed finding (A, red dots represent seeds) followed by EGVD in 2-D (B, C, outer loop for level set evolution and inner loop for EGVD prevents splitting and merging of objects) resulting in segmented nuclei (D, E) and cells (F, G). This work was carried out in collaboration with Weimiao Yu (Institute of Molecular Biology) and Hwee Kuan Lee (Bioinformatics Institute).

3.2.2. Estimation of cell number

Segmentation by EGVD allowed estimation of cell number per neurosphere based on days of growth (figure 3.3A) and neurosphere diameter (figure 3.3A). I found that under low cell density conditions, cell number within a neurosphere increased exponentially with time (figure 3.3A). When cell number was plotted again neurosphere diameter, a similar exponential curve was observed (figure 3.3A, inset A). Cells propagated under bulk conditions also showed an exponential growth curve (figure 3.3B). From these growth curves, I was able to estimate the doubling time of NSCs/NPs to be 24 h.

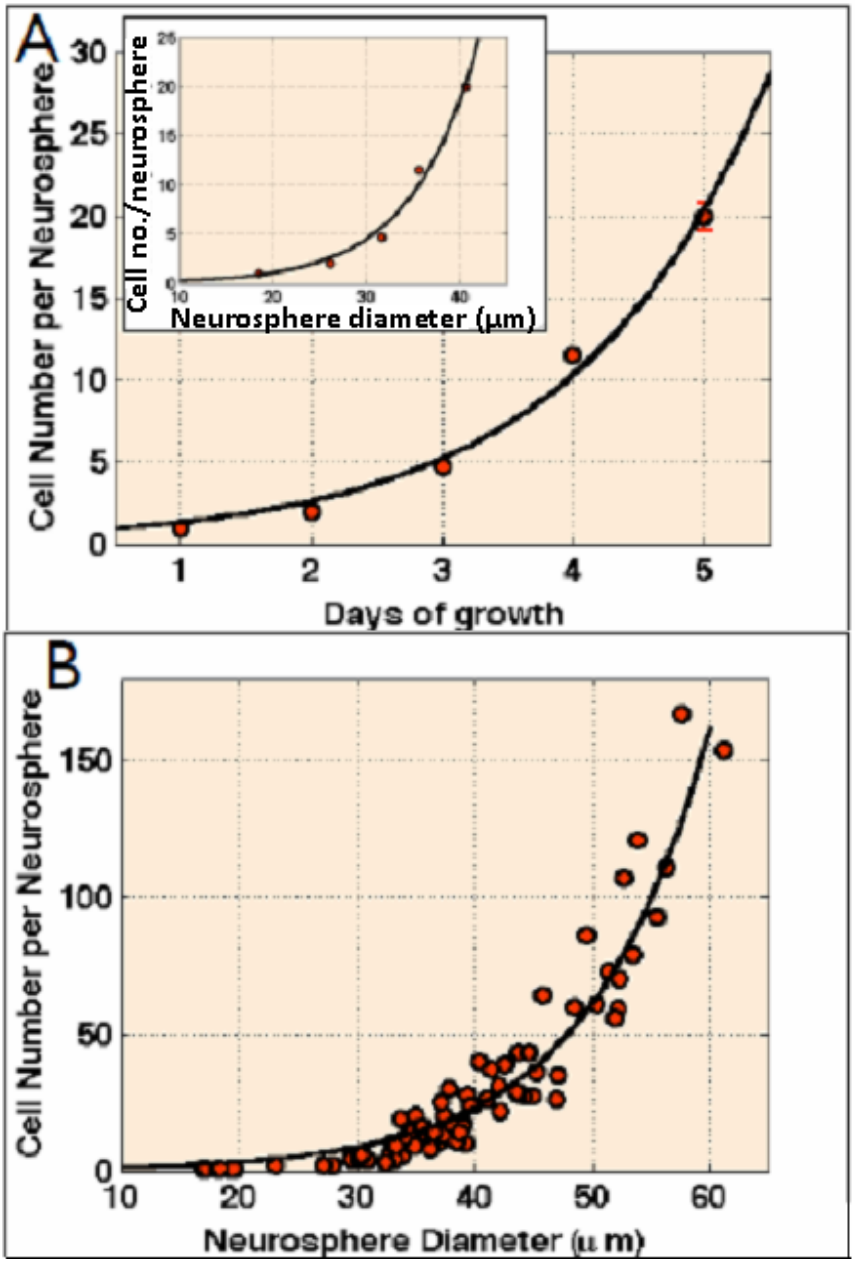

Figure 3.3. Estimation of cell number by EGVD.
Segmentation by EGVD yielded cell number which increases exponentially with days of growth (A) and increasing neurosphere diameter (B). (A) Under low density culture conditions (n= 47), cell number increases exponentially with days of growth and the growth curve is obtained from y = 0.6767 × e0.6809x. Cell number in low density also shows an exponential increase with increasing neurosphere diameter (A, inset) and the function describing this correlation is given by y = 0.06597 × e0.1411x. (B) Cell number increases exponentially with neurosphere diameter. This is represented by the equation y = 0.4725 × e0.0972x for neurospheres from low and bulk (n= 88) densities. Numbers represent mean of several neurospheres. Curve fitting was done by using the minimum mean square error method.

3.2.3. Cell, nuclear volumes and cell number

The cell number per neurosphere was enumerated and nuclear and cellular volumes were calculated for individual cells within the neurosphere. As shown in figure 3.4A, both cell (green curve) and nuclear volume (blue curve) decreased with increasing cell number per neurosphere. Once the neurosphere reached a certain cell number threshold (20-30 cells, figure 3.4A), the values for nuclear and cell volumes remained constant; these values were 2-4 times lesser than at the beginning of neurosphere formation.

3.2.4. Nuclear/cell volume ratio and cell number

The nuclear/cell volume ratio is an indicator of the relative size of the two components. Individual nuclear and cell volumes were computed and the ratio was plotted against cell number per neurosphere (figure 3.4B). There was an initial steep increase in the nuclear/cell volume ratio in a growing neurosphere under both low and bulk density conditions. In bulk density cultures as the neurospheres grew bigger (figure 3.4B, red curve), the nuclear/cell volume ratio reached a plateau. Data for the low density culture conditions was recorded only up to day 5 when neurospheres were <50 cells. Thus only a steep curve was observed (figure 3.4B, blue curve).

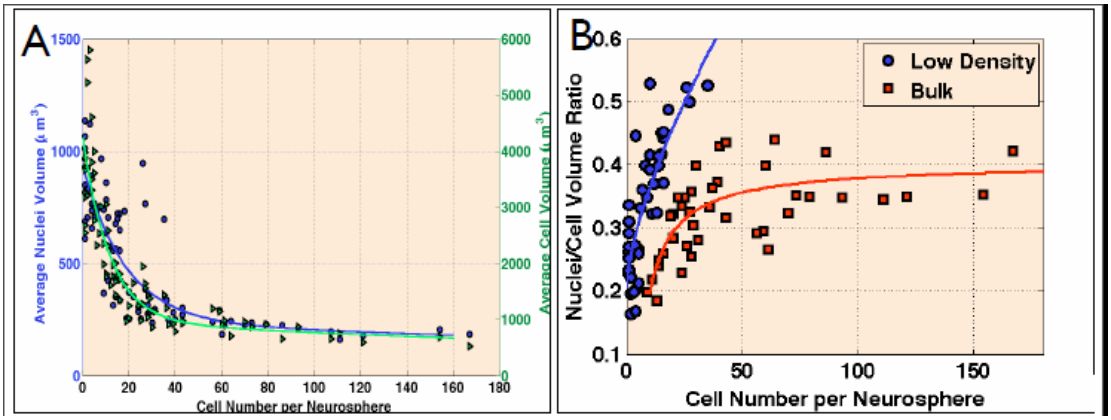

Figure 3.4. Estimation of cellular and nuclear volumes by EGVD.
(A) Average cell (green) and nuclear (blue) volumes decrease 2-4 times before reaching a plateau. Values for volume are derived from the equations $y = 694.8 \times e(-0.0546x)+241.0 \times e(-0.00182x)$ for the nuclear volume, and $y = 3271.0 \times e(-0.0858x)+964.3 \times e(-0.00229x)$ for the cell volume. (B) Change of nuclear-to-cell volume ratio under low (blue curve, $y = -1.66 \times x^{-0.9019x} +0.405$) and bulk density (red curve, $y = -0.0328 \times x^{-0.6803x} +0.2062$) culture conditions. Data for the low density condition was only collected for up to day 5 and hence only a steep curve was observed.

3.2.5. Sphericity

Sphericity is an indicator of shape and can be expressed as a ratio between the surface area of a sphere of the same volume as the given object to the actual surface area of the object. For example, a sphere has sphericity (S) = 1. Lower sphericity indicates that an object has relatively bigger surface per unit volume. Figure 3.5 illustrates the relationship between cell and nuclear sphericity with increasing cell number. When the cell number per neurosphere was less than 20 a higher variation in cell and nuclear sphericity was observed. As the neurosphere grew bigger than 20 cells, both nuclear and cell sphericity stabilised at a constant value. Nuclear sphericity was in the range of 0.8-1 while cell sphericity was 0.6 suggesting that the nuclei retain their sphericity in a growing neurosphere while cells appear to have relatively more surface and are not as spherical.

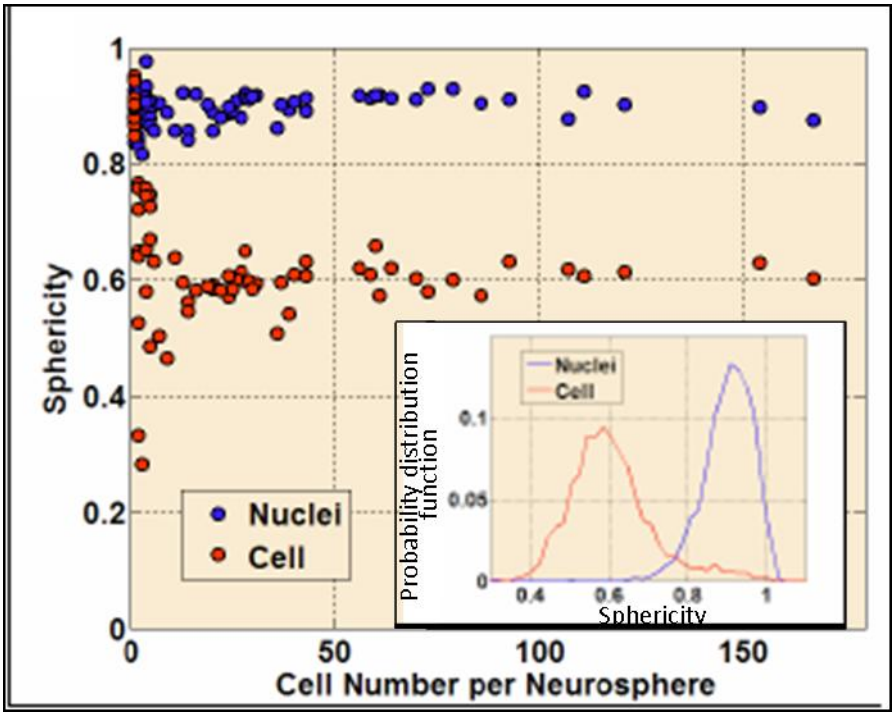

Figure 3.5. Changes in sphericity relative to size of the neurosphere.
Nuclear (blue dots) and cell (red dots) sphericity show low variability when cell number >20 regardless of exponential increase in cell number. Inset shows the distribution of the nuclear (blue curve) and cell (red curve) sphericity of all analysed cells.

3.2.6. Positional information

Spatial mapping of cells is made possible by 3-D imaging. The position of a cell is defined as the Euclidean distance between the centres of the cell and neurosphere (figure 3.6, inset and B). The question I wanted to address was whether a cell's position is in any way related to its structural features as defined by its nuclear/cell volume ratio and sphericity. Figure 3.6 shows that within a neurosphere the nuclear/cell volume ratio and sphericity are related to the position of a cell. In general, lower the nuclear/cell volume ratio the closer is the cell to the neurosphere-centre as shown in the region highlighted by blue in figure 3.6A. Cells with higher nuclei-to-cell volume ratio on the other hand are more likely to be located at the periphery of the neurosphere (represented by yellow and red

dots). Also, cells with lower sphericity values (blue highlighted region) are more likely to be located closer to the neurosphere-centre suggesting that cells in the centre of the neurosphere are possibly more compact compared to those at the periphery.

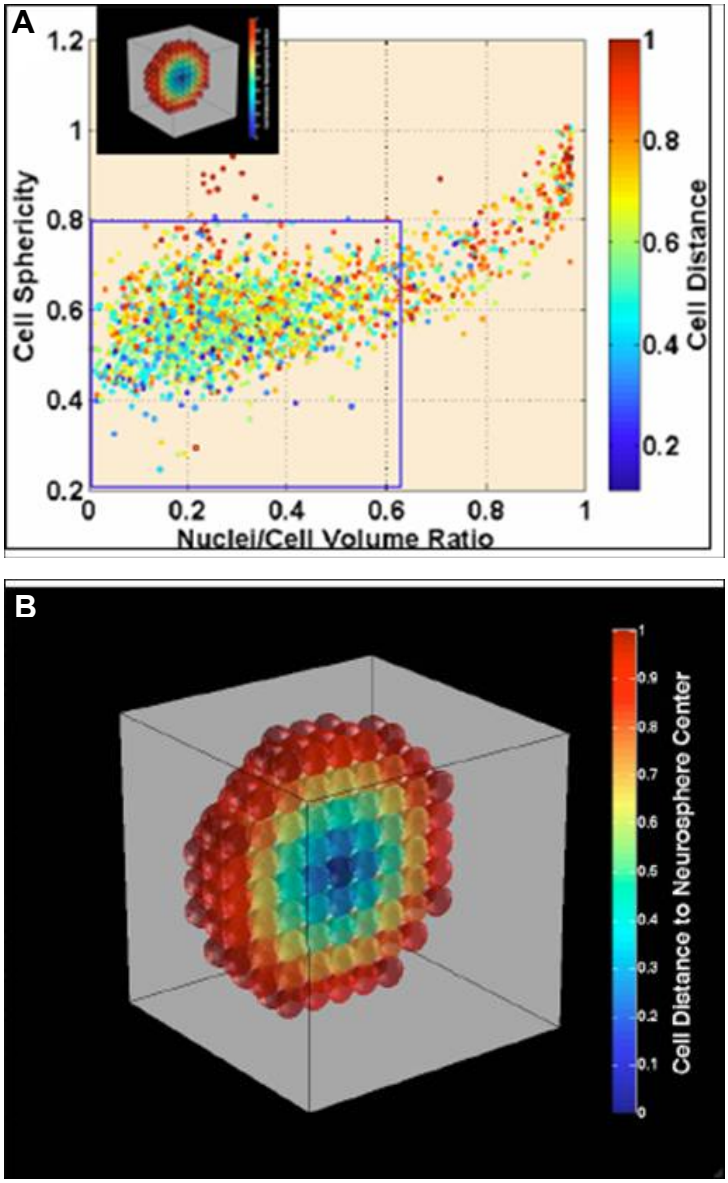

Figure 3.6. Positional information of cells.
The cell distance to neurosphere center (inset, B) is defined by the Euclidean distance between the cell and neurosphere geometric center. This measurement is then normalized from 0 to 1.0 for each neurosphere. This positional information relating to cell distance and sphericity is colour coded (inset) with red representing the outer cell layer and blue the central cell layer.

3.2.7. ECS and neurosphere volume

To estimate the amount of ECS a neurosphere contains I have used high molecular weight dextran as a marker of the ECS (figure 3.7). Dextran being cell-impermeable will occupy the space between cells while being excluded from the cell interior. Cells expressing eYFP-PMT were labelled with Hoechst 33342 and dextran and imaged in 3-D. From preliminary quantitative analysis the ECS was estimated to occupy 1% of the total neurosphere volume. Image of a reconstructed neurosphere labelled with eYFP-PMT and dextran are shown in figure 3.7A with an example of a reconstructed image of a neurosphere with ECS shown in four different angles in figure 3.7B.

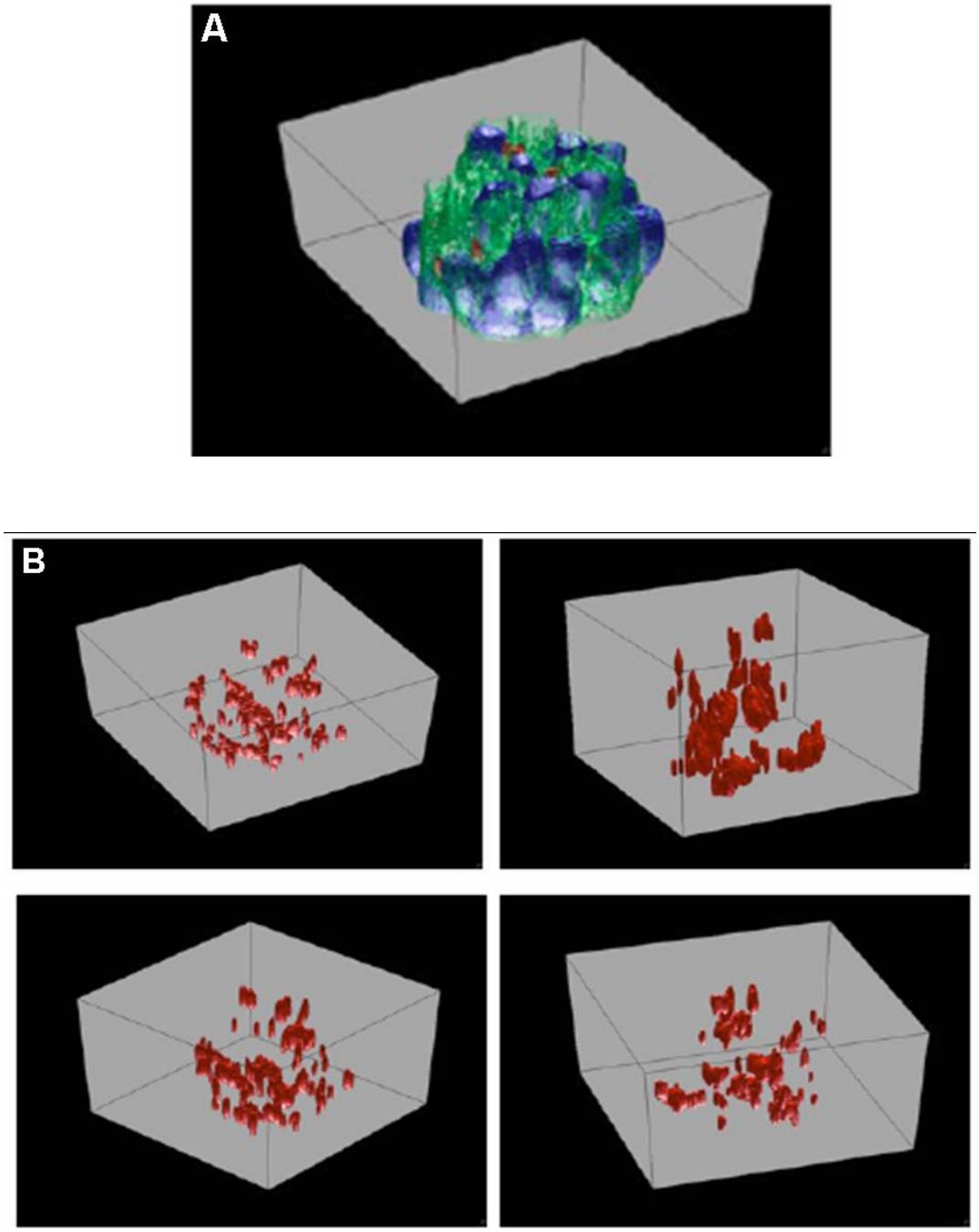

Figure 3.7. Extracellular space (ECS) within neurospheres.
(A) The reconstructed neurosphere is represented by nuclei in blue and cell surface in green. The ECS is labeled by dextran shown in red. (B) Visualisation of ECS from four difference angles shows the 3-D distribution of ECS within the neurosphere.

Elucidation of the 3-D architecture of the neurosphere was hence made possible with EGVD-based segmentation.

3.3. Identification and characterisation of the NFC

Neurospheres are a heterogeneous mix of NSCs, NPs and differentiated cells. Currently many of the NSC markers also label NPs *in vitro* necessitating efforts to identify novel markers and selection methods to distinguish between the two populations. Both NSCs and NPs could be NFCs and can be distinguished from each other by means of their multipotency. While NSCs can give rise to all the three lineages namely astrocytes, neurons and oligodendrocytes, NPs are either uni- or bi-potent. The clonal multipotency assay is a direct test of potency- presence of all three lineages indicates that they were derived from an NSC whereas cell populations that consist of astrocytes alone (unipotent), or astrocytes and neurons (bipotent) for instance, are derived from a bipotent NP.

I have used a combination of time-lapse analysis, investigation of single cell features, mode of cell division, and single cell PCR (scPCR) to characterise the NFCs. To do this, optimisation of methods to track suspension cells over time and enrich for NFCs was first required.

3.3.1. Online 3-D tracking of neurosphere formation

To directly correlate features of single cells such as size, motility, and dynamics with neurosphere formation and potency in real time, it is necessary to investigate neurosphere formation from the single cell stage. In a typical time-lapse experiment NSCs/NPs cells are imaged every few hours for 5-7 days. Such an analysis requires that cells remain within the field of view for the duration of imaging. NSC/NPs are grown as suspension cultures and cells are highly motile under these conditions. I found that NSCs/NPs frequently leave the field of view

mostly within hours of acquisition of the first image (figure 4.1A). In the absence of tracking algorithms, this can cause a potential loss of data since the total number of cells being analysed is reduced. Moreover, not all cells form neurospheres. Hence, there was a clear need to develop an automated tracking algorithm that can track, register the position, and re-align cells through the duration of the time-course experiment.

A novel online tracking algorithm was hence developed for time-lapse image acquisition using phase-contrast microscopy (Huang et al., 2012). The design of the algorithm includes the following components: the cell localiser, controller, and the microscope, camera, and motorised stage. The flow of the cell tracking procedure is shown in figure 4.1C. Registration of cell position and image acquisition is carried out using the MDA feature of Metamorph. First the cell localiser identifies individual cells and provides their positions and snapshots. Next, using the information provided by the cell localiser the controller automatically controls the microscope, camera and stage, which is a typical set-up that is used for image acquisition. These three components work in tandem to update the positions of the tracked cells at each acquisition.

Figure 4.1D shows the design of the tracking algorithm. The microscope, digital camera, and motorised stage constitute the hardware. Images from the microscope feed into a database that manages the information produced by the system. The tracking system is composed of four functions namely, object detection, feature extraction, object position retrieval, and position refinement. Object detection provides the location of all objects in the given image. The features of the detected

objects are provided by feature extraction. Based on the extracted features the object position retrieval identifies and updates the positions of the objects of interests. Finally, fine-tuning of the positions of the objects is carried out by position refinement if necessary. Thus information related to the tracked cells during the entire course of time-lapse image acquisition can be recorded for further analysis.

When tested on NSCs/NPs the algorithm was found to successfully retain cells within the field of view for the duration of imaging (figure 4.1B).

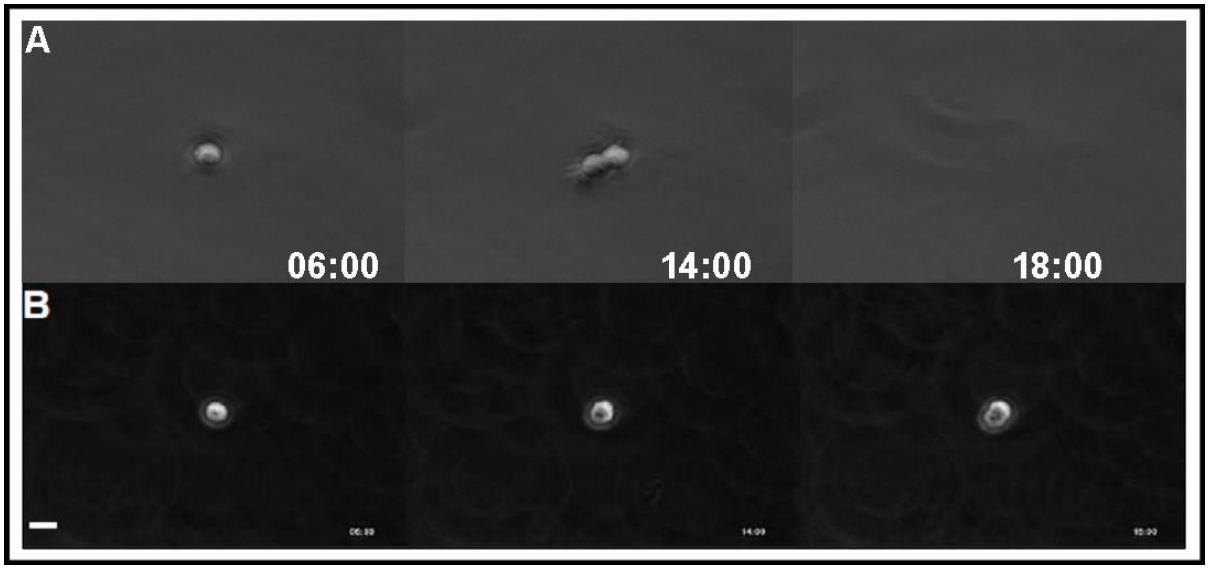

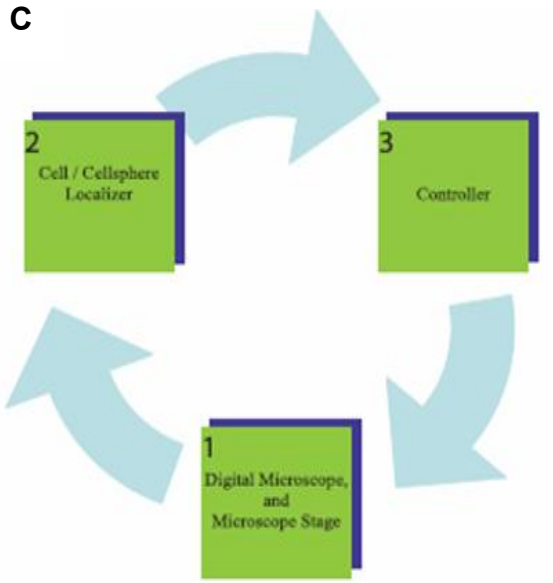

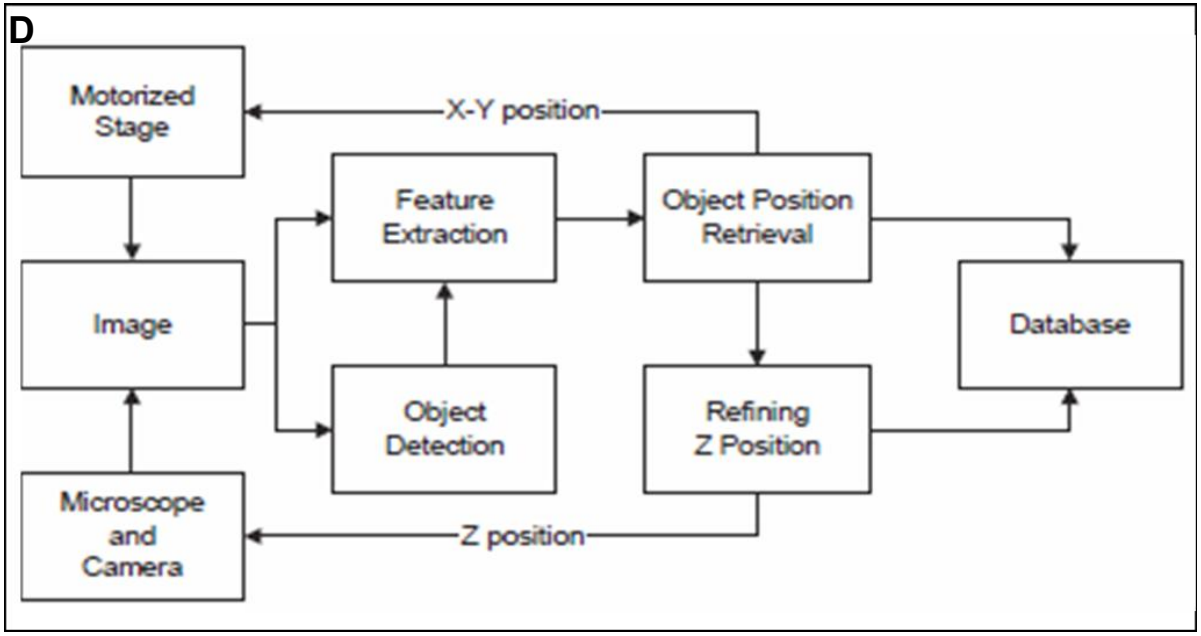

Figure 4.1. Automated online tracking of cells over time.

Single NSCs/NPs were seeded at clonal density in a 3 cm Mattek dish and followed by time-lapse videomicroscopy with (B) and without (A) the aid of the online tracking algorithm. (C) Flow of the cell tracking procedure. (D) Components of the tracking algorithm (Huang et al., 2012). This work was carried out in collaboration with Chao-Hui Huang and Hwee Kuan Lee (Bioinformatics Institute). Time, h. Scale bar, 10 µm.

3.3.2. FACS-based enrichment of NFCs

As mentioned earlier the NFU in a control population of NSCs/NPs is usually in the range of 10-15% (Gan et al., 2011). This implies that not all cells form neurospheres and necessitates the use of a bigger starting pool of cells to be analysed by time-lapse imaging. This can be circumvented by starting with a relatively smaller pool of cells that can yield a high NFU.

Previous work on NSC surface markers had led to the identification of C1qR1 as a potential NSC marker (Mike Yu and Sohail Ahmed, unpublished data). It was already known that eNSCs could be purified by using LeX (or CD15) as a surface marker for FACS (Capela and Temple, 2006). Cells double selected with CD15 and C1qR1 were found to yield significantly higher NFU compared to control. CD15+/C1qR1+ were FACS-sorted (figure 4.2A) and found to generate 45-55% NFU, which is 3-fold higher than the NFU of unsorted control cells (figure 4.2B). CD15+/C1qR1+ cells were hence used in subsequent experiments.

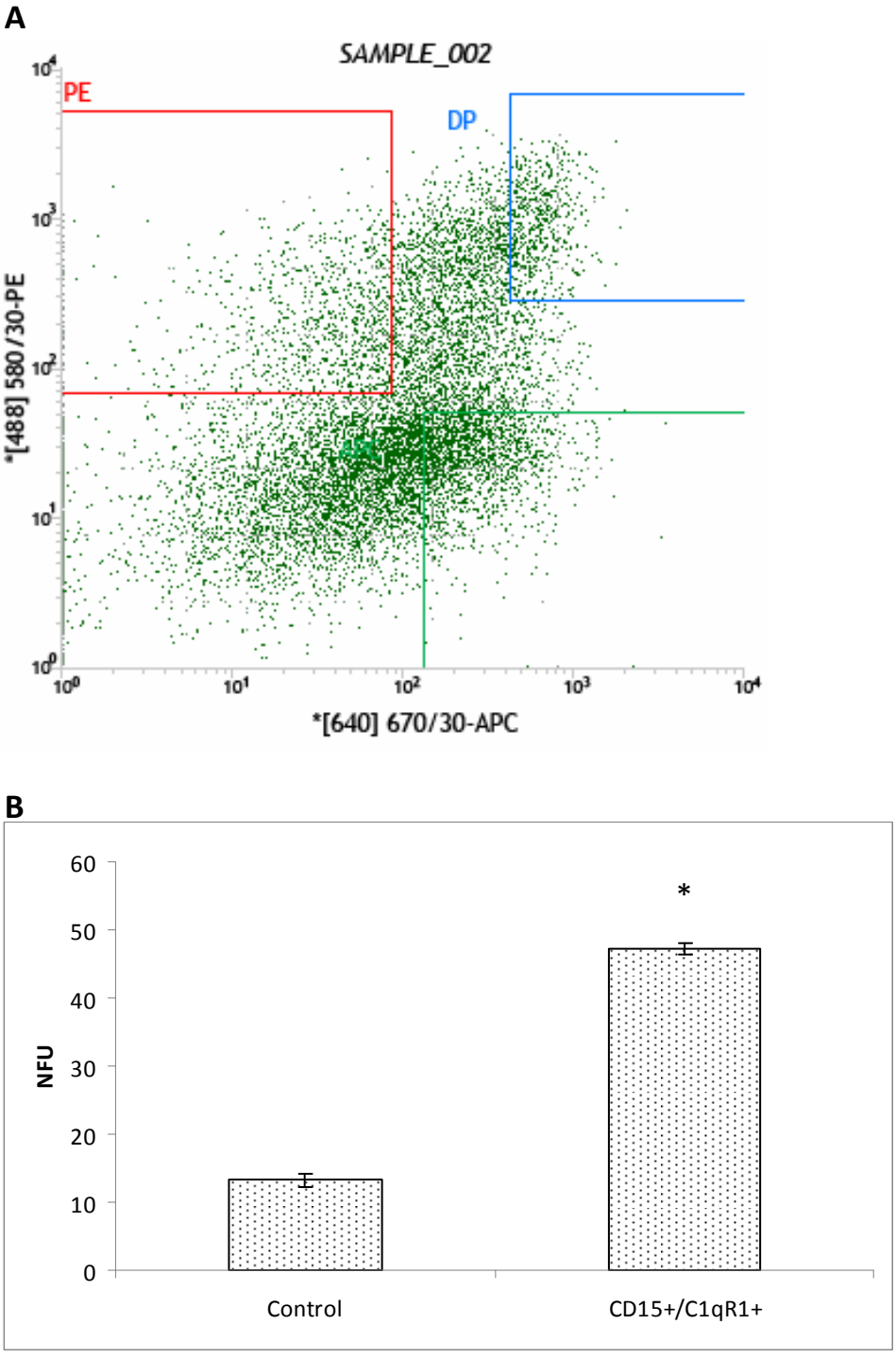

Figure 4.2. FACS enrichment of NFCs.
FACS enrichment of cells with surface markers CD15 and C1qR1 yielded higher NFUs. Single cells labelled with CD15 (APC) and C1qR1 (PE) were analysed by FACS (A). CD15+/C1qR1+ (A, DP) were found to yield higher NFUs compared to control (B). (Mean ± SEM; n= 5; *$p < 0.001$.) DP, double positive.

3.3.3. Time-lapse analysis of neurosphere formation

To correlate features of single cells with neurosphere formation, I performed time-lapse experiments by using the CD15+/C1qR1+ cell population. Typically, 50-70 single cells seeded at clonal density were followed from the single cell stage up to neurosphere formation (5-7 days) by time-lapse videomicroscopy. Analysis of time-lapse sequences showed the existence of 4 distinct groups of cells- cells that formed neurospheres (NFCs, 45%, figure 4.3A, E), cells that died without dividing (25%, figure 4.3B, E), cells that died after 1 division (15%, figure 4.3C, E), and cells that died after 2 divisions (15%, figure 4.3D, E).

To further characterise and distinguish the NFCs from the other cells, features of individual cells obtained from the time-lapse imaging analysis were used to identify links between the single cell and neurosphere formation as described below.

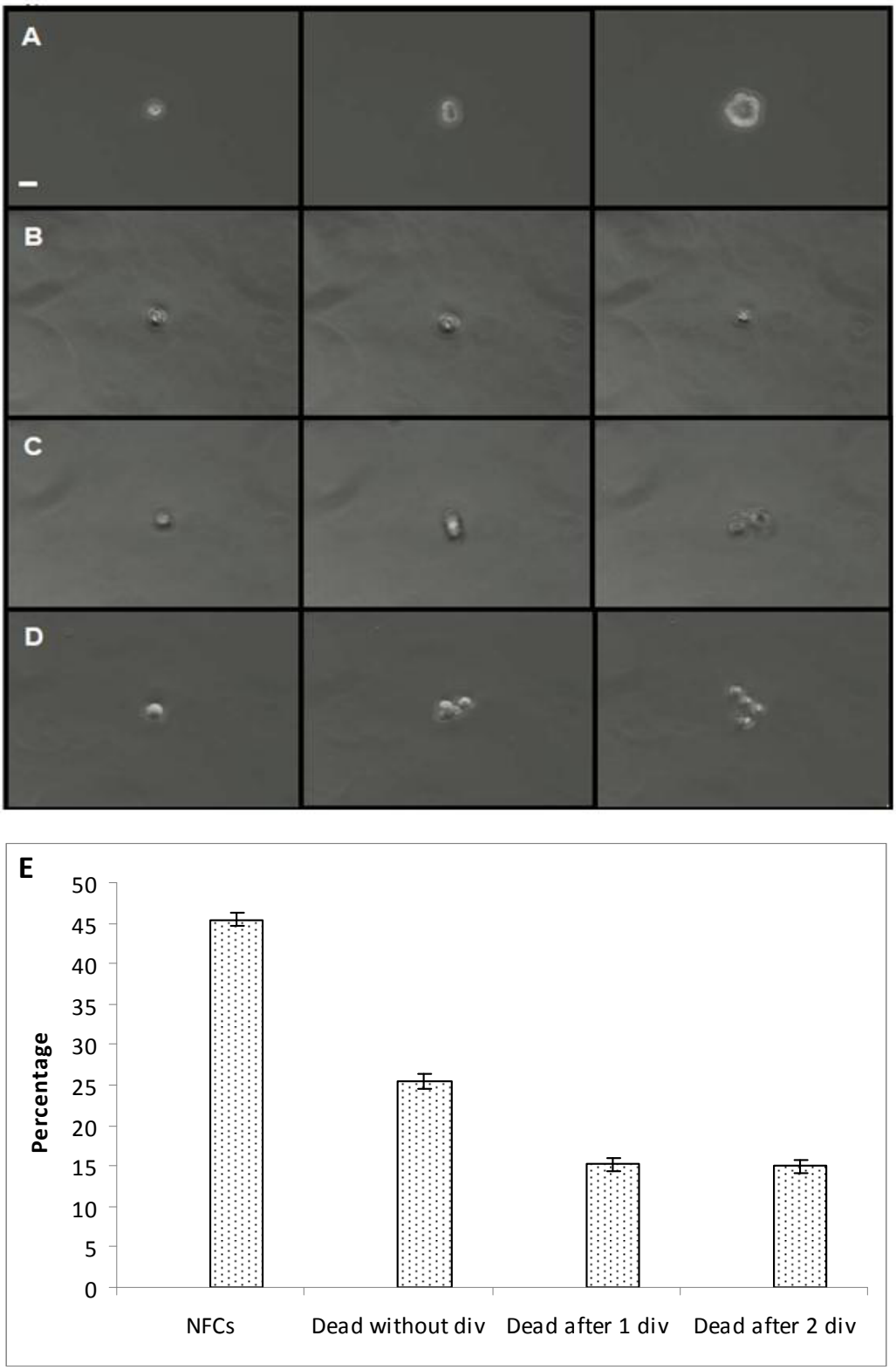

Figure 4.3. Imaging neurosphere formation.
CD15+/C1qR1+ cells were seeded at clonal density in a 96 well plate, and imaged from the single cell stage for 5 days. Based on cell fate cells were categorised as NFCs (A), dead without dividing (B), dead after one division (C), and dead after two divisions (D). Images shown are representative single images from varying time points from a time-lapse sequence for each of the four groups of cells. (E) Percentage of the four groups. Scale bar, 10 µm. (Mean ± SEM; n= 5.)

3.3.4. Cell size predicts neurosphere formation

Enrichment for NSCs based on cell size and granularity has been described by Murayama et al., where they found that cells with a FSC^{high}/SSC^{high} profile were enriched for NSCs (Murayama et al., 2002). To directly explore the relationship between cell size and neurosphere formation, CD15+/C1qR1+ cells were seeded at clonal density in a 96 well plate and followed by time-lapse videomicroscopy for five days. The NFU of cells measuring 10-20 μm in size was at least four times higher than that of cells <10 μm (figure 4.4). Single cell size can hence be used as a selective marker to enrich for NFCs.

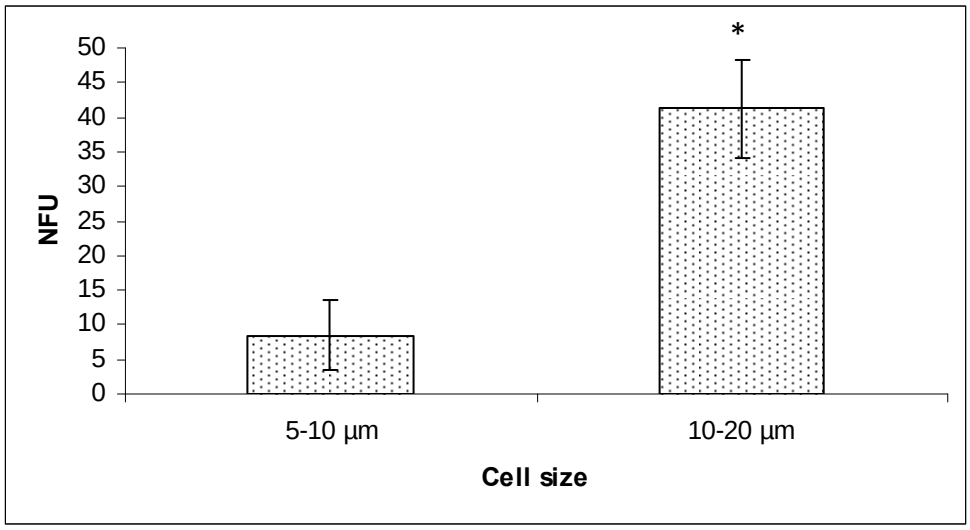

Figure 4.4. Cell size predicts neurosphere formation.
Bigger cells yield higher NFUs. CD15+/C1qR1+ were seeded at clonal density in a 96 well plate and neurosphere formation was followed by time-lapse videomicroscopy. Single cell size at t= 0 was manually measured by using Metamorph image analysis software and correlated with neurosphere formation on day 5. (Mean ± SEM; 184 cells, n= 4; *$p < 0.01$.)

3.3.5. Single cell dynamics are indicative of neurosphere formation

By using the automatic online cell tracker it was possible to quantify cell movement over time. This tool was used to plot and compare the tracks of the four groups of cells over the first 24 h as shown in figure 4.5. From the plots, it appeared that the NFCs (figure 4.5A, A′) were more dynamic compared to others (figure 4.5B-D, B′-D′). To test if this was indeed true the single cell track was used to predict cell fate by means of the receiver operating characteristic (ROC) curve. The ROC curve is derived from the false and true positive values resulting from varying the discriminatory threshold and can be used as a method to evaluate the accuracy of the test. Closer the curve to the left and upper borders of the plotted region higher is the accuracy. When applied on the 24 h cell tracks, the ROC curve showed an accuracy of 60% (figure 4.5E). This observation suggests that cell movement is predictive of neurosphere formation or death and represents an important aspect of NFC identity.

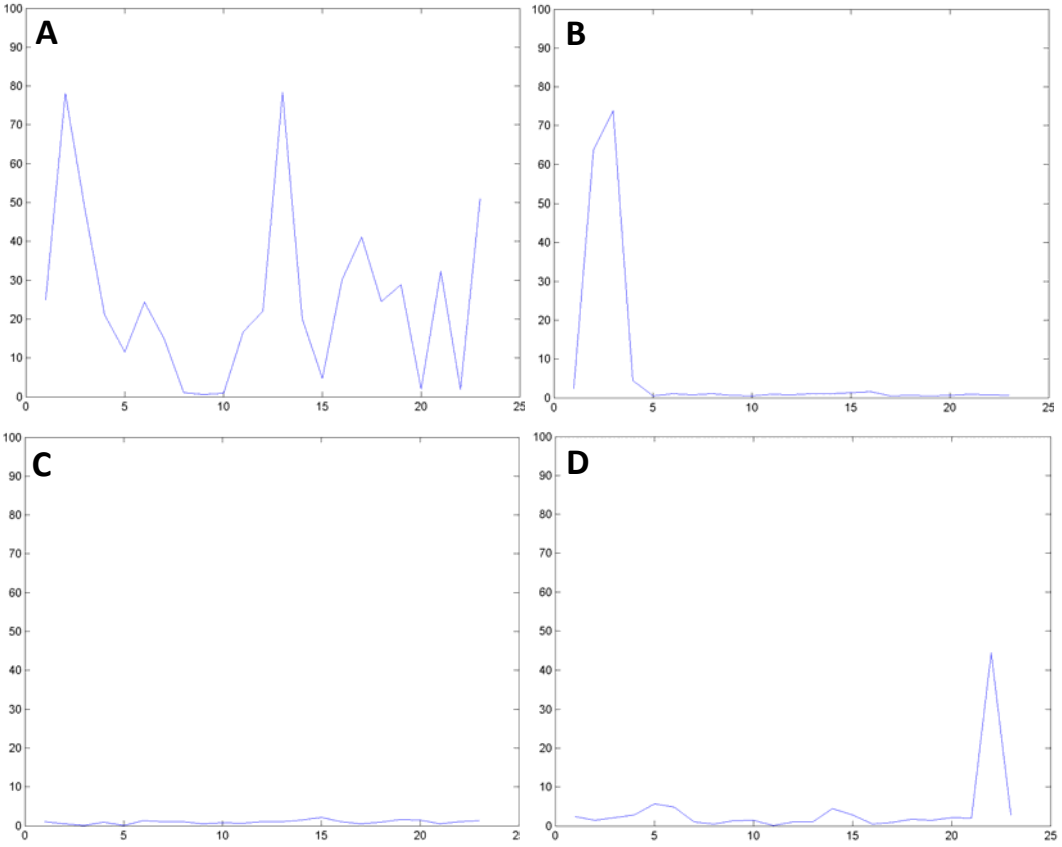
A
B
C
D

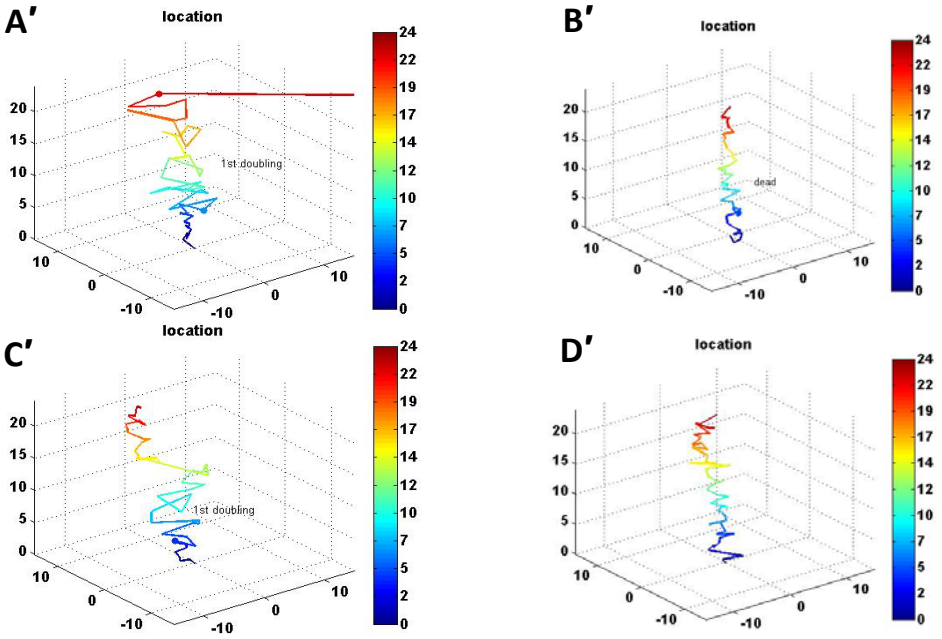
A′
location
1st doubling
B′
location
dead
C′
location
1st doubling
D′
location

E

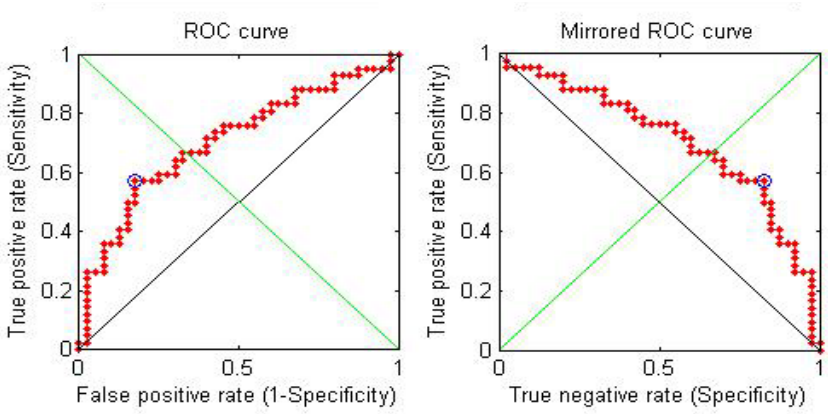

Figure 4.5. Cellular dynamics during the first 24h.
NFCs are more motile. CD15+/C1qR1+ cells were seeded at clonal density in a 96 well plate and followed by time-lapse imaging for up to 5 days by using the online tracking algorithm. Cell movement over 24 h were calculated for each cell and correlated to cell fate. Boxplots of cell movement are shown in A-D, where *x* denotes time in h and *y* denotes distance in µm. Tracks shown here are representative individual cell movements over the first 24 h for NFC (A, A'), cell dead without dividing (B, B'), cell dead after one division (C, C'), and cell dead after two divisions (D, D'). In A'-D' *x* and *y* denote distance in µm; *z* denotes time in h. (E) ROC curve for predicting cell fate based on cell movement shows that the curve is closer to the left and top border of the plotted region yielding an accuracy of 60%. This analysis was carried out in collaboration with Chaohui Huang (Bioinformatics Institute).

3.3.6. NFCs have a shorter doubling time

To distinguish between NFCs and cells that die after two divisions the doubling time for both populations was calculated and compared. The time taken for the first division was similar for both groups of cells. However, the time taken for the second division was longer for the group of cells that died after two divisions (figure 4.6A). Likewise the doubling time i.e., the time taken between the first and second divisions was 1.6 times longer for the group of cells that died (30 h) compared to the NFCs (18.5 h) (figure 4.6B).

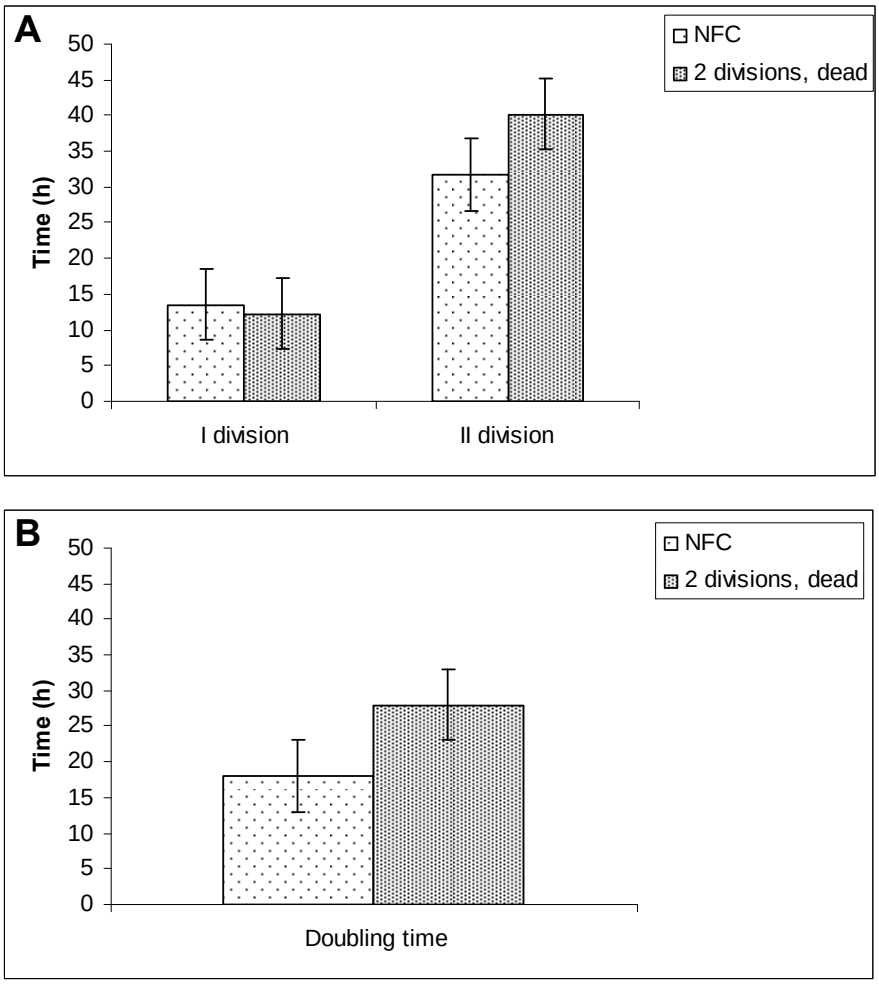

Figure 4.6. NFCs have a shorter doubling time.
To distinguish between an NFC and a cell that dies after two divisions, **t**he time taken for a single cell to divide two times was measured for both groups of cells (A). From these values, the doubling time for each group was calculated (B). (Mean ± SEM; 60 cells, n= 3; *$p < 0.001$.)

Specific features such as bigger cell size, rapid cell motility, and shorter doubling time can therefore be attributed to NFCs and used to distinguish them from cells that do not form neurospheres.

3.4. Correlation between mechanism of cell division and potency

Studies on the cell division patterns of stem cells have shown the importance of asymmetric divisions to stem cell behaviour (Zhong et al., 1996;

Shen et al., 2002; Sun et al., 2005). I sought to inspect if neurospheres exhibited distinct marker distribution patterns and if these patterns correlated with the potency of the neurosphere. In other words, could the marker distribution reflect if the cell was a stem cell or a progenitor?

3.4.1. Time point analysis of cell division using eYFP-PMT

3-D imaging of neurospheres expressing eYFP-PMT had indicated that PMT was not distributed uniformly in all the cells within a neurosphere (figure 2.2). Since eYFP-PMT is a plasmid transfected into clonal cultures of NSCs/NPs, its distribution is a direct result of segregation of the plasmid during cell division.

To determine the distribution pattern of eYFP-PMT in neurospheres, cells were transfected with eYFP-PMT and imaged everyday from day 1 (figure 4.7A- single cell stage) up to day 5 (figure 4.7A and B, D5- neurosphere). The distribution pattern of eYFP-PMT suggests that there are distinct modes of cell division adopted by different cells. For instance, cells shown in figure 4.7B divided symmetrically to give rise to progeny with a uniform eYFP-PMT distribution. On the other hand, cells shown in figure 4.7C likely divided asymmetrically followed subsequently by symmetric divisions thus resulting in a mosaic pattern.

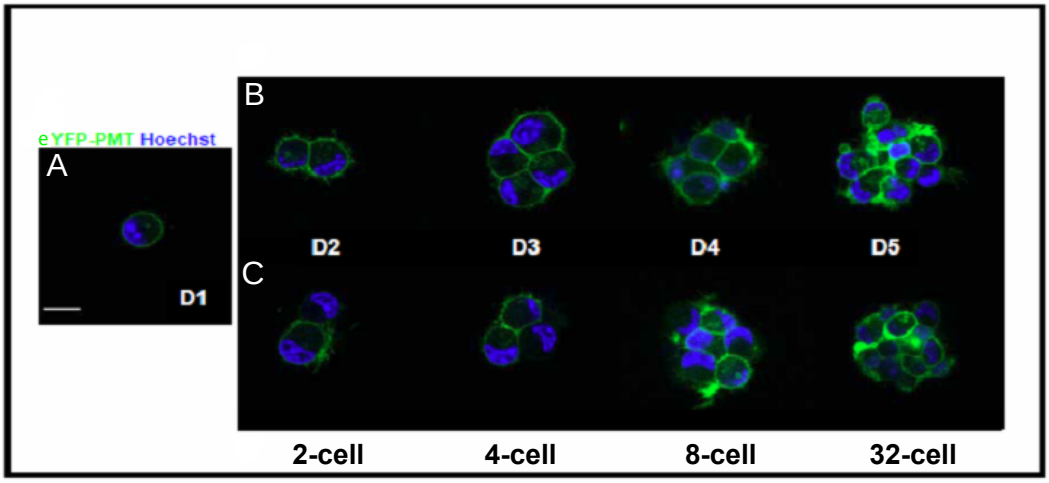

Figure 4.7. Cell division patterns in NSCs/NPs.
Cells transfected with eYFP-PMT were seeded at clonal density and imaged from single cell stage (A) everyday up to day 5 (B, C). Hoechst 33342 (nuclei, blue) was added to the samples prior to imaging to reveal cell number. Dividing cells were observed to display symmetric (B) or asymmetric (C) distribution of eYFP-PMT. Scale bar, 10 µm.

3.4.2. Surface marker distribution reflects potency

Since eYFP-PMT displayed distinct modes of marker distribution, I wanted to find out if similar distribution patterns could be observed potential NSC surface markers like CD15 and C1qR1. I also wanted to ascertain if there was a correlation between marker distribution and neurosphere potency. To do this, day 5 neurospheres derived from CD15+/C1qR1+ cells were labelled with antibodies against CD15 and C1qR1. They were then examined by 3-D imaging and grouped as neurospheres with uniform or non-uniform CD15/C1qR1 distributions. Neurospheres with uniform marker distribution exhibited even labelling among the cells while those with non-uniform distribution had 1-4 cells that were brighter than the others cells within the same neurosphere (discussed in section 3.5.2).

The two groups of neurospheres were then differentiated followed by triple labelling for markers against astrocytes, neurons, and oligodendrocytes. Analysis of the potency of the two groups of neurospheres revealed that 70% of neurospheres with non-uniform CD15/C1qR1 distribution were multipotent (figure 4.8). In other words, a neurosphere displaying non-uniform surface marker distribution is 7 times more likely to be multipotent compared to one with a uniform marker distribution.

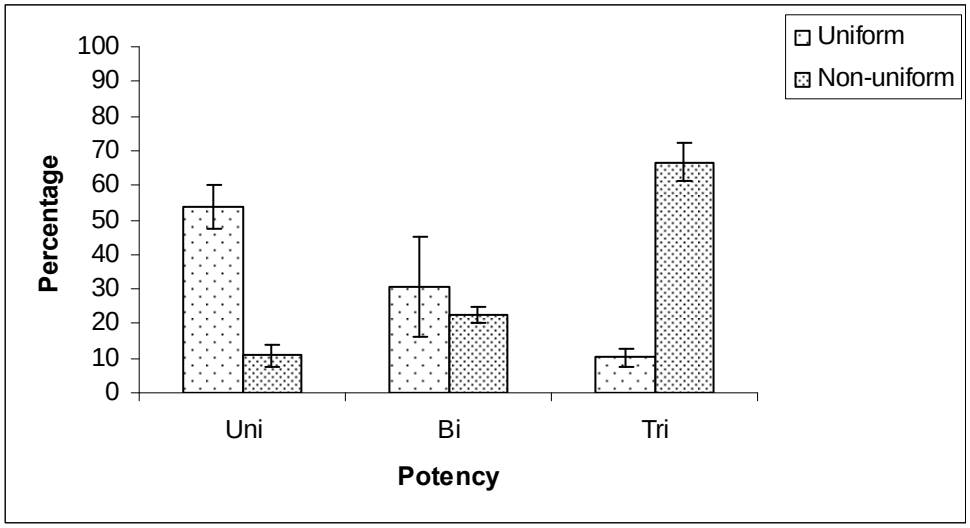

Figure 4.8. Non-uniform marker distribution indicates multipotency.
Clonal neurospheres from CD15+/C1qR1+ cells were labelled with antibodies against CD15 and C1qR1 and 3-D images were generated to assess marker distribution patterns. Neurospheres were grouped into uniform and non- uniform distributions and subjected to the clonal differentiation assay. Differentiated neurospheres were labelled with lineage- specific markers O4, β-III tubulin and GFAP and the potency of individual neurospheres was scored. (Mean ± SEM; 60 neurospheres, n= 4; $*p \leq 0.01$.)

Hence symmetric and asymmetric marker distribution patterns resulting from cell division can be observed in neurospheres transfected with eYFP-PMT. CD15 and C1qR1 surface markers also show distinct labelling patterns among neurospheres.

Further, non-uniform CD15/C1qR1 distribution strongly correlates with multipotency.

3.5. Use of surface markers to study NSC/NP behaviour

To examine if a correlation exists between the identity of the single cell (NSC Vs NP) and the type of cell division I used a combination of fluorescently-labelled surface markers, phase intensity, expression vectors, and cell permeable dyes to label cells and study the resulting distribution patterns and find if they correlated with neurosphere formation and multipotency.

3.5.1. Marker distributions in doublets

The CD15+/C1qR1+ cell population showed enrichment of NFCs. To assess if CD15+/C1qR1+ doublets possess features that could help distinguish NFCs from the others CD15 and C1qR1 antibodies were used to label doublets arising from four different cell populations: unsorted control, CD15+, C1qR1+, and CD15+/C1qR1+. Confocal imaging of immunolabelled doublets revealed two distinct distribution patterns- uniform and non-uniform (figure 4.9A, B). However, when the percentage of the label distribution was quantified and compared (figure 4.9C) no significant differences were found in the labelling pattern of CD15+/C1qR1+ doublets compared to the other populations.

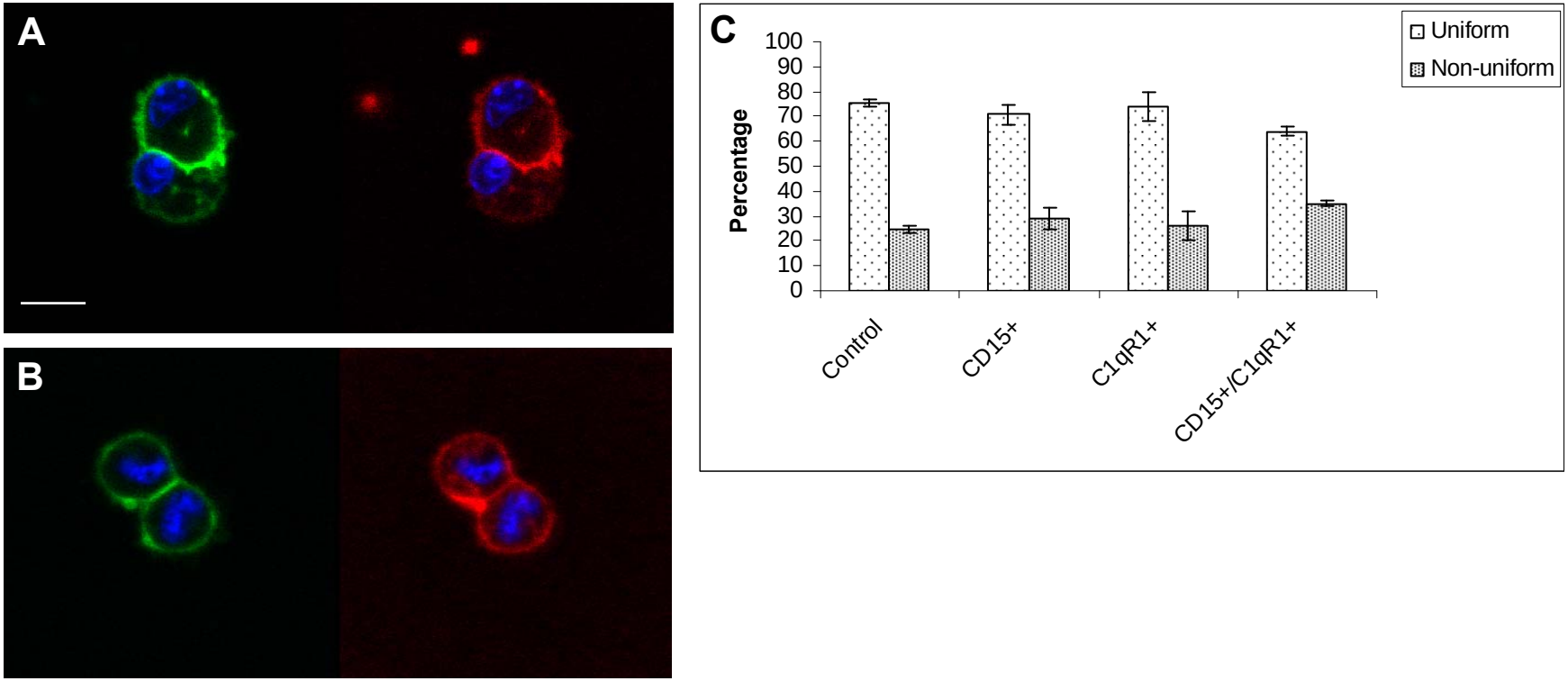

Figure 4.9. Distribution of CD15 and C1qR1 in FACS-sorted doublets.
Clonally generated CD15+/C1qR1+ doublets were labelled with CD15 and C1qR1 antibodies and imaged to reveal marker distribution patterns which were non-uniform (A) or uniform (B). The percentage of uniform and non-uniform marker distributions was quantified and compared between different cell populations (C). Control refers to unsorted live cells. CD15, green; C1qR1, red, Hoechst 33342, blue. Scale bar, 10 µm. (Mean ± SEM; 60 doublets, n=3.)

3.5.2. Marker distributions in neurospheres

To assess if neurospheres labelled with surface markers displayed distinct distribution patterns they were labelled with SSEA-1 and C1qR1 antibodies and imaged in 3-D. Again, uniform and non-uniform labelling patterns were observed. Uniform marker distribution was characterised by an even distribution of SSEA-1 and C1qR1 signals between the cells in a neurosphere. In contrast, in neurospheres with a non-uniform surface marker distribution there were 1-4 cells significantly brighter than the others within the same neurosphere (figure 4.10A). Quantification of the fluorescence intensity of SSEA-1 revealed that bright cells were on average 2-5 times more fluorescent than other cells in the same neurosphere (figure 4.10B and C). Bright cells also appeared to have bigger surface (Figure 4.10D). Similarly, neurospheres labelled with the cell permeable dye CDy5 also displayed uniform and non-uniform distribution patterns (figure 4.11).

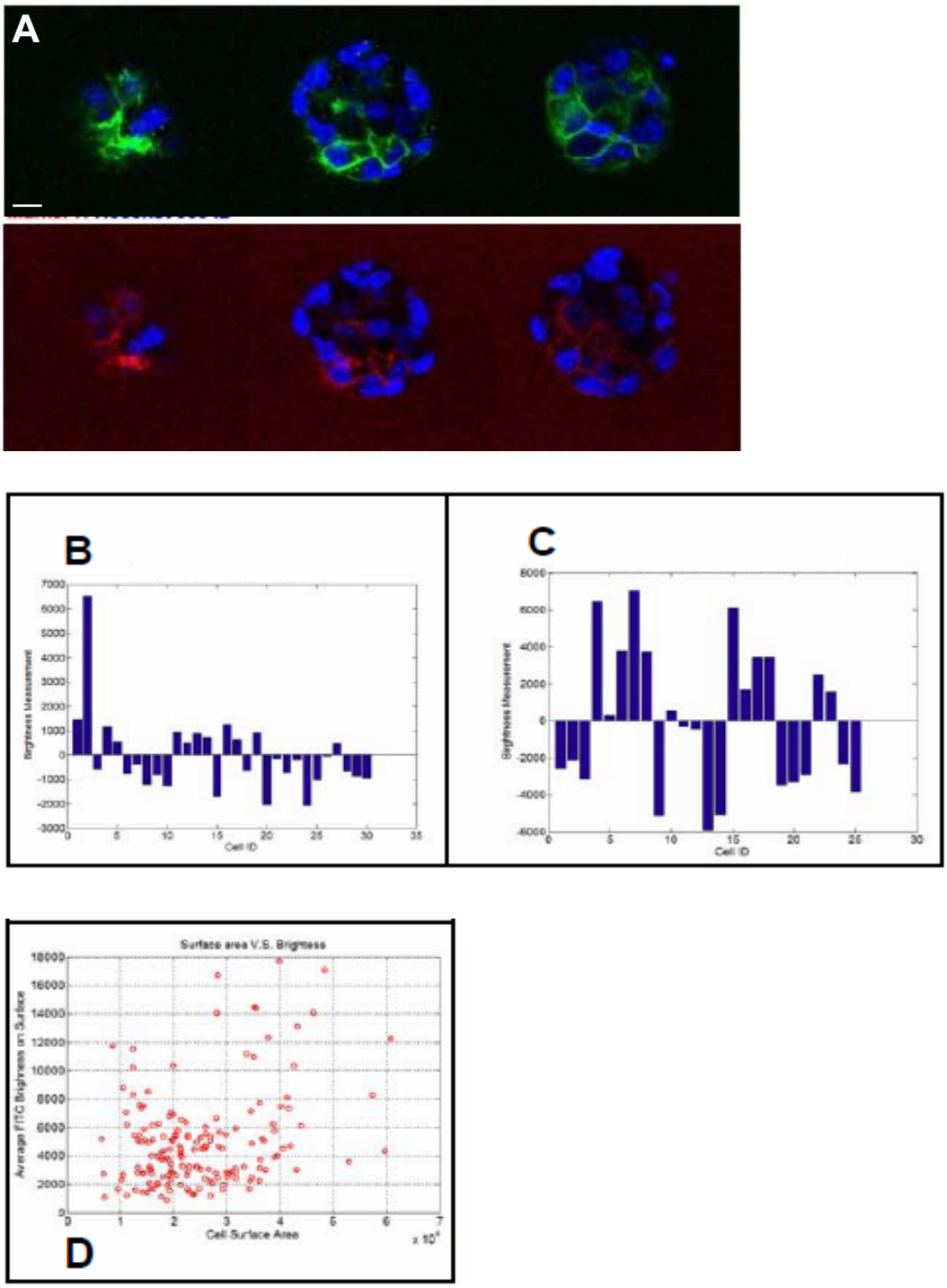

Figure 4.10. Non-uniform surface marker distributions in neurospheres.
Day 5 neurospheres labelled with SSEA-1 (A, green) or C1qR1 (A, red) antibodies and imaged in 3-D on a LSCM to reveal distribution patterns. Slices from one 3-D stack are shown in A. Quantification of the fluorescence intensity of SSEA-1 in two different neurospheres (B and C) revealed a difference in fluorescence intensity between bright cells relative to other cells within the same neurosphere. *x*-axis represents individual cells and *y*-axis represents mean SSEA-1 intensity in B and C. The surface area of single cells were measured and plotted against SSEA-1 intensity (D). Hoechst 33342 labels the nuclei (A, blue). Scale bar, 10 µm.

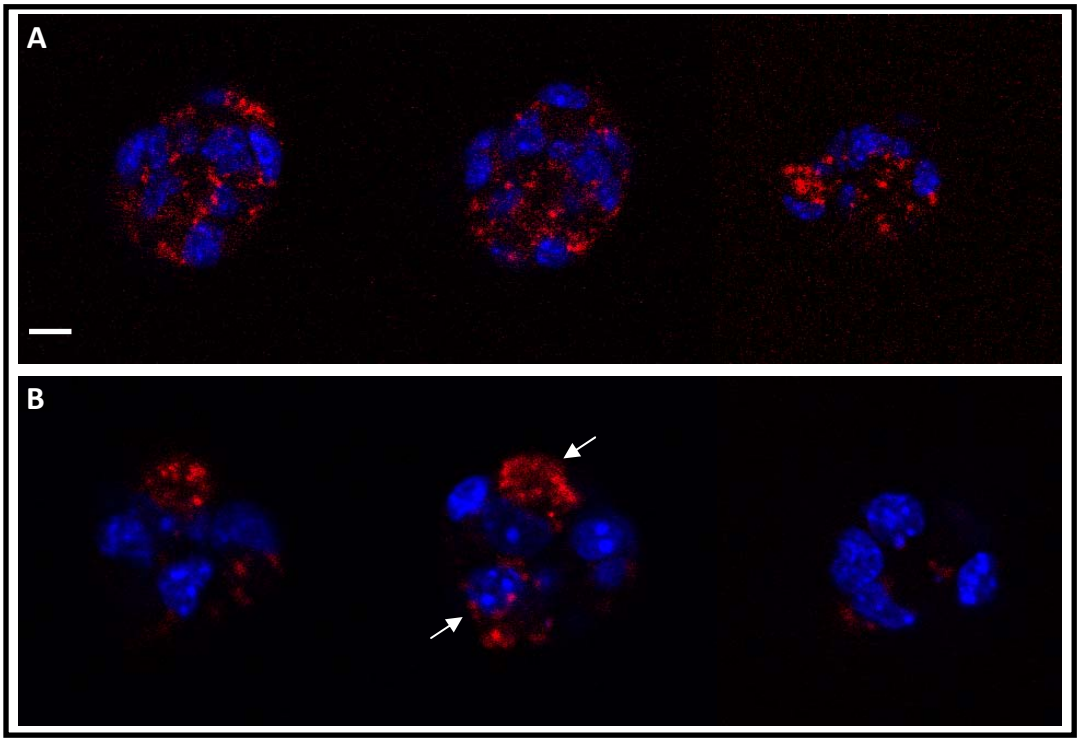

Figure 4.11. Distribution of CDy5 in FACS-sorted neurospheres.
CD15+/C1qR1+ cells were labelled with cell-permeable dye CDy5 and seeded at clonal density in 96 well plates and allowed to grow for 5 days. Day 5 neurospheres were imaged on a LSCM to reveal marker distribution patterns which were observed to be uniform (A) or non-uniform (B). Individual slices from a single neurosphere are shown in A and B. Arrows in B indicate CDy5 labelling in a few cells. Hoechst 33342 (blue) labels the nuclei. Scale bar, 20 µm.

3.6. Purification of NSCs

FACS-sorting cells using surface markers CD15 and C1qR1 enriched for cells with higher NFUs. However, the NSC frequency within the CD15+/C1qR1+ population was 46%. I wanted to explore specific imaging-related features that could enrich for the NSC frequency within the CD15+/C1qR1+ population. To do this I analysed cells that were imaged by phase contrast microscopy from the single cell stage till neurosphere formation. I then sought to identify features of single cells that correlated strongly with neurosphere formation and multipotency.

3.6.1. Phase intensity predicts neurosphere formation

Use of the phase contrast mode for imaging allowed the measurement of the phase intensity of a cell. Due to the optics of the phase contrast mode the objects being observed are surrounded by a luminous halo. The phase intensity of a cell can then be defined as the intensity of the halo surrounding the cell in gray values. The phase intensity was manually measured by drawing a region of interest around the single cell using Metamorph. Following background correction, phase intensities of cells were measured and correlated with cell fate. Phase intensity was found to be highest for the NFCs (figure 4.12A) with a score >200 gray values. By using a threshold of >200 gray values for phase intensity cells that do not form neurospheres can be excluded from analysis.

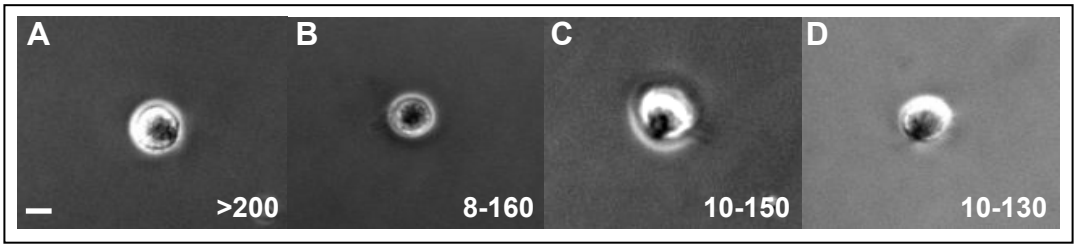

Figure 4.12. Phase intensity predicts neurosphere formation.
NFCs have higher phase intensity values. CD15+/C1qR1+ cells were seeded at clonal density in 96 well plates and neurosphere formation was followed by time-lapse videomicroscopy. Phase intensity of the single cell at t= 0 was manually measured for all the cells. Representative examples of NFCs (A), cells dead without dividing (B), cells dead after one division (C), and cells dead after two divisions (D) are shown. Numbers represent phase intensity in gray values for each group. Scale bar, 10 μm.

Thus, selecting for cells with CD15+/C1qR1+/Phasebright (Phbrt)+ profile yields a 100% NFC population (figure 4.13A). To evaluate the potency of the clonal neurosphere and correlate it with single cell phase intensity, neurosphere formation was tracked by time-lapse videomicroscopy. Individual neurospheres were then differentiated and immunolabelled with antibodies against GFAP, O4, and βIII tubulin. Imaging of immunolabelled neurospheres revealed the potency of the CD15+/C1qR1+/Phbrt+ population to be 72%. The potency of the CD15+/C1qR1+/Phbrt+ was similar to that of the CD15+/C1qR1+ population (figure 4.13B) although the NFU of the former is 100%. To determine if an increase in the cut-off of phase intensity would result in increase in multipotency of the CD15+/C1qR1+/Phbrt+ population, phase intensity was increased to >240 gray values. This resulted in a further purification of the CD15+/C1qR1+/Phbrt+ population to yield 100% multipotent neurospheres (figure 4.13B). Thus the CD15+/C1qR1+/Phbrt+>240 population consisted entirely of cells giving rise to

multipotent neurospheres i.e., NSCs. Representative examples of neurospheres formed by an NSC and NP are shown (figure 4.13 E, F).

3.6.2. Phase bright cells are enriched for NSCs

The stem cell frequency can be derived from two known values: the NFU and the percentage of multipotent neurospheres. It can be calculated by using the formula: NSC frequency = NFU x % multipotent neurospheres. As shown in figure 4.13C, enriching for CD15+/C1qR1+/Phbrt>240+ yielded a population of cells consisting 100% of NSCs. NSC yield was then calculated from known values of NSC frequency and the composition of the selected cells as a percentage of the total starting population (figure 4.13D). The CD15+/C1qR1+ population constitutes on average of 3.8% of the total cell population with an NSC frequency of 34%. The NSC yield of CD15+/C1qR1+ was thus calculated to be 1.3%. Similarly the NSC yield of CD15+/C1qR1+/Phbrt+ and CD15+/C1qR1+/Phbrt>240 cells was 0.65% and 0.17%, respectively (figure 4.13D).

Thus I was able to purify a population consisting of 100% NSCs using a combination of surface marker-based purification and phase intensity of the single cell.

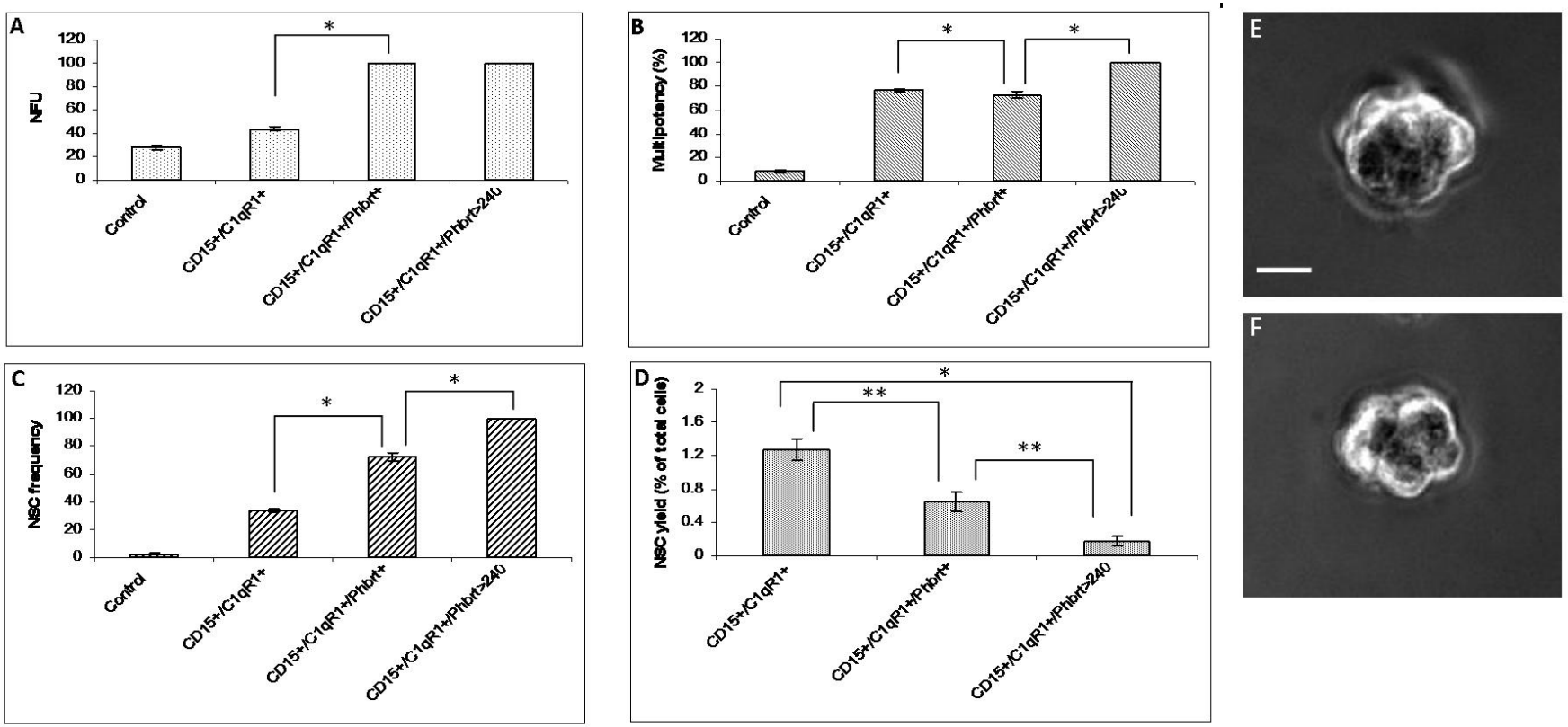

Figure 4.13. Analysis of CD15+/C1qR1+/Phbrt+ cells.

CD15+/C1qR1+ were tracked by time-lapse videomicroscopy and NFU and multipotency were evaluated for various cell populations. Values for NFU (A) multipotency (B), NSC frequency (C), and NSC yield (D) are shown. NFU and multipotency were used to estimate NSC frequency. NSC yield is represented as a percentage of the total starting cell population. Unsorted live cells were used as control. Examples of neurospheres formed by NSC (E) and NP (F) are shown. (Mean ± SEM; n= 3; *$p \leq 0.01$, **$p < 0.05$.) Scale bar, 20 µm.

3.7. mRNA profile of CD15+/C1qR1+/Phbrt+ cells

Having established that CD15+/C1qR1+/Phbrt+ cells yielded 100% neurosphere formation, I attempted to identify the mRNA signature of this population. Single-cell mRNA profiling was used to identify different sub-populations of cells within neurospheres (Narayanan et al., 2012). To understand if there were novel NSC markers associated with CD15+/C1qR1+/Phbrt+ cells single-cell mRNA profiling of 48 genes was performed using unsorted and CD15+/C1qR1+/Phbrt+ cell populations. Genes from the major NSC signalling pathways such as Notch, Wnt, and Shh as well as classes of genes such as POU factors and bHLH factors were included in the list of 48 genes and were chosen since they are important cell fate regulators.

Average expression levels of each of the 48 genes were compared between unsorted and CD15+/C1qR1+/Phbrt+ populations. As shown in figure 4.14**,** 22 genes were found to show significant changes in expression levels in the CD15+/C1qR1+/Phbrt+ population compared to the unsorted population. *Notch1* which is involved in the Notch signalling pathway was found to be elevated in the CD15+/C1qR1+/Phbrt+ population. Similarly, *Pax6* was also expressed at higher levels in CD15+/C1qR1+/Phbrt+ cells as were *Jag1* and *Prominin* compared to unsorted cells. Other genes associated with NSC function that showed marginally higher expression levels include *BLBP, FGFR1, Dll1, c-kit*, *FoxG1*, *CBF1* and differentiation markers such as *Sox9* and *Mash1*.

Although the current analysis did not yield any new NSC markers, further examination of the NSC-enriched population (CD15+/C1qR1+/Phbrt+>240) is required for a conclusive commentary on the mRNA profile of NSCs.

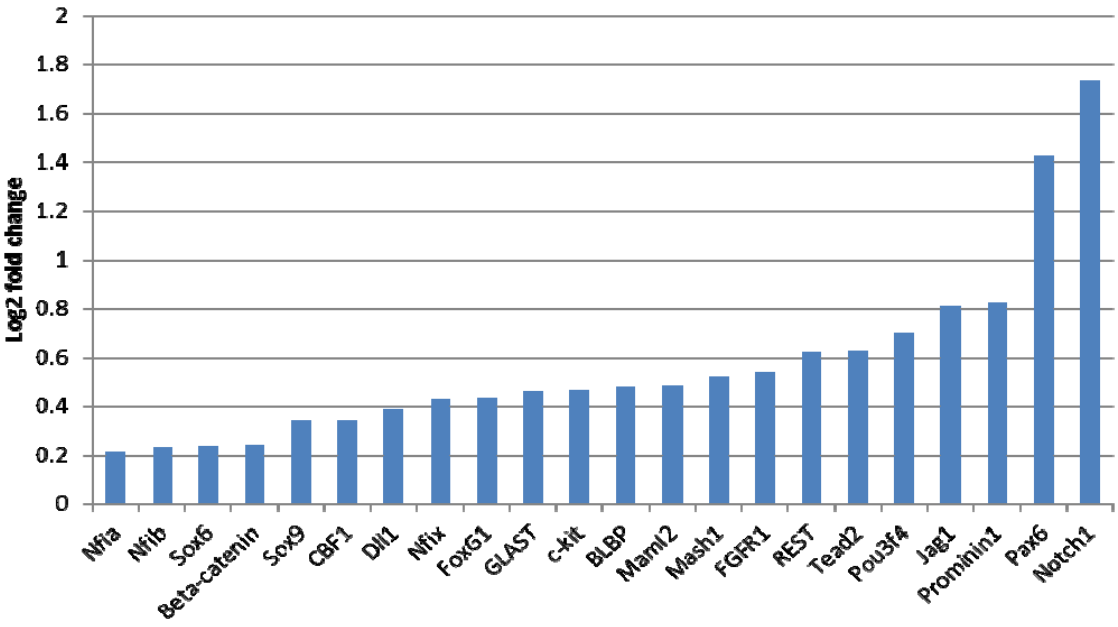

Figure 4.14. mRNA signature of CD15+/C1qR1+/Phbrt+ cells.
CD15+/C1qR1+/Phbrt+ cells were analysed by scPCR against 48 chosen genes. The bar plots represent a $\log_2$-fold change in gene expression compared to unsorted control cells. This work was carried out in collaboration with Gunaseelan Narayanan (Institute of Medical Biology, A-STAR, Singapore).

3.8. A HTS assay to study changes in neurosphere growth and gene expression

High content screens (HCS) and HTS are powerful methods to analyse large cell populations. While the former is used to generate detailed information pertaining to individual cells such as cell structure and function, the latter is vital for quantifying global changes occurring in cell populations. For instance, a HTS assay can be used study the effects of drugs on NFU or gene expression and was developed to analyse large populations of neurospheres.

NSCs are crucial to the study of therapy against several neurodegenerative disorders such as AD, PD, schizophrenia, depression, stroke and brain tumours (Lindvall et al., 2004; Kim, 2010). More importantly, the discovery of the BTSC (Singh et al., 2003) has caused a paradigm shift in the approach to anti-tumour therapy research and design. While conventional approaches to treating tumours involve radiation, cytotoxic chemotherapeutic agents, surgery, and hormone treatments, there has been a serious lack of understanding of the cellular and molecular basis of the initiation and proliferation of cancerous cells. As a result, patient prognosis can be poor especially with brain tumours (Dirks, 2008). Hence there is an urgent need to re-think tumour therapy from the study of NSCs. Moreover, a number of studies are beginning to uncover a correlation between the low incidence of cancers in patients receiving treatment for neuropsychiatric disorders (Dalton et al., 2002; Barak et al., 2005; Grinshpoon et al., 2005; Diamandis et al., 2009). The speculation is that the neuromodulatory drugs could exhibit a protective anti-cancer effect by reducing pools of NSCs in the patients receiving treatment (Diamandis et al., 2009).

Hence I sought to test a panel of drugs commonly used in treating neurological disorders and glioma (table 2) to determine their effects on NSC/NPs. Measures of neurosphere growth (NFU, size) and gene expression (*Sox2* promoter activity) were used to assess the effects of the drugs. Sox2 is an established stem cell marker (Ellis et al., 2004). A decrease in NFU, neurosphere diameter, and *Sox2* promoter activity (GFP intensity) would suggest that the tested drug could potentially have anti-tumour properties.

3.8.1. Design of the HTS assay

To image large populations of samples rapidly and efficiently a Metamorph-based assay was developed and optimised. The sequence of steps in the process is shown in figure 5.1. First, samples were cultured in a multiwell dish such as a 96 well plate. Next, using the 'Screen acquisition' feature in Metamorph individual wells in the dish were imaged by capturing images of 15-20 regions per well. This process was repeated until all the wells in the multiwell dish were imaged. Post-imaging, individual wells were reconstructed by stitching together all the regions in the well. Based on the fluorescent markers used for imaging the reconstructed well can be segmented to yield information on neurosphere numbers or changes in fluorescence intensity. Results of control and drug treatment for instance, can thus be compared. The entire process usually takes between 2-4 h.

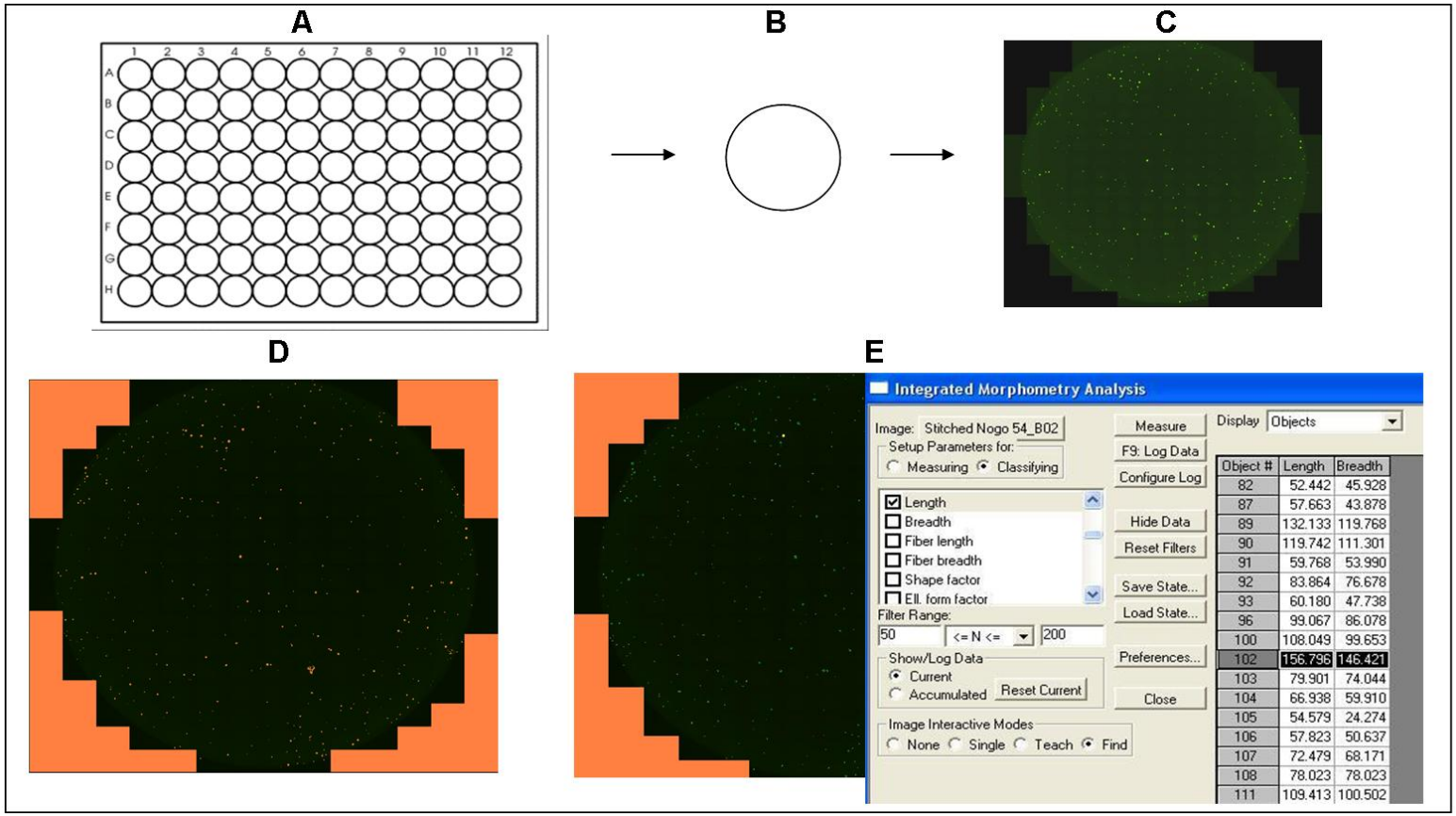

Figure 5.1. Design of the HTS assay.
Single cells were cultured in a multiwell dish (A) and allowed to form neurospheres. Using Metamorph images of neurospheres in individual wells (B) were generated (C) which were then segmented (D) and quantified for neurosphere number or fluorescence intensity of the reporter gene (E).

3.8.2. Proof-of-principle test: effects of Ifenprodil on NSCs/NPs

In the work done by Peter Dirks' group (Diamandis et al., 2007), it was revealed that a complex neural network exists to allow NSCs to retain their ground state. In this study it was also shown that certain classes of molecules had stronger effects on neurosphere numbers. Ifenprodil, which is an NMDA receptor antagonist was shown to impact neurosphere numbers most significantly. Hence, Ifenprodil was chosen to test the response of E14.5 NSCs/NPs to drug treatment.

The read-out for the effects of the drug was assessed in terms of changes in i) neurosphere numbers (NFU), and ii) *Sox2* promoter activity. As shown in figure 5.2, treatment of NSCs/NPs with 0.6 μM Ifenprodil resulted in a 1.5-fold reduced NFU compared to DMSO-treated control. Similarly, Ifenprodil treatment resulted in decreasing GFP intensity by 3-fold showing that Ifenprodil has an effect on E14.5 NSCs/NPs.

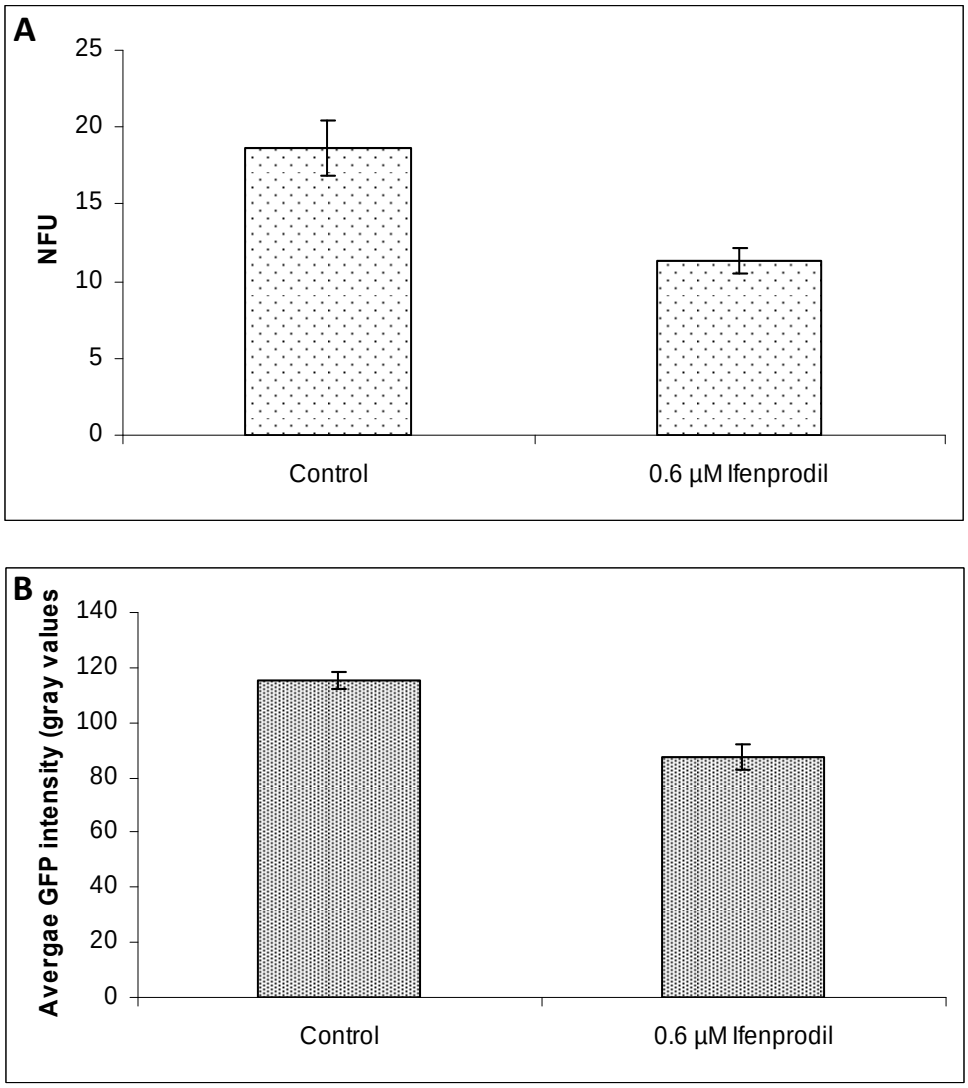

Figure 5.2. Effects of Ifenprodil on E14.5 NSCs/NPs.
Ifenprodil reduces NFU and Sox2-GFP promoter activity. Single cells were treated with Ifenprodil at the EC_{50} dose and allowed to proliferate. Day 5 neurospheres from untreated and drug-treated populations were analysed by the HTS assay for NFU (A) and GFP fluorescence (B).

3.8.3. Effects of neuromodulators on NFU, neurosphere diameter, and *Sox2* promoter activity

Experiments with Ifenprodil showed that an automated HTS assay could indeed be used to monitor the effect of drugs on neurospheres cultures. Having optimised the HTS assay, I next tested the effects of a chosen group of neuromodulatory drugs

(table 2) on neurospheres. *Sox2*-GFP cells were treated with drug or solvent control and the effects on NFU, neurosphere diameter, and GFP intensity were quantified. Results are represented as dose response curves for drug or solvent control (figure 5.3A-D). The drugs could be classified under two groups based on their effects: a) those that reduced NFU, neurosphere diameter, and GFP intensity, and b) those that did not show any effects. With the exception of clozapine and Prozac (prescribed for the treatment of schizophrenia and depression, respectively), all the drugs reduced NFU, neurosphere diameter, and GFP intensity. Table 2 summarises the drugs tested and their effects on NSCs/NPs.

Name of drug	Used in the treatment of	Effects on NFU, neurosphere size, and Sox2-GFP promoter activity
Clozapine	Schizophrenia	Did not show any changes.
Paliperidone		Reduction
Ziprasidone hydrochloride		Reduction
Biperidin hydrochloride	Parkinson's disease	Reduction
L-3,4-Dihydroxyphenylalanine methyl ester hydrochloride		Reduction
Fluoxetine (Prozac)	Depression	Did not show any changes.
Imipramine		Reduction
Desipramine		Reduction
Temozolomide	Glioma	Reduction

Table 2. Summary of the effects of neuromodulatory drugs tested on E14.5 NSCs/NPs.

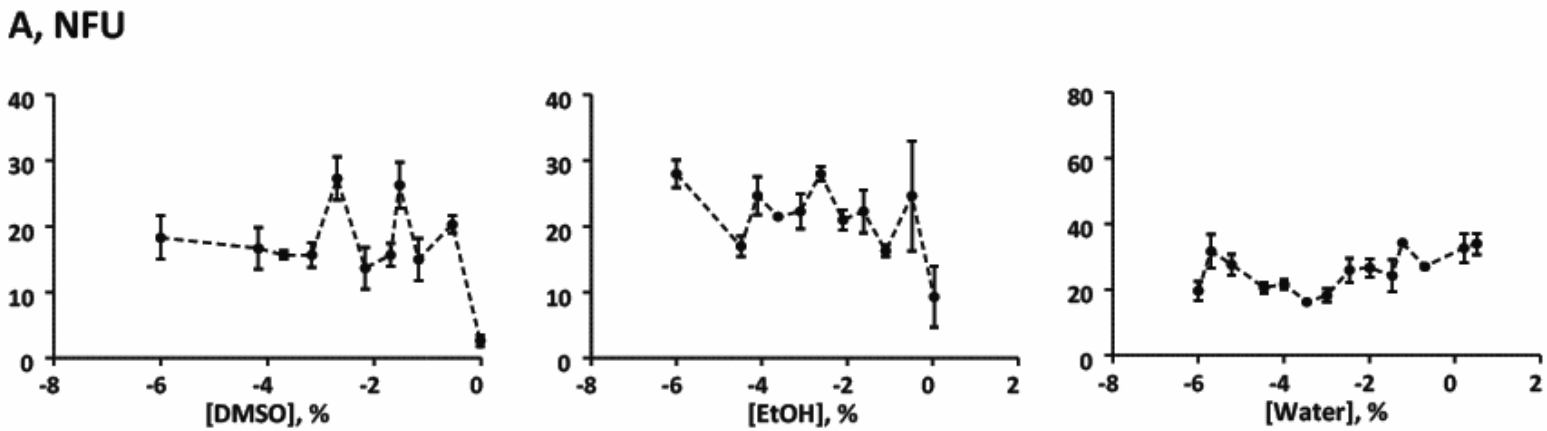

Figure 5.3. Effects of neuromodulatory drugs on NFU, neurosphere size, and *Sox2* promoter activity.
Sox2-GFP single cells were treated with varying drug concentrations or solvent control and allowed to form neurospheres. Day 7 neurospheres were evaluated for NFU, neurosphere size, and GFP intensity by using the HTS assay. Data is presented as dose response curves for solvent control (A, *y*-axis represents NFU) or drugs (B-D). Effects of drugs as changes in NFU (B, *y*-axis represents NFU), neurosphere size (C, *y*-axis represents size of the neurosphere in µm), and GFP intensity (D, *y*-axis represents average gray values) are shown.

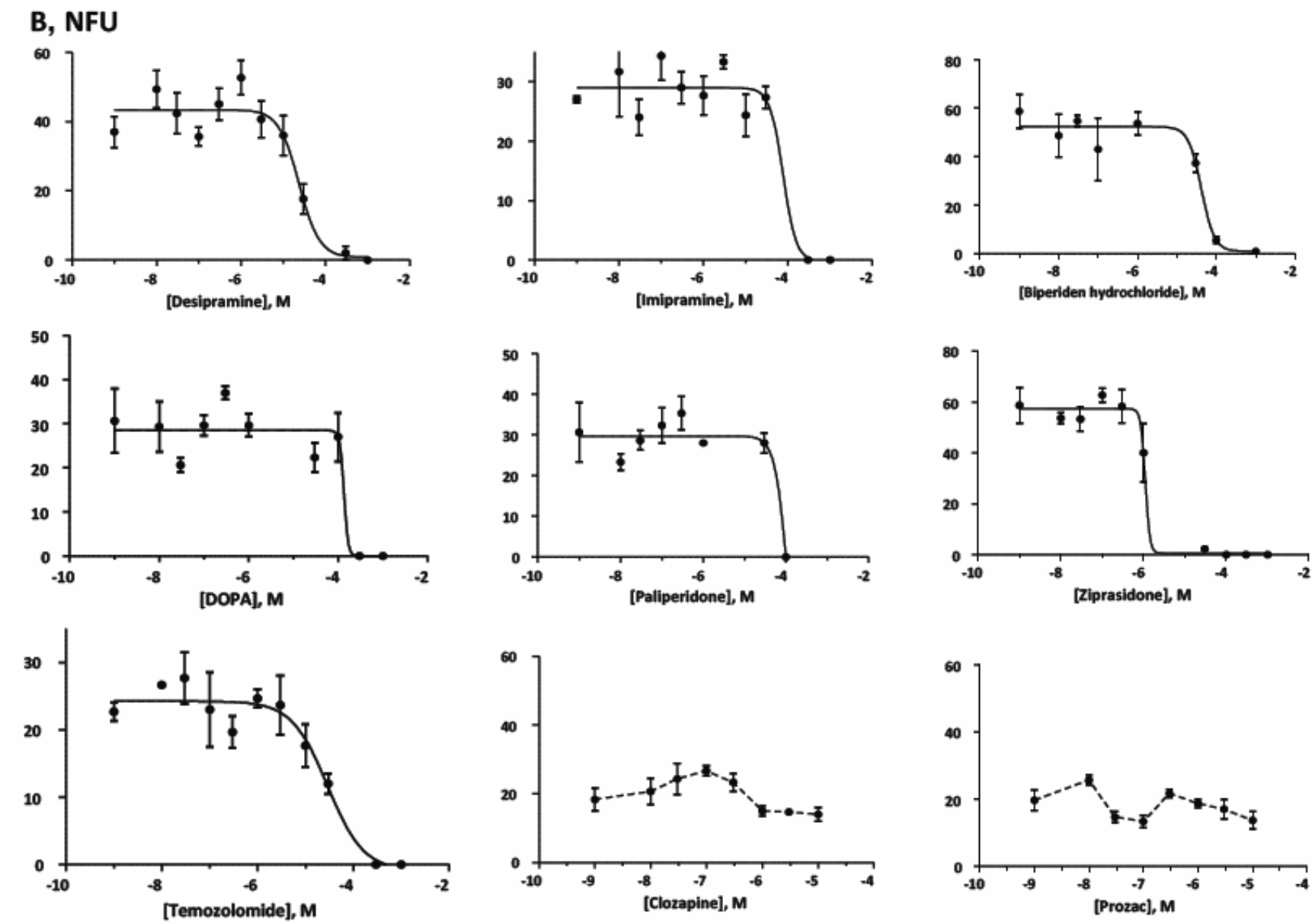
B, NFU
[Desipramine], M
[Imipramine], M
[Biperiden hydrochloride], M
[DOPA], M
[Paliperidone], M
[Ziprasidone], M
[Temozolomide], M
[Clozapine], M
[Prozac], M

C, Neurosphere size

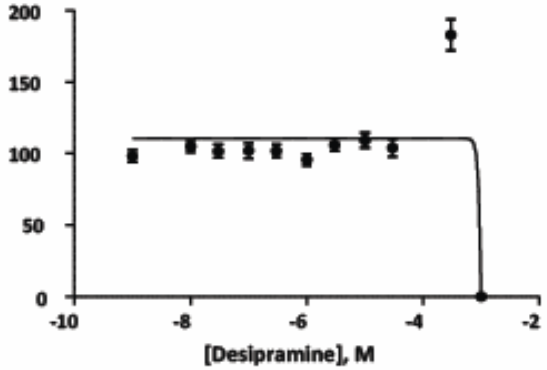

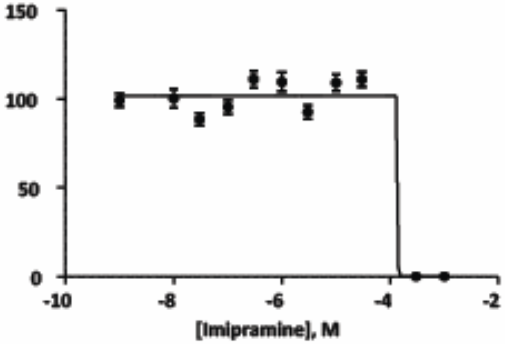

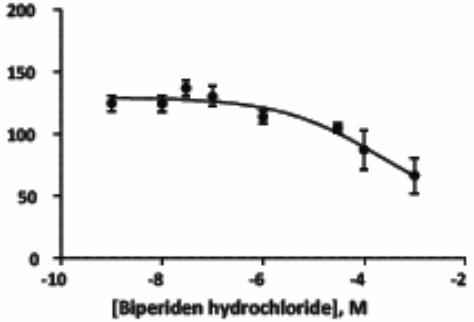

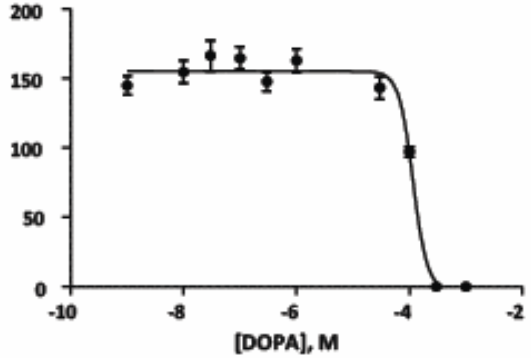

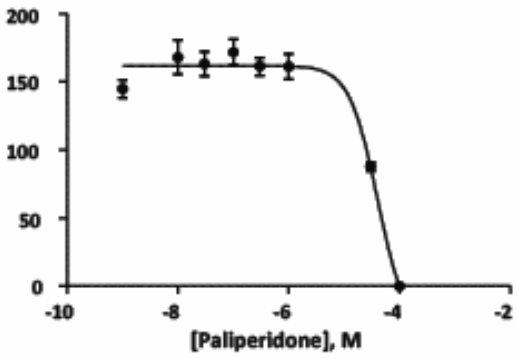

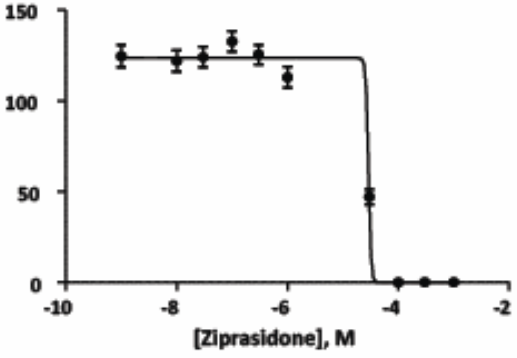

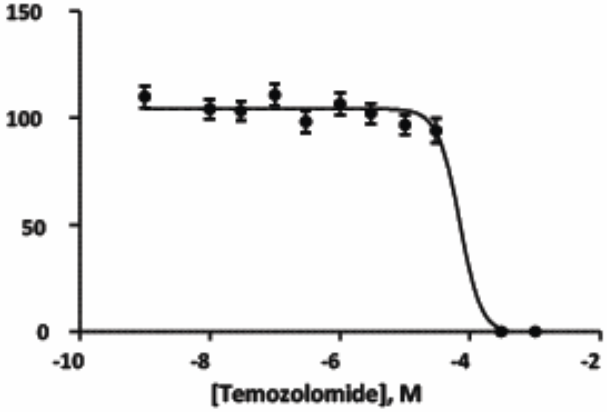

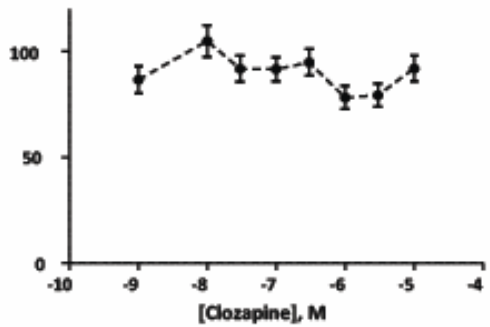

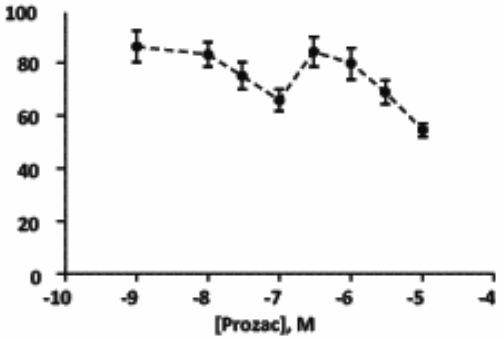

D, GFP intensity

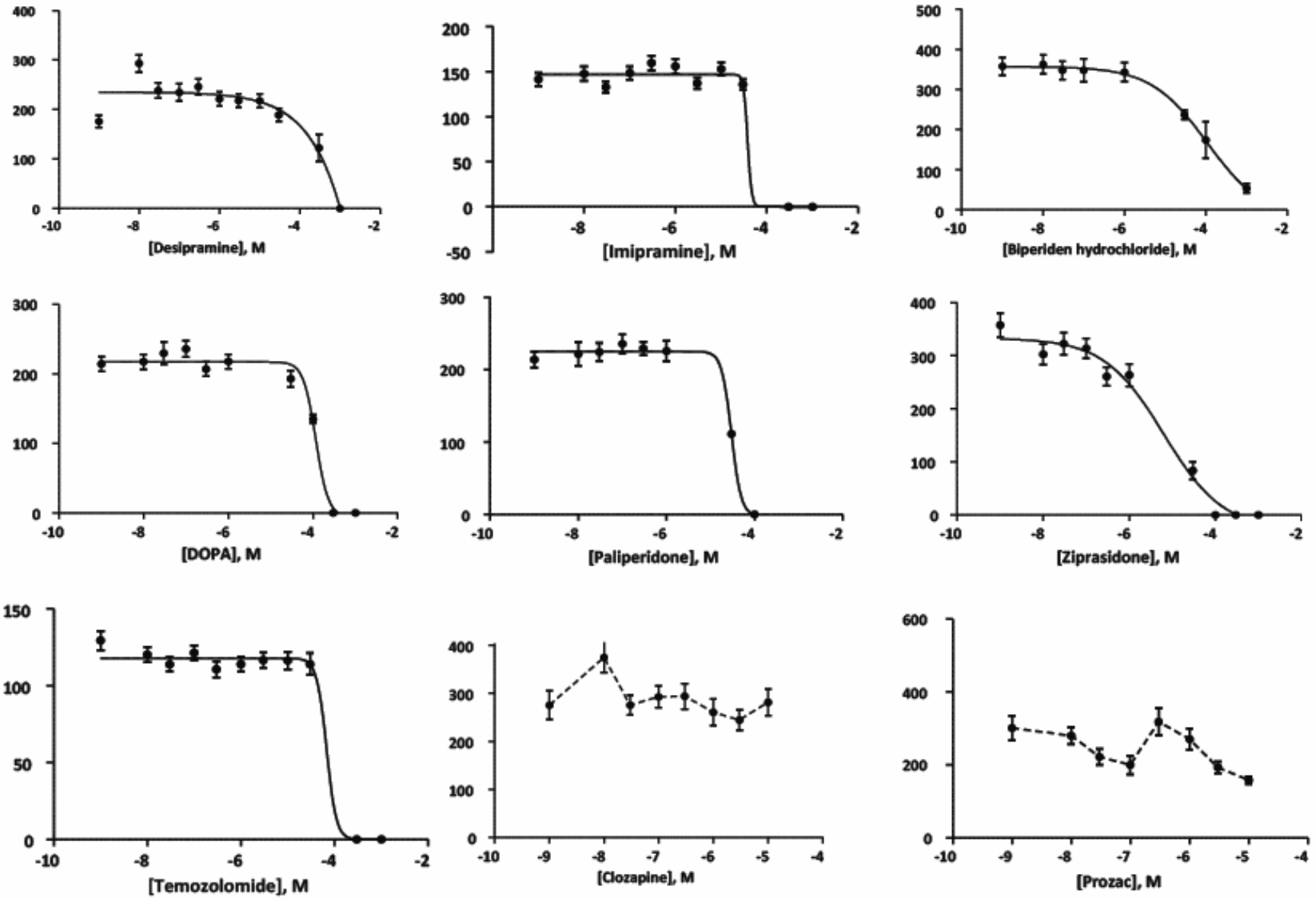

3.8.4. Use of brightfield and phase imaging modalities in a HTS assay

HCS and HTS assays depend on the use of fluorescent markers for sample imaging and analysis. NSCs/NPs are highly sensitive to exposure to fluorescent light and cannot be re-used once imaged with fluorescently labelled markers. In order to allow imaged samples to be used for downstream analysis, use of non-interfering and non-toxic imaging modalities is essential. For this reason a novel approach using phase contrast and brightfield imaging modalities were developed for use in HTS assays involving NSCs/NPs. We reported the sensitivity and prediction rates for the phase contrast modality to be 99.58 and 72.28, respectively (Xiong et al., 2011). However, in the phase contrast mode several neurospheres lying on the periphery of the well were not detected by the segmentation method. Besides phase contrast posed the added problem of uneven illumination within wells, and between different wells of the same plate which led us to explore the use of brightfield imaging modality for image acquisition and segmentation.

Unlabelled day 5 neurospheres were imaged in the brightfield mode (figure 5.4) using the Screen acquisition feature in Metamorph. Images of 480 sites which included 32 wells with 738 neurospheres were tested with the novel segmentation method (M0) and compared to ground truth (GT). The sensitivity and positive prediction rates for the brightfield modality were determined to be 89.13 and 82.25, respectively. Further improvements to sensitivity and detection would allow the novel segmentation method to be applied on images generated by the HTS assay without the use of fluorescent labels.

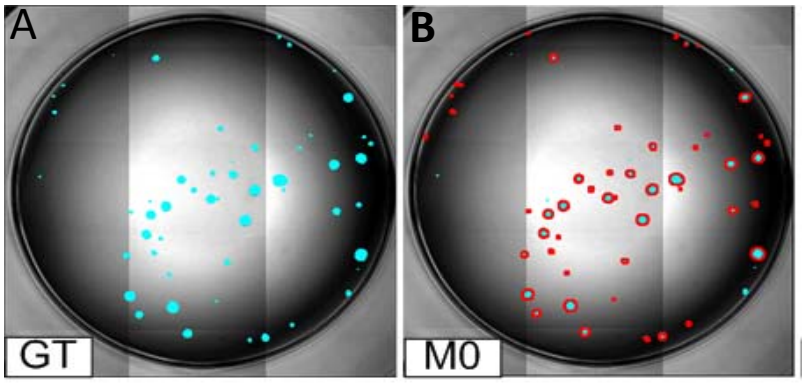

Figure 5.4. Development of label-free segmentation methods for HTS.
Neurospheres cultured in 96 well plate were imaged in brightfield modality. Segmentation results of neurospheres in a single well are shown. In (A), the blue dots outline the contours of the cells labelled in the ground truth (GT). Segmentation results obtained from the application of the new method (MO) are represented as red dots in (B).

4. DISCUSSION

NSCs/NPs are cells that can give rise to neurons, astrocytes and oligodendrocytes. *In vitro* they form 3-D clusters called neurospheres (Reynolds et al., 1992; Weiss et al., 1996). Neurospheres are heterogeneous in composition consisting of NSCs, NPs, and differentiated cells. In this thesis I have outlined the use of non-invasive imaging as a powerful tool to investigate the properties of NSCs/NPs and neurospheres. I have investigated the 3-D architecture of neurospheres, characterised the NFC, developed a purification method that yields 100% NSCs, and discussed the use of a HTS assay to study the effects of drugs on neurosphere cultures.

4.1. 3-D imaging of neurospheres

In animal tissues cells are connected to one another and to an external structure called the ECM. The ECM which is composed of proteins such as laminin, collagen, and elastin enables communication between cells and the external environment by means of receptors such as the integrins. Compared to 2-D culture, 3-D culture is physiologically more relevant as shown by studies on cancer cell biology, metastasis, and drug resistance (Weaver et al., 1997; dit Faute et al., 2002). For successful 3-D imaging a number of parameters need to be considered including the imaging modality, size of the sample, penetration and stability of dyes used, and image analysis algorithms.

Neurospheres grow as 3-D cultures but not much is known about their 3-D architecture. Hence, in an effort to understand the 3-D architecture of the neurosphere I imaged fluorescently-labelled live neurospheres in 3-D on different

imaging modalities and applied a novel segmentation algorithm to derive quantitative information from the 3-D structure. I describe how quantitative analysis of the 3-D images provides insight into the structure and organisation of a growing neurosphere.

4.1.1. Comparison of microscopes for 3-D neurosphere imaging

To study the 3-D structure of the neurosphere it was important to determine the microscope that could generate 3-D image stacks without adversely affecting cells or causing rapid bleaching. Images were acquired on LSCM and SDC microscopes and compared. I found that the Olympus FV1000 LSCM produced 3-D images of neurospheres with clearly visible individual cell contours. The images thus acquired would be amenable to segmentation by automated segmentation algorithms. For this reason the Olympus FV1000 LSCM was used for 3-D neurosphere imaging. Recent advances in 3-D imaging techniques allow multi-angle 3-D imaging of live whole embryos (Keller et al., 2008). Samples imaged by DSLM displayed an isotropic view in addition to increased light penetration. Most importantly, imaging on the DSLM significantly reduced bleaching and phototoxicity (data not shown). The DSLM is therefore a superior system for imaging 3-D cluster of cells such as neurospheres.

4.1.2. Labelling of live cells

For live labelling of cells and subcellular structures in the neurosphere it is important that the dyes are able to penetrate the 3-D structure and label individual cells. To test this various membrane and nuclear dyes were used to label neurospheres. Among the nuclear dyes, Hoechst 33342 produced consistent

nuclear labelling and was least prone to bleaching. All the commonly used membrane dyes produced punctate staining in the cytoplasm apart from weak membrane labelling in neurospheres. Incubation of the sample at 4°C or addition of PAO prior to the addition of the dye did not improve membrane labelling and the cytoplasmic punctae persisted. Hence, neurospheres transfected with eYFP-PMT were used for 3-D imaging since it was found to be the best membrane label for NSCs/NPs.

4.2. Segmentation by EGVD

Segmentation is the process by which the boundaries of objects are delineated. To allow the extraction of information from 3-D images of a neurosphere, individual nuclei and cells need to be segmented. EGVD was used for the segmentation of neurosphere images. Use of Hoechst 33342 to mark the nuclei in neurospheres allowed the cell centres to be identified with 90% accuracy. Since the intensity of the eYFP-PMT signal that labelled the plasma membrane was non-uniform an edge detector called phase congruency was used to detect the edges based on phase rather than magnitude. Nuclei and cell membrane were thus efficiently segmented by EGVD. EGVD was shown to produce a higher segmentation accuracy compared to commercially available software packages (Yu et al., 2010). Hence, EGVD is an efficient segmentation algorithm that can be applied on 3-D neurosphere images even when membrane markers displaying non-uniform intensity profiles are used for labelling.

4.3. Quantitative analysis of the neurosphere structure

Following segmentation by EGVD quantitative measurements of several neurosphere features such as cell size, cell number, cellular and nuclear volumes were obtained. Analysis of the neurosphere in 3-D provides insight into its architecture. To ensure reproducibility of results in a given *in vitro* setting, it is important to understand the culture system and maintain the 3-D neurosphere structure if the information is to be relevant.

For a typical immunocytochemistry procedure neurospheres are fixed and then labelled with specific markers for confocal microscopy. Using fixatives on cells kills them and may even introduce artifacts. For this reason live neurospheres were immobilized in a hydrogel that is transparent to allow imaging while simultaneously providing the biochemical matrix to keep the cells alive during imaging. All 3-D imaging was performed on neurospheres embedded in 2% hydrogel.

Quantitative analysis of the reconstructed 3-D neurosphere images revealed that cell number increased exponentially to the size of the neurosphere. This in turn was a direct reflection of the number of days the neurosphere were in culture. The doubling time was derived from the growth curve to be 24 h. One of the most widely employed methods for estimating the number of live cells in a population is the adenosine triphosphate (ATP) assay. This method is based on the principle that ATP is an indicator of metabolically active cells; the ATP concentration reflects whether a cell is live or necrotic. A major limitation of this method is that the assay requires the cells to be lysed for the endogenous ATP to be accessible rendering

them unusable for further downstream analysis. With EGVD-based segmentation it is possible to accurately estimate cell numbers in growing neurospheres.

The study of the relationship between cell and nuclear volumes and cell number showed that the average cell and nuclear volumes decreased significantly with increasing cell number. Cells likely experience tension and forces from the neurosphere structure directly and hence display a more rapid decrease in volume compared to nuclei. As cell numbers increase it is likely that greater forces are required to bind individual cells as well as the neurosphere structure together. Nuclei on the other hand, buffered by the presence of the cytoplasm and cell membrane around them demonstrate a less drastic change in volume. The nuclear/cell volume ratio shows an initial increase with cell number followed by a plateau. This likely indicates that as the neurosphere grows pressure increases preventing expansion of the cytoplasm. The nuclei are more stable presumably because they pack the same amount of chromatin as before. The nuclear/cell volume ratio showed an initial peak under low density conditions. Under bulk conditions the nuclear/cell volume ratio displayed a less rapid rise which was followed by a plateau, and this is indicative of the involvement of aggregation events.

The probability distribution function of cell and nuclear sphericity showed that in a given cell population nuclei were more rounded relative to cells over time. This can again be attributed to the 'shielding' effects of the cytoplasm and plasma membrane on the nuclei, as well as the absence of direct contacts with other nuclei or substrate. Although cells exhibited initial variations in sphericity, as the

neurosphere grew bigger cell sphericity stabilised at an average value of 0.6. Sphericity was also found to have an effect on the position of a cell within a neurosphere. Cells with smaller sphericity and nuclear/cell volume ratios were located closer to the centre of the neurosphere hinting at the effects of tension and forces produced by the growing neurosphere structure on the cells contained within.

I have thus demonstrated that high resolution 3-D imaging of neurospheres can be performed and the resulting 3-D images can be segmented efficiently to provide information about the 3-D architecture of the neurosphere. Next, I sought to study the behaviour of single NSCs/NPs in an effort to correlate feature of the single cell with neurosphere formation and multipotency.

4.4. Salient features of NFCs and NSCs

The NFU in a control population of NSCs/NPs is typically in the range of 10-15% (Gan et al., 2011) indicating that not all cells form neurospheres. Additionally, the NSC frequency within a culture is variable and could range from 0.07%-20% depending on the exact growth conditions used (Kim and Morshead, 2003; Tham et al., 2010; Gan et al., 2011). To enrich for NSCs/NPs several methods have been used. These include selection of cells based on gene expression (Kawaguchi et al., 2001; Sunabori et al., 2008), binding to peanut agglutinin (PNA) (Rietze et al., 2001), and expression of surface receptors (Johansson et al., 1999; Uchida et al., 2000; Ciccolini et al., 2005; Capela and Temple, 2006; Corti et al., 2007). Surface receptors have been widely used to select for specific cell populations. Some of the

more commonly used surface markers for NSCs/NPs include CD15, CD133, EGF receptor, and Notch 1. The methods mentioned above have been used successfully to yield pure populations of NSCs/NPs to varying degrees. However, a 100% pure population of NSCs has proven elusive.

The first step towards enriching for a pure NSC population *in vitro* is to isolate cells that are able to form neurospheres. What are the features of cells that successfully form neurospheres? There is a lack of markers to definitively distinguish NSCs from NPs *in vitro*. I hence set out to analyse features of single cells and their behaviour during neurosphere formation to determine if they could potentially be used to distinguish between NSCs and NPs. Moreover, information on neurosphere formation and multipotency can be used to estimate the NSC frequency within the culture (where, NSC frequency = NFU x % of multipotent neurospheres), and this was used to predict the NSC frequencies in purified cell populations.

In this section, I have used a combination of time-lapse analysis, study of the mode of cell division, and mRNA profiling to distinguish the NFC from the others.

4.4.1. Time-lapse analysis of neurosphere formation

4.4.1.1. Challenges of imaging live NSCs/NPs

Since NSCs/NPs grow as suspension cultures it raises a number of challenges for long-term videomicroscopy. Cell motility is one of the major issues with ~90% of the cells leaving the field of view within a few hours of imaging. To overcome this

problem an automated tracking method was developed (explained in the following section).

It would be very useful to observe neurosphere formation in cells labelled with fluorescent markers. Insight into cell division patterns, marker segregation, and lineage analysis can potentially be derived. However, I found that fluorescent illumination affected cell behaviour. For instance, cells labelled with eYFP-PMT, Cell Tracker Green CMFDA, or Actin-GFP cells when exposed to fluorescent illumination died. On the other hand, when the cells were left in the tissue culture incubator or in the microscope without being illuminated or imaged they proliferated and formed neurospheres. This suggests that NSCs/NPs are highly sensitive to fluorescent light exposure. Also, Hoechst 33342 could not be used for live cell imaging of NSCs/NPs. Labelled cells either stalled in the cell cycle (single cells did not form doublets) or died (data not shown). Intriguingly, when NSCs/NPs were labelled for surface markers such as Phosphacan, LeX or C1qR1, exposure to fluorescent light did not kill them (data not shown). Marker-labelled cells proliferated normally and form neurospheres. One possible reason that cells labelled with intracellular markers (eYFP-PMT, Cell Tracker Green CMFDA) died when exposed to fluorescent light could be due to the generation of free radicals within the cell. Use of surface markers probably overcomes this problem thus limiting cytotoxicity. The use of surface markers to study the behaviour of NSCs/NPs during cell division is currently under investigation.

4.4.1.2. Automated tracking of NSCs/NPs over time

Tracking of suspension cells is a difficult problem to tackle. The only method to ensure that the cells are maintained in the field of view for the duration of imaging is for the operator to manually adjust the stage positions, which makes the exercise impractical for imaging that is spread over 5-7 days. To address this issue, a number of methods have been reported. The most commonly used techniques to overcome the problem of cell motility are physical entrapment using microwells (Guldevall et al., 2010), and use of fluorescence to track single cells (Rabut and Ellenberg, 2004). Although some studies have suggested biomarker-free visual tracking algorithms (Langehanenberg et al., 2009), they have certain disadvantages. For instance, dependence on specialized equipment (Langehanenberg et al., 2009) could result in high costs or they might only be suitable for adherent cells. Hence, there was a pressing need to devise a method that could track live cells in suspension during prolonged time-lapse image acquisitions.

A novel online tracking algorithm thus developed in collaboration with Chaohui Huang and Hwee Kuan Lee at BII was integrated within an operational system (Huang et al., 2012). The algorithm utilises information solely from phase contrast images without the need for fluorescent dyes and has been successfully implemented to track NSCs/NPs in time-lapse experiments lasting 5-7 days. NSCs/NPs are thus retained within the field of view during continuous image acquisition.

4.4.2. Enriching for NFCs

The occurrence of low NFUs in neurosphere cultures necessitated the enrichment of NFCs, which is an essential pre-requisite for analysis by time-lapse videomicroscopy. Low NFUs require that a bigger starting pool of cells be used. An optimal solution is to begin with a population of cells that will yield a higher NFU. It was found that cells selected for the surface markers CD15 and C1qR1 were enriched for NFCs (Mike Yu and Sohail Ahmed, unpublished data). Hence CD15+/C1qR1+ double selected cells made the time-lapse imaging experiments viable.

Identification and characterisation of the NFC requires clonal expansion. This is to overcome aggregation events that occur in bulk density conditions of neurosphere propagation (Singec et al., 2006; Mori et al., 2007; Coles-Takabe et al., 2008). CD15+/C1qR1+ were used at a clonal density of 100 cells/mL in a 96 well plate format, where 100% of the neurospheres generated are clonal (Gan et al., 2011).

4.4.2.1. Big cells form more neurospheres

The relationship between morphological features of the single cell such as cell size and their correlation to neurosphere formation has not been fully explored. A number of previous studies have attempted to test the existence of such a correlation. For instance, cells with a FSC^{high}/SSC^{high} profile were found to be enriched for NSCs (Murayama et al., 2002). A similar enrichment was found in cells isolated by the Hoechst 33342 exclusion-side population method (Kim and Morshead, 2003).

Although the side population strategy has been used by several groups for isolating stem cells from different tissues, it was subsequently shown that it was not specific for NSCs since they were contained in a population distinct from the side population (Mouthon et al., 2006). Hence, to directly interrogate the relationship between cell size and neurosphere formation single cell size at day 0 was measured and correlated to neurosphere formation on day 5. Cells >10 μm in size were found to have an NFU that is at least four times higher than that of cells <10 μm suggesting that cell size can be used to enrich for NFCs.

4.4.2.2. Cell dynamics as a predictor of neurosphere formation

Comparison of cell movement over the first 24 h of imaging showed that NFCs were more motile than the other groups of cells. To see if cell movement could predict cell fate, individual cell tracks generated by the tracking algorithm were used to predict neurosphere formation or death. I found that cell motility could predict cell fate with an accuracy of 60%. NFCs display higher motility relative to dying cells. Assessment of cell motility and its correlation to multipotency would provide clues to the behaviour of NSCs. This study could be extended to evaluate motility of normal NSCs and BTSCs in the light of the observation that stem cells with increased motility are involved in metastasis (Palmer et al., 2011).

4.4.2.3. NFCs have a shorter doubling time

Under culture conditions used in this study, the average doubling time for the NFCs was calculated to be 18.5 h whereas it was 1.6 times longer for cells that

died after two divisions. Hence, during time-lapse analysis of NSCs/NPs cells with a doubling time >24 h can be excluded from analysis on the basis that they will die after the second division.

4.4.2.4. NFCs are phase bright

Imaging of cells in the phase contrast mode allowed the measurement of the phase intensity of individual cells. I found that cells with bright phase intensity in combination with the CD15+/C1qR1+ profile yielded 100% NFU. By setting a threshold for the phase intensity at >200 gray values non-NFCs could be easily excluded from the analysis.

It is known that NSCs/NPs secrete proteoglycans into the culture medium during growth and proliferation (Kabos et al., 2004; Tham et al., 2010). Could the halo then reflect enhanced proteoglycan secretion? This can be investigated by using specific CSPGs epitopes such as 473HD, which was shown to correlate with increased neurosphere formation (von Holst et al., 2006). Hence it is worth testing 473HD in combination with CD15+/C1qR1+ selection to evaluate NFC enrichment.

4.4.3. Evaluation of multipotency

4.4.3.1. Relevance of surface marker distributions to multipotency

Several studies have demonstrated asymmetric division to be a defining characteristic of NSCs in invertebrates as well as mammals. When a stem cell

divides to generate another stem cell (self-renewal) along with a fate-limited, or a differentiated daughter cell it is said to be undergoing asymmetric cell division. Symmetric divisions on the other hand, give rise to two daughter cells that are identical to each another. The balance between self-renewal and differentiation characterises embryonic growth and development as well as homeostasis in adults (Roegiers and Jan, 2004; Huttner and Kosodo, 2005; Knoblich, 2008). The balance is critical to ensuring normal development since aberrations in this process could lead to tumours (Neumuller and Knoblich 2009).

Neurospheres were observed to display uniform and non-uniform distribution of markers such as eYFP-PMT, CD15 and C1qR1. I was interested to investigate if the type of cell division as indicated by the marker distribution patterns reflected neurosphere forming potential and multipotency. To assess the correlation between uniform and non-uniform marker distributions and neurosphere potency, neurospheres labelled with CD15 and C1qR1 antibodies were imaged and manually selected for a clonal differentiation assay. The clonal multipotency assay revealed that non-uniform CD15/C1qR1 distribution in neurospheres was 7 times more likely to yield multipotent neurospheres than uniform distribution, suggesting that non-uniform marker distribution does indeed indicate potency of the neurosphere.

4.4.3.2. Features of the single cell and multipotency

Enriching for NFCs based on cell size showed that cells >10 μm yielded higher NFUs. The NFU was further enriched when a phase intensity filter of >200 gray

values was imposed on the CD15+/C1qR1+ cells as a selection criterion. How did cell size and phase intensity impact the potency of the neurospheres formed? The CD15+/C1qR1+/Phbrt+ cell population was found to be 72% multipotent. When the threshold for phase intensity was extended further to >240 gray values, the multipotency rose to 100%. The single cells that formed multipotent neurospheres in this population were found to be >13 μm. These results suggest that a combination of cell size and phase intensity can be used to select specifically for NSCs *in vitro*.

4.4.4. Purification of NSCs

The NSC frequency can be estimated from NFU and multipotency values. The NSC frequency in neurosphere cultures have been enumerated in a number of earlier studies (Rietze 2001; Capela 2002; Kim 2003). However, the cells used in these studies were propagated under bulk density conditions. The N-CFCA has also been used to estimate NSC frequency by using the size of the colony as an indicator of the presence of NSCs (Louis 2008). There are a number of disadvantages to both approaches. While NSC frequencies obtained from bulk density neurosphere culture tend to overestimate the presence of NSCs (Reynolds and Rietze, 2005), colony size may in the N-CFCA may not be a true indicator of NSC activity since the assay overlooks the property of stem cell quiescence. For instance, a study showed that the astroglial stem cell was activated to repopulate the SVZ only after anti-mitotic treatment (Doetsch et al., 1999). Although eNSCs are required to proliferate rapidly to give rise to the different cell lineages of the developing brain, the possibility that NSCs in culture undergo a series of divisions before turning quiescent cannot be excluded.

Clonal NSA and multipotency tests allow the accurate estimation of NSC frequency. The NSC frequency of the CD15+/C1qR1+/Phbrt>240+ cell population assessed under clonal cell density conditions was found to be 100%, which is the highest enrichment for NSCs *in vitro.*

4.4.5. NSC purification by imaging- implications for future work

I have described a novel method of enriching for NSCs by using a combination of FACS- and imaging-based purification. CD15+/C1qR1+/Phbrt>240+ cell population was found to consist 100% of NSCs. However, this method of NSC purification has certain limitations. These include manual analysis and low yield of NSCs. Since the population consisting 100% NSCs constitutes <0.2% of the total cell population the number of cells that would have to be manually screened and the time taken for image-based screening is very high. In effect, there is an immediate need for automated screening of vast numbers of cells.

While the hunt for surface and intracellular stem cell markers for FACS-based purification is bound to persist, it is necessary to evaluate the NSCs from an alternate perspective in parallel. Imaging single cells at high resolution can often provide clues that might not be forthcoming from other approaches. In HSCs for instance, the projections on the leading edge and cell periphery are believed to be one of the defining stemness features (Frimberger et al., 2001). Hence, a computational strategy that can identify unique single cell features that link to neurosphere formation and multipotency would be invaluable to the screening

process. An algorithm with such capabilities is currently under development in collaboration with Chaohui Huang and Hwee Kuan Lee (BII, Singapore). The hope is that a single image of the single cell would be sufficient to predict its fate and affirm its identity as an NSC or NP.

4.4.6. mRNA profile

Single cell RNA profiling is a popular method to identify different cell types within a population. A recent study found the existence of different progenitor subclasses within neurospheres (Narayanan et al., 2012). Cluster analysis of cells with similar mRNA profiles showed that the molecular signature of the different groups of cells could be extracted. To uncover the signature of the CD15+/C1qR1+/Phbrt+ cells they were analysed by scPCR by using a panel of 48 genes associated with NSCs/NPs. Expression of genes involved in the regulation of stem cell behaviour such as *Notch1*, *Pax6*, *Jag1*, and *Prominin* was higher in CD15+/C1qR1+/Phbrt+ cells. The roles of *Notch1* and *Pax6* in early brain patterning, NSC self-renewal, neuronal specification and migration are well established (Osumi, 2001; Lasky and Wu, 2005). *Jag1* plays a crucial role in self-renewal, proliferation and maintenance of NSCs in their undifferentiated state (Nyfeler et al., 2005). Expression of other genes such as *BLBP*, *NFIX*, *Tead2*, *NFIA*, *NFIB* and *POU3F3* was also slightly upregulated in CD15+/C1qR1+/Phbrt+ cells. Their exact function in NSC growth and behaviour is however unclear. Further work is required to study and understand the roles of these genes in NSC development and maintenance.

Among the genes that showed unexpected changes in the CD15+/C1qR1+/Phbrt+ cells are *Sox9*, *Mash1,* and *Dll1*. *Sox9* and *Mash1* regulate cell differentiation in the developing CNS (Torii et al., 1999; Stolt et al., 2003; Hagiwara, 2012) and showed a positive change in expression in CD15+/C1qR1+/Phbrt+ cells compared to unsorted cells. Similarly, the expression of *Dll1* was found to be higher in CD15+/C1qR1+/Phbrt+ cells, although single cell analysis had revealed low *Dll1* expression in the NSC cluster (Gunaseelan Narayanan and Sohail Ahmed, unpublished data). The reasons for these observed inconsistencies in the mRNA profile of CD15+/C1qR1+/Phbrt+ cells could be because i) results are from a single scPCR analysis of CD15+/C1qR1+/Phbrt+ cells, ii) CD15+/C1qR1+/Phbrt+ could be a heterogeneous mix of NSCs and more fate-restricted NPs, hence, a purer population of cells needs to be analysed, iii) the current method of comparison uses unsorted cells which has a low NSC frequency. Perhaps comparison with a cell population that consists predominantly of early/late progenitors is necessary to definitively identify genes associated with a pure NSC population. Thus scPCR analysis of NSCs/NPs warrants a more thorough investigation.

Single cell mRNA profiling is a potentially useful method to help decipher the molecular signature for *bona fide* NSCs. This can be further applied to the identification of genes required for NSC identity and help tease out their functions in NSC survival and proliferation.

4.5. HTS

NSCs hold considerable promise for the development of therapies against tumours and other neurodegenerative disorders such as AD, PD, schizophrenia, and depression (Lindvall et al., 2004). Since the discovery of the BTSC (Singh et al., 2003), efforts to find suitable anti-tumour therapies have been re-aligned to focus on NSCs. Moreover, a number of studies are beginning to uncover a correlation between the low incidence of cancers in patients receiving treatment for neuropsychiatric disorders (Dalton et al., 2002; Barak et al., 2005; Grinshpoon et al., 2005; Diamandis et al., 2009). Moreover, the importance of NSCs as stem cell therapy models for diseases such as stroke is invaluable (Choi, 2007). Replacement of specific neurons would address multiple issues such as reconstruction of neural circuits, aiding the release of neurotransmitters or enzymes, correcting biochemical deficits, and acting as support cells providing neurotrophic factors.

Most HCS and HTS assays rely on the use of immortalised cell lines to study the effects of drugs. While this is invaluable, it is important to assess the effects of novel compounds and drugs on 3-D culture systems for the results to be physiologically relevant. The ease of culture of NSCs/NPs *in vitro* permits the evaluation of large scale drug screens. An automated HTS assay was thus developed and tested on neurosphere cultures.

4.5.1. Design of the HTS assay

A typical HCS or HTS assay consists of the following steps: image acquisition, image processing, and data output. Image acquisition depends on the

instrumentation and the software driving the process. Image processing relies heavily on the type of images produced for analysis. For instance, images of several neurospheres spread over multiwell dishes necessitated the development of a content-specific analytical strategy. This led to the development of a HTS assay on the Metamorph platform.

In the newly developed HTS assay fluorescently labelled neurospheres were first imaged and segmented followed by quantification of the required parameters such as NFU or fluorescence intensity. Segmentation was carried out in a two-step process. First, images pertaining to a single well were stitched together, followed by global stitching of all the wells in a given multiwell dish. Image segmentation was followed by automatic quantification of the read-out in the form of neurosphere numbers and fluorescence intensity making the HTS assay easy and convenient to use.

4.5.2. Testing the HTS assay on neurospheres

To test the efficacy of the HTS assay on neurospheres a proof-of-principle analysis was performed using Ifenprodil (Diamandis et al., 2007). In their study Diamandis et al. found that Ifenprodil, a clinically prescribed glutamate antagonist was one of the most potent anti-BTSC agents. Tests with Ifenprodil on E14.5 NSCs/NPs showed that the EC_{50} dose could reduce both NFU as well as *Sox2* promoter activity. The HTS assay to assess changes in NFU and gene expression was reproducible and produced consistent results and can potentially be applied on larger drug screens using NSCs/NPs.

4.5.3. Effects of neuromodulatory drugs on E14.5 NSCs/NPs

Optimisation of the HTS assay allowed the testing of the effects of various neuromodulatory drugs on E14.5 NSCs/NPs (summarised in table 2). The list included drugs that are prescribed for treating schizophrenia, depression, PD, and gliomas. All the drugs tested with the exception of two (fluoxetine and clozapine), negatively impacted NFU, neurosphere size, and *Sox2* promoter activity. The results demonstrate the effects of prescribed neuromodulatory drugs on E14.5 NSCs/NPs. The effect on *Sox2* promoter activity is of particular interest since Sox2 is an established stem cell marker (Ellis et al., 2004). Current results demonstrate the effects of the drugs on the transcriptional activity of *Sox2*. Further work assessing the effects of the drugs on Sox2 protein levels would be invaluable.

Current results with the neuromodulatory drugs are interesting in the light of recent observations on reduced cancer incidence in patients treated for neuropsychiatric disorders (Dalton et al., 2002; Barak et al., 2005; Grinshpoon et al., 2005; Diamandis et al., 2009). Although evaluation of the correlation in these reports was done by means of retrospective studies, they likely hint at the effects of neuromodulatory drugs on NSC pools in the patient. It has been speculated that protection against cancer could arise from the depletion of NSC pools targeted by the drugs used for treatment (Diamandis et al., 2009). This is consistent with the current findings of lower neurosphere numbers in drug treated cell populations. However, whether the drugs specifically target the NSCs or both NSCs and NPs is not evident in the current results and needs to be examined by carrying out NSA and multipotency assays on control and drug treated neurospheres.

The drugs that did not show any effects include fluoxetine (depression) and clozapine (schizophrenia). The target of fluoxetine, which is commonly known as Prozac has been elucidated. In the adult brain, it was found to specifically target symmetrically dividing neural progenitors and not stem-like cells in the dentate gyrus (Encinas et al., 2006). Also noteworthy is the finding that fluoxetine did not affect the neural stem and precursor cells in the SVZ. This could potentially explain the lack of effects of fluoxetine on eNSCs/NPs used in this study. Moreover, since it works by specifically promoting neurogenesis in the adult DG (Jacobs et al., 2000) changes in NSC numbers or marker expression patterns in the SVZ are probably unlikely.

The reasons for the lack of effects on NSCs/NPs using clozapine are unclear. Clozapine has a range of effects on cell signalling; of note are its dopamine receptor and α-adrenergic blocking abilities (Naheed and Green, 2001). Perhaps effects on growth of NSCs/NPs fall beyond the realm of its mode of action.

4.5.4. Label-free assay

Current methods to follow neurospheres with fluorescent markers limit subsequent analysis because neurospheres are killed from exposure to fluorescent light. Non-fluorescent imaging modalities would circumvent this problem. In this regard, in collaboration with Shue Ching Chia and Wei Xiong at I^2R, use of phase contrast (Xiong et al., 2011) and brightfield imaging modalities have been developed. Samples are imaged on a microscope equipped with live cell supporting system and can hence be used for downstream analysis following image acquisition.

4.6. Conclusions and future work

In this thesis I have demonstrated the power of imaging techniques to investigate the behaviour of NSCs/NPs as single cells and in 3-D culture. Investigating single cells has the advantage that subpopulations can be followed and distinguished from the bulk. From work on single cells I have been able to generate an mRNA signature for NSCs. This could potentially be useful in identifying NSC markers that could be used for isolation and purification of NSC populations. Most importantly I have been able to purify NSCs to 100% by using a combination of cell surface markers and phase intensity. NSC biology can now be investigated in detail with a pure population of cells.

Future studies should focus on extending the assays and techniques that have been developed in the current work to address several important questions pertaining to the growth, behaviour, and response to external stimuli of NSCs/NPs *in vitro*. Firstly, how do mechanical forces impact on the behaviour and response of NSCs/NPs? This can be investigated by analysing the characteristics of neurospheres cultured in hydrogels of varying stiffness. Cross-linking in the Gtn-HPA polymers is achieved by using HRP and H_2O_2, which can be used in varying concentrations to control gelation rate and degree of cross-linking. Furthermore, 3-D analysis of cells isolated from tumourigenic tissues would provide glimpses into the architecture and organisation of tumour versus normal neurosphere cultures. Secondly, analysis of aspects of NSC behaviour such as cell movement and single cell morphology can be used to develop an automated method to identify and purify NSCs without the need for fluorescent labelling methods. Thirdly, label-free HTS assays would allow further downstream analysis of samples that have been

imaged thus circumventing the current practice of using fluorescent biomarkers. A combination of 3-D analysis of NSCs/NPs in a HTS assay would be a powerful method to evaluate the effects of candidate drugs on NSCs/BTSCs providing valuable results that would be more physiologically relevant.

PUBLICATIONS

1. Lee HK, Uddin MS, **Sankaran S**, Hariharan S, Ahmed S. 2009. A field theoretical restoration method for images degraded by non-uniform light attenuation: an application for light microscopy. Opt Express17:11294–11308.
2. Yu M, Lee HK, Hariharan S, **Sankaran S**, Vallotton P, Ahmed S. 2009. Segmentation of Neural Stem/Progenitor Cells Nuclei within 3-D Neurospheres. International Symposium on Advances in Visual Computing (1) 2009: 531-543.
3. Xiong W, Chia SC, Lim JH, **Shvetha S**, Ahmed S. 2011. Detection of unstained living neurospheres from phase contrast images with very large illumination variations. Conf Proc IEEE Eng Med Biol Soc 6154-6157.
4. Huang CH, **Sankaran S**, Racoceanu D, Hariharan S, Ahmed S. 2012. Online 3-D tracking of suspension living cells imaged with phase-contrast microscopy. IEEE Trans Biomed Eng 59:1924-1933.
5. Narayanan G, Poonepalli A, Chen J, **Sankaran S**, Hariharan S, Yu YH, Robson P, Yang H, Ahmed S. 2012. Single-Cell mRNA Profiling Identifies Progenitor Subclasses in Neurospheres. Stem Cells Dev 21(18):3351-62.
6. Rigaud SU, Loménie N, **Sankaran S**, Ahmed S, Lim JH, Racoceanu D. 2012. Neurosphere fate prediction: An analysis-synthesis approach for feature extraction. IEEE International Joint Conference on Neural Networks: 1-7.

REFERENCES

Abbott A. 2003. Cell culture: biology's new dimension. Nature 424:870-872.

Ahmed S. 2009. The culture of neural stem cells. J Cell Biochem 106:1-6.

Altman J. 1969. Autoradiographic and histological studies of postnatal neurogenesis. IV. Cell proliferation and migration in the anterior forebrain, with special reference to persisting neurogenesis in the olfactory bulb. J Comp Neurol 137:433-457.

Altman J, Das GD. 1965. Autoradiographic and histological evidence of postnatal hippocampal neurogenesis in rats. J Comp Neurol 124:319-335.

Alvarez-Buylla A, Theelen M, Nottebohm F. 1988. Birth of projection neurons in the higher vocal center of the canary forebrain before, during, and after song learning. Proc Natl Acad Sci U S A 85:8722-8726.

Atkinson JM, Shelat AA, Carcaboso AM, Kranenburg TA, Arnold LA, Boulos N, Wright K, Johnson RA, Poppleton H, Mohankumar KM, Feau C, Phoenix T, Gibson P, Zhu L, Tong Y, Eden C, Ellison DW, Priebe W, Koul D, Yung WK, Gajjar A, Stewart CF, Guy RK, Gilbertson RJ. 2011. An integrated in vitro and in vivo high-throughput screen identifies treatment leads for ependymoma. Cancer Cell 20:384-399.

Avilion AA, Nicolis SK, Pevny LH, Perez L, Vivian N, Lovell-Badge R. 2003. Multipotent cell lineages in early mouse development depend on SOX2 function. Genes Dev 17:126-140.

Badr CE, Wurdinger T, Tannous BA. 2011. Functional drug screening assay reveals potential glioma therapeutics. Assay Drug Dev Technol 9:281-289.

Bao S, Wu Q, McLendon RE, Hao Y, Shi Q, Hjelmeland AB, Dewhirst MW, Bigner DD, Rich JN. 2006. Glioma stem cells promote radioresistance by preferential activation of the DNA damage response. Nature 444:756-760.

Barak Y, Achiron A, Mandel M, Mirecki I, Aizenberg D. 2005. Reduced cancer incidence among patients with schizophrenia. Cancer 104:2817-2821.

Barker N, van Es JH, Kuipers J, Kujala P, van den Born M, Cozijnsen M, Haegebarth A, Korving J, Begthel H, Peters PJ, Clevers H. 2007. Identification of stem cells in small intestine and colon by marker gene Lgr5. Nature 449:1003-1007.

Becker BE, Gard DL. 2006. Visualization of the cytoskeleton in Xenopus oocytes and eggs by confocal immunofluorescence microscopy. Methods Mol Biol 322:69-86.

Blanpain C, Fuchs E. 2009. Epidermal homeostasis: a balancing act of stem cells in the skin. Nat Rev Mol Cell Biol 10:207-217.

Brazel CY, Limke TL, Osborne JK, Miura T, Cai J, Pevny L, Rao MS. 2005. Sox2 expression defines a heterogeneous population of neurosphere-forming cells in the adult murine brain. Aging Cell 4:197-207.

Breier JM, Gassmann K, Kayser R, Stegeman H, De Groot D, Fritsche E, Shafer TJ. 2009. Neural progenitor cells as models for high-throughput screens of developmental neurotoxicity: state of the science. Neurotoxicol Teratol 32:4-15.

Bruggeman SW, Valk-Lingbeek ME, van der Stoop PP, Jacobs JJ, Kieboom K, Tanger E, Hulsman D, Leung C, Arsenijevic Y, Marino S, van Lohuizen M. 2005. Ink4a and Arf differentially affect cell proliferation and neural stem cell self-renewal in Bmi1-deficient mice. Genes Dev 19:1438-1443.

Bylund M, Andersson E, Novitch BG, Muhr J. 2003. Vertebrate neurogenesis is counteracted by Sox1-3 activity. Nat Neurosci 6:1162-1168.

Campos LS, Leone DP, Relvas JB, Brakebusch C, Fassler R, Suter U, ffrench-Constant C. 2004. Beta1 integrins activate a MAPK signalling pathway in neural stem cells that contributes to their maintenance. Development 131:3433-3444.

Capela A, Temple S. 2002. LeX/ssea-1 is expressed by adult mouse CNS stem cells, identifying them as nonependymal. Neuron 35:865-875.

Capela A, Temple S. 2006. LeX is expressed by principle progenitor cells in the embryonic nervous system, is secreted into their environment and binds Wnt-1. Dev Biol 291:300-313.

Carlson MW, Alt-Holland A, Egles C, Garlick JA. 2008. Three-dimensional tissue models of normal and diseased skin. Curr Protoc Cell Biol Chapter 19:Unit 19 19.

Cattaneo E, McKay R. 1990. Proliferation and differentiation of neuronal stem cells regulated by nerve growth factor. Nature 347:762-765.

Chalfie M, Tu Y, Euskirchen G, Ward WW, Prasher DC. 1994. Green fluorescent protein as a marker for gene expression. Science 263:802-805.

Chapple JP, Hardcastle AJ, Grayson C, Willison KR, Cheetham ME. 2002. Delineation of the plasma membrane targeting domain of the X-linked retinitis pigmentosa protein RP2. Invest Ophthalmol Vis Sci 43:2015-2020.

Chen W, Chen M, Barak LS. 2010. Development of small molecules targeting the Wnt pathway for the treatment of colon cancer: a high-throughput screening approach. Am J Physiol Gastrointest Liver Physiol 299:G293-300.

Choi CQ. 2007. A stroke for stem cells. Sci Am 296:8-9.

Chubb C, Inagaki Y, Sheu P, Cummings B, Wasserman A, Head E, Cotman C. 2006. BioVision: an application for the automated image analysis of histological sections. Neurobiol Aging 27:1462-1476.

Chudakov DM, Matz MV, Lukyanov S, Lukyanov KA. 2010. Fluorescent proteins and their applications in imaging living cells and tissues. Physiol Rev 90:1103-1163.

Ciccolini F, Mandl C, Holzl-Wenig G, Kehlenbach A, Hellwig A. 2005. Prospective isolation of late development multipotent precursors whose migration is promoted by EGFR. Dev Biol 284:112-125.

Clarke RB, Spence K, Anderson E, Howell A, Okano H, Potten CS. 2005. A putative human breast stem cell population is enriched for steroid receptor-positive cells. Dev Biol 277:443-456.

Coles-Takabe BL, Brain I, Purpura KA, Karpowicz P, Zandstra PW, Morshead CM, van der Kooy D. 2008. Don't look: growing clonal versus nonclonal neural stem cell colonies. Stem Cells 26:2938-2944.

Corti S, Nizzardo M, Nardini M, Donadoni C, Locatelli F, Papadimitriou D, Salani S, Del Bo R, Ghezzi S, Strazzer S, Bresolin N, Comi GP. 2007. Isolation and characterization of murine neural stem/progenitor cells based on Prominin-1 expression. Exp Neurol 205:547-562.

Coussens LM, Werb Z. 2002. Inflammation and cancer. Nature 420:860-867.

Dahlstrand J, Lardelli M, Lendahl U. 1995. Nestin mRNA expression correlates with the central nervous system progenitor cell state in many, but not all, regions of developing central nervous system. Brain Res Dev Brain Res 84:109-129.

Dalton SO, Mellemkjaer L, Olsen JH, Mortensen PB, Johansen C. 2002. Depression and cancer risk: a register-based study of patients hospitalized with affective disorders, Denmark, 1969-1993. Am J Epidemiol 155:1088-1095.

Darzynkiewicz Z, Huang X. 2004. Analysis of cellular DNA content by flow cytometry. Curr Protoc Immunol Chapter 5:Unit 5 7.

Diamandis P, Sacher AG, Tyers M, Dirks PB. 2009. New drugs for brain tumors? Insights from chemical probing of neural stem cells. Med Hypotheses 72:683-687.

Diehn M, Clarke MF. 2006. Cancer stem cells and radiotherapy: new insights into tumor radioresistance. J Natl Cancer Inst 98:1755-1757.

Dirks PB. 2008. Brain tumour stem cells: the undercurrents of human brain cancer and their relationship to neural stem cells. Philos Trans R Soc Lond B Biol Sci 363:139-152.

dit Faute MA, Laurent L, Ploton D, Poupon MF, Jardillier JC, Bobichon H. 2002. Distinctive alterations of invasiveness, drug resistance and cell-cell organization in 3D-cultures of MCF-7, a human breast cancer cell line, and its multidrug resistant variant. Clin Exp Metastasis 19:161-168.

Doetsch F, Caille I, Lim DA, Garcia-Verdugo JM, Alvarez-Buylla A. 1999. Subventricular zone astrocytes are neural stem cells in the adult mammalian brain. Cell 97:703-716.

Dragunow M. 2008. High-content analysis in neuroscience. Nat Rev Neurosci 9:779-788.

Egles C, Garlick JA, Shamis Y. 2009. Three-dimensional human tissue models of wounded skin. Methods Mol Biol 585:345-359.

Ellis P, Fagan BM, Magness ST, Hutton S, Taranova O, Hayashi S, McMahon A, Rao M, Pevny L. 2004. SOX2, a persistent marker for multipotential neural stem cells derived from embryonic stem cells, the embryo or the adult. Dev Neurosci 26:148-165.

Encinas JM, Vaahtokari A, Enikolopov G. 2006. Fluoxetine targets early progenitor cells in the adult brain. Proc Natl Acad Sci U S A 103:8233-8238.

Engler AJ, Sen S, Sweeney HL, Discher DE. 2006. Matrix elasticity directs stem cell lineage specification. Cell 126:677-689.

Ernst C, Christie BR. 2005. Nestin-expressing cells and their relationship to mitotically active cells in the subventricular zones of the adult rat. Eur J Neurosci 22:3059-3066.

Ernst C, Christie BR. 2006. The putative neural stem cell marker, nestin, is expressed in heterogeneous cell types in the adult rat neocortex. Neuroscience 138:183-188.

Evans GS, Potten CS. 1991. Stem cells and the elixir of life. Bioessays 13:135-138.

Eyler CE, Rich JN. 2008. Survival of the fittest: cancer stem cells in therapeutic resistance and angiogenesis. J Clin Oncol 26:2839-2845.

Ferri AL, Cavallaro M, Braida D, Di Cristofano A, Canta A, Vezzani A, Ottolenghi S, Pandolfi PP, Sala M, DeBiasi S, Nicolis SK. 2004. Sox2 deficiency causes neurodegeneration and impaired neurogenesis in the adult mouse brain. Development 131:3805-3819.

Fuchs E, Jaffe J, Long R, Azam F. 2002. Thin laser light sheet microscope for microbial oceanography. Opt Express 10:145-154.

Gan HT, Tham M, Hariharan S, Ramasamy S, Yu YH, Ahmed S. 2011. Identification of ApoE as an autocrine/paracrine factor that stimulates neural stem cell survival via MAPK/ERK signaling pathway. J Neurochem 117:565-578.

George TC, Basiji DA, Hall BE, Lynch DH, Ortyn WE, Perry DJ, Seo MJ, Zimmerman CA, Morrissey PJ. 2004. Distinguishing modes of cell death using the ImageStream multispectral imaging flow cytometer. Cytometry A 59:237-245.

George TC, Fanning SL, Fitzgerald-Bocarsly P, Medeiros RB, Highfill S, Shimizu Y, Hall BE, Frost K, Basiji D, Ortyn WE, Morrissey PJ, Lynch DH. 2006. Quantitative measurement of nuclear translocation events using similarity analysis of multispectral cellular images obtained in flow. J Immunol Methods 311:117-129.

Gilbert SF. 2000. Developmental Biology. Massachusetts: Sinauer Associates.

Gotz C, Pfeiffer R, Tigges J, Ruwiedel K, Hubenthal U, Merk HF, Krutmann J, Edwards RJ, Abel J, Pease C, Goebel C, Hewitt N, Fritsche E. 2012. Xenobiotic metabolism capacities of human skin in comparison with a 3D-epidermis model and keratinocyte-based cell culture as in vitro alternatives for chemical testing: phase II enzymes. Exp Dermatol 21:364-369.

Graham V, Khudyakov J, Ellis P, Pevny L. 2003. SOX2 functions to maintain neural progenitor identity. Neuron 39:749-765.

Grinshpoon A, Barchana M, Ponizovsky A, Lipshitz I, Nahon D, Tal O, Weizman A, Levav I. 2005. Cancer in schizophrenia: is the risk higher or lower? Schizophr Res 73:333-341.

Guldevall K, Vanherberghen B, Frisk T, Hurtig J, Christakou AE, Manneberg O, Lindstrom S, Andersson-Svahn H, Wiklund M, Onfelt B. 2010. Imaging immune surveillance of individual natural killer cells confined in microwell arrays. PLoS One 5:e15453.

Gupta PB, Onder TT, Jiang G, Tao K, Kuperwasser C, Weinberg RA, Lander ES. 2009. Identification of selective inhibitors of cancer stem cells by high-throughput screening. Cell 138:645-659.

Hagiwara N. 2012. Sox6, jack of all trades: a versatile regulatory protein in vertebrate development. Dev Dyn 240:1311-1321.

Hatakeyama J, Bessho Y, Katoh K, Ookawara S, Fujioka M, Guillemot F, Kageyama R. 2004. Hes genes regulate size, shape and histogenesis of the nervous system by control of the timing of neural stem cell differentiation. Development 131:5539-5550.

Haubensak W, Attardo A, Denk W, Huttner WB. 2004. Neurons arise in the basal neuroepithelium of the early mammalian telencephalon: a major site of neurogenesis. Proc Natl Acad Sci U S A 101:3196-3201.

Hertzberg RP, Pope AJ. 2000. High-throughput screening: new technology for the 21st century. Curr Opin Chem Biol 4:445-451.

Hiratsuka S, Watanabe A, Aburatani H, Maru Y. 2006. Tumour-mediated upregulation of chemoattractants and recruitment of myeloid cells predetermines lung metastasis. Nat Cell Biol 8:1369-1375.

Hu M, Schurdak ME, Puttfarcken PS, El Kouhen R, Gopalakrishnan M, Li J. 2007. High content screen microscopy analysis of A beta 1-42-induced neurite outgrowth reduction in rat primary cortical neurons: neuroprotective effects of alpha 7 neuronal nicotinic acetylcholine receptor ligands. Brain Res 1151:227-235.

Huang CH, Sankaran S, Racoceanu D, Hariharan S, Ahmed S. 2012. Online 3-D tracking of suspension living cells imaged with phase-contrast microscopy. IEEE Trans Biomed Eng 59:1924-1933.

Huttner WB, Kosodo Y. 2005. Symmetric versus asymmetric cell division during neurogenesis in the developing vertebrate central nervous system. Curr Opin Cell Biol 17:648-657.

Jacobs BL, van Praag H, Gage FH. 2000. Adult brain neurogenesis and psychiatry: a novel theory of depression. Mol Psychiatry 5:262-269.

Jacobs JJ, Kieboom K, Marino S, DePinho RA, van Lohuizen M. 1999. The oncogene and Polycomb-group gene bmi-1 regulates cell proliferation and senescence through the ink4a locus. Nature 397:164-168.

Jacques TS, Relvas JB, Nishimura S, Pytela R, Edwards GM, Streuli CH, ffrench-Constant C. 1998. Neural precursor cell chain migration and division are regulated through different beta1 integrins. Development 125:3167-3177.

Jiang Y, Jahagirdar BN, Reinhardt RL, Schwartz RE, Keene CD, Ortiz-Gonzalez XR, Reyes M, Lenvik T, Lund T, Blackstad M, Du J, Aldrich S, Lisberg A, Low WC, Largaespada DA, Verfaillie CM. 2002. Pluripotency of mesenchymal stem cells derived from adult marrow. Nature 418:41-49.

Johansson CB, Momma S, Clarke DL, Risling M, Lendahl U, Frisen J. 1999. Identification of a neural stem cell in the adult mammalian central nervous system. Cell 96:25-34.

Jurvansuu J, Zhao Y, Leung DS, Boulaire J, Yu YH, Ahmed S, Wang S. 2008. Transmembrane protein 18 enhances the tropism of neural stem cells for glioma cells. Cancer Res 68:4614-4622.

Justice BA, Badr NA, Felder RA. 2009. 3D cell culture opens new dimensions in cell-based assays. Drug Discov Today 14:102-107.

Kabos P, Kabosova A, Neuman T. 2002. Blocking HES1 expression initiates GABAergic differentiation and induces the expression of p21(CIP1/WAF1) in human neural stem cells. J Biol Chem 277:8763-8766.

Kabos P, Matundan H, Zandian M, Bertolotto C, Robinson ML, Davy BE, Yu JS, Krueger RC, Jr. 2004. Neural precursors express multiple chondroitin sulfate proteoglycans, including the lectican family. Biochem Biophys Res Commun 318:955-963.

Kageyama R, Ohtsuka T. 1999. The Notch-Hes pathway in mammalian neural development. Cell Res 9:179-188.

Kanazawa T, Takematsu H, Yamamoto A, Yamamoto H, Kozutsumi Y. 2008. Wheat germ agglutinin stains dispersed post-golgi vesicles after treatment with the cytokinesis inhibitor psychosine. J Cell Physiol 215:517-525.

Kaneko Y, Sakakibara S, Imai T, Suzuki A, Nakamura Y, Sawamoto K, Ogawa Y, Toyama Y, Miyata T, Okano H. 2000. Musashi1: an evolutionally conserved marker for CNS progenitor cells including neural stem cells. Dev Neurosci 22:139-153.

Kang X, Xie Y, Kniss DA. 2005. Adipose tissue model using three-dimensional cultivation of preadipocytes seeded onto fibrous polymer scaffolds. Tissue Eng 11:458-468.

Kaplan RN, Riba RD, Zacharoulis S, Bramley AH, Vincent L, Costa C, MacDonald DD, Jin DK, Shido K, Kerns SA, Zhu Z, Hicklin D, Wu Y, Port JL, Altorki N, Port ER, Ruggero D, Shmelkov SV, Jensen KK, Rafii S, Lyden D. 2005. VEGFR1-positive haematopoietic bone marrow progenitors initiate the pre-metastatic niche. Nature 438:820-827.

Kawaguchi A, Miyata T, Sawamoto K, Takashita N, Murayama A, Akamatsu W, Ogawa M, Okabe M, Tano Y, Goldman SA, Okano H. 2001. Nestin-EGFP transgenic mice: visualization of the self-renewal and multipotency of CNS stem cells. Mol Cell Neurosci 17:259-273.

Keller PJ, Pampaloni F, Stelzer EH. 2006. Life sciences require the third dimension. Curr Opin Cell Biol 18:117-124.

Keller PJ, Schmidt AD, Wittbrodt J, Stelzer EH. 2008. Reconstruction of zebrafish early embryonic development by scanned light sheet microscopy. Science 322:1065-1069.

Khairy K, Reynaud E, Stelzer E. 2008. Detection of deformable objects in 3D images using Markov-Chain Monte Carlo and spherical harmonics. Med Image Comput Comput Assist Interv 11:1075-1082.

Kim M, Morshead CM. 2003. Distinct populations of forebrain neural stem and progenitor cells can be isolated using side-population analysis. J Neurosci 23:10703-10709.

Kim SU. 2010. Neural stem cell-based gene therapy for brain tumors. Stem Cell Rev 7:130-140.

Knoblich JA. 2008. Mechanisms of asymmetric stem cell division. Cell 132:583-597.

Kunz-Schughart LA, Freyer JP, Hofstaedter F, Ebner R. 2004. The use of 3-D cultures for high-throughput screening: the multicellular spheroid model. J Biomol Screen 9:273-285.

Lai Y, Asthana A, Cheng K, Kisaalita WS. 2011. Neural cell 3D microtissue formation is marked by cytokines' up-regulation. PLoS One 6:e26821.

Langehanenberg P, Ivanova L, Bernhardt I, Ketelhut S, Vollmer A, Dirksen D, Georgiev G, von Bally G, Kemper B. 2009. Automated three-dimensional tracking of living cells by digital holographic microscopy. J Biomed Opt 14:014018.

Lasky JL, Wu H. 2005. Notch signaling, brain development, and human disease. Pediatr Res 57:104R-109R.

Lee J, Kotliarova S, Kotliarov Y, Li A, Su Q, Donin NM, Pastorino S, Purow BW, Christopher N, Zhang W, Park JK, Fine HA. 2006. Tumor stem cells derived from glioblastomas cultured in bFGF and EGF more closely mirror the phenotype and genotype of primary tumors than do serum-cultured cell lines. Cancer Cell 9:391-403.

Lendahl U, Zimmerman LB, McKay RD. 1990. CNS stem cells express a new class of intermediate filament protein. Cell 60:585-595.

Lerner B, Clocksin WF, Dhanjal S, Hulten MA, Bishop CM. 2001. Automatic signal classification in fluorescence in situ hybridization images. Cytometry 43:87-93.

Levenberg S, Huang NF, Lavik E, Rogers AB, Itskovitz-Eldor J, Langer R. 2003. Differentiation of human embryonic stem cells on three-dimensional polymer scaffolds. Proc Natl Acad Sci U S A 100:12741-12746.

Li L, Xie T. 2005. Stem cell niche: structure and function. Annu Rev Cell Dev Biol 21:605-631.

Lie DC, Dziewczapolski G, Willhoite AR, Kaspar BK, Shults CW, Gage FH. 2002. The adult substantia nigra contains progenitor cells with neurogenic potential. J Neurosci 22:6639-6649.

Lind CR, Gray CW, Pearson AG, Cameron RE, O'Carroll SJ, Narayan PJ, Lim J, Dragunow M. 2006. The mitogen-activated/extracellular signal-regulated kinase kinase 1/2 inhibitor U0126 induces glial fibrillary acidic protein expression and reduces the proliferation and migration of C6 glioma cells. Neuroscience 141:1925-1933.

Lindvall O, Kokaia Z, Martinez-Serrano A. 2004. Stem cell therapy for human neurodegenerative disorders-how to make it work. Nat Med 10 Suppl:S42-50.

Liu Y, Himes BT, Solowska J, Moul J, Chow SY, Park KI, Tessler A, Murray M, Snyder EY, Fischer I. 1999. Intraspinal delivery of neurotrophin-3 using neural stem cells genetically modified by recombinant retrovirus. Exp Neurol 158:9-26.

Lobo MV, Alonso FJ, Redondo C, Lopez-Toledano MA, Caso E, Herranz AS, Paino CL, Reimers D, Bazan E. 2003. Cellular characterization of epidermal growth factor-expanded free-floating neurospheres. J Histochem Cytochem 51:89-103.

Lockett SJ, Herman B. 1994. Automatic detection of clustered, fluorescent-stained nuclei by digital image-based cytometry. Cytometry 17:1-12.

Louis SA, Rietze RL, Deleyrolle L, Wagey RE, Thomas TE, Eaves AC, Reynolds BA. 2008. Enumeration of neural stem and progenitor cells in the neural colony-forming cell assay. Stem Cells 26:988-996.

Loulier K, Lathia JD, Marthiens V, Relucio J, Mughal MR, Tang SC, Coksaygan T, Hall PE, Chigurupati S, Patton B, Colognato H, Rao MS, Mattson MP, Haydar TF, Ffrench-Constant C. 2009. beta1 integrin maintains integrity of the embryonic neocortical stem cell niche. PLoS Biol 7:e1000176.

Malpica N, de Solorzano CO, Vaquero JJ, Santos A, Vallcorba I, Garcia-Sagredo JM, del Pozo F. 1997. Applying watershed algorithms to the segmentation of clustered nuclei. Cytometry 28:289-297.

Marani E, van Oers JW, Tetteroo PA, Poelmann RE, van der Veeken J, Deenen MG. 1986. Stage specific embryonic carbohydrate surface antigens of primordial germ cells in mouse embryos: FAL (S.S.E.A.-1) and globoside (S.S.E.A.-3). Acta Morphol Neerl Scand 24:103-110.

Medina RJ, Kataoka K, Takaishi M, Miyazaki M, Huh NH. 2006. Isolation of epithelial stem cells from dermis by a three-dimensional culture system. J Cell Biochem 98:174-184.

Merkle FT, Alvarez-Buylla A. 2006. Neural stem cells in mammalian development. Curr Opin Cell Biol 18:704-709.

Mi R, Luo Y, Cai J, Limke TL, Rao MS, Hoke A. 2005. Immortalized neural stem cells differ from nonimmortalized cortical neurospheres and cerebellar granule cell progenitors. Exp Neurol 194:301-319.

Miraglia S, Godfrey W, Yin AH, Atkins K, Warnke R, Holden JT, Bray RA, Waller EK, Buck DW. 1997. A novel five-transmembrane hematopoietic stem cell antigen: isolation, characterization, and molecular cloning. Blood 90:5013-5021.

Miyake T, McDermott JC, Gramolini AO. 2011. A method for the direct identification of differentiating muscle cells by a fluorescent mitochondrial dye. PLoS One 6:e28628.

Mohanty SK, Sharma M, Gupta PK. 2003. Laser-assisted microinjection into targeted animal cells. Biotechnol Lett 25:895-899.

Molofsky AV, He S, Bydon M, Morrison SJ, Pardal R. 2005. Bmi-1 promotes neural stem cell self-renewal and neural development but not mouse growth and survival by repressing the p16Ink4a and p19Arf senescence pathways. Genes Dev 19:1432-1437.

Mori H, Fujitani T, Kanemura Y, Kino-Oka M, Taya M. 2007. Observational examination of aggregation and migration during early phase of neurosphere culture of mouse neural stem cells. J Biosci Bioeng 104:231-234.

Morrison SJ, Spradling AC. 2008. Stem cells and niches: mechanisms that promote stem cell maintenance throughout life. Cell 132:598-611.

Morshead CM, Reynolds BA, Craig CG, McBurney MW, Staines WA, Morassutti D, Weiss S, van der Kooy D. 1994. Neural stem cells in the adult mammalian forebrain: a relatively quiescent subpopulation of subependymal cells. Neuron 13:1071-1082.

Mouthon MA, Fouchet P, Mathieu C, Sii-Felice K, Etienne O, Lages CS, Boussin FD. 2006. Neural stem cells from mouse forebrain are contained in a population distinct from the 'side population'. J Neurochem 99:807-817.

Murayama A, Matsuzaki Y, Kawaguchi A, Shimazaki T, Okano H. 2002. Flow cytometric analysis of neural stem cells in the developing and adult mouse brain. J Neurosci Res 69:837-847.

Naheed M, Green B. 2001. Focus on clozapine. Curr Med Res Opin 17:223-229.

Nakamura M, Okano H, Blendy JA, Montell C. 1994. Musashi, a neural RNA-binding protein required for Drosophila adult external sensory organ development. Neuron 13:67-81.

Narayan PJ, Gibbons HM, Mee EW, Faull RL, Dragunow M. 2007. High throughput quantification of cells with complex morphology in mixed cultures. J Neurosci Methods 164:339-349.

Narayanan G, Poonepalli A, Chen J, Sankaran S, Hariharan S, Yu YH, Robson P, Yang H, Ahmed S. 2012. Single-cell mRNA profiling identifies progenitor subclasses in neurospheres. Stem Cells Dev 21:3351-3362.

Neumuller RA, Knoblich JA. 2009. Dividing cellular asymmetry: asymmetric cell division and its implications for stem cells and cancer. Genes Dev 23:2675-2699.

Neve RL, Dawes LR, Yankner BA, Benowitz LI, Rodriguez W, Higgins GA. 1990. Genetics and biology of the Alzheimer amyloid precursor. Prog Brain Res 86:257-267.

Noctor SC, Martinez-Cerdeno V, Ivic L, Kriegstein AR. 2004. Cortical neurons arise in symmetric and asymmetric division zones and migrate through specific phases. Nat Neurosci 7:136-144.

Nottebohm F. 1989. From bird song to neurogenesis. Sci Am 260:74-79.

Nyfeler Y, Kirch RD, Mantei N, Leone DP, Radtke F, Suter U, Taylor V. 2005. Jagged1 signals in the postnatal subventricular zone are required for neural stem cell self-renewal. EMBO J 24:3504-3515.

Ohtsuka T, Ishibashi M, Gradwohl G, Nakanishi S, Guillemot F, Kageyama R. 1999. Hes1 and Hes5 as notch effectors in mammalian neuronal differentiation. EMBO J 18:2196-2207.

Osumi N. 2001. The role of Pax6 in brain patterning. Tohoku J Exp Med 193:163-174.

Palmer TD, Ashby WJ, Lewis JD, Zijlstra A. 2011. Targeting tumor cell motility to prevent metastasis. Adv Drug Deliv Rev 63:568-581.

Palmer TD, Markakis EA, Willhoite AR, Safar F, Gage FH. 1999. Fibroblast growth factor-2 activates a latent neurogenic program in neural stem cells from diverse regions of the adult CNS. J Neurosci 19:8487-8497.

Parker MA, Anderson JK, Corliss DA, Abraria VE, Sidman RL, Park KI, Teng YD, Cotanche DA, Snyder EY. 2005. Expression profile of an operationally-defined neural stem cell clone. Exp Neurol 194:320-332.

Pastrana E, Silva-Vargas V, Doetsch F. 2011. Eyes wide open: a critical review of sphere-formation as an assay for stem cells. Cell Stem Cell 8:486-498.

Pinaud F, Michalet X, Bentolila LA, Tsay JM, Doose S, Li JJ, Iyer G, Weiss S. 2006. Advances in fluorescence imaging with quantum dot bio-probes. Biomaterials 27:1679-1687.

Plikus MV, Mayer JA, de la Cruz D, Baker RE, Maini PK, Maxson R, Chuong CM. 2008. Cyclic dermal BMP signalling regulates stem cell activation during hair regeneration. Nature 451:340-344.

Poole CA, Brookes NH, Gilbert RT, Beaumont BW, Crowther A, Scott L, Merrilees MJ. 1996. Detection of viable and non-viable cells in connective tissue explants using the fixable fluoroprobes 5-chloromethylfluorescein diacetate and ethidium homodimer-1. Connect Tissue Res 33:233-241.

Potten CS, Booth C, Tudor GL, Booth D, Brady G, Hurley P, Ashton G, Clarke R, Sakakibara S, Okano H. 2003. Identification of a putative intestinal stem cell and early lineage marker; musashi-1. Differentiation 71:28-41.

Potten CS, Loeffler M. 1990. Stem cells: attributes, cycles, spirals, pitfalls and uncertainties. Lessons for and from the crypt. Development 110:1001-1020.

Rabut G, Ellenberg J. 2004. Automatic real-time three-dimensional cell tracking by fluorescence microscopy. J Microsc 216:131-137.

Raven P. 2007. Biology by Peter Raven (NASTA Hardcover Reinforced High School Binding) Student Edition. McGraw-Hill Companies,Incorporated.

Reynolds BA, Rietze RL. 2005. Neural stem cells and neurospheres--re-evaluating the relationship. Nat Methods 2:333-336.

Reynolds BA, Weiss S. 1992. Generation of neurons and astrocytes from isolated cells of the adult mammalian central nervous system. Science 255:1707-1710.

Richards GR, Smith AJ, Parry F, Platts A, Chan GK, Leveridge M, Kerby JE, Simpson PB. 2006. A morphology- and kinetics-based cascade for human neural cell high content screening. Assay Drug Dev Technol 4:143-152.

Rietze RL, Valcanis H, Brooker GF, Thomas T, Voss AK, Bartlett PF. 2001. Purification of a pluripotent neural stem cell from the adult mouse brain. Nature 412:736-739.

Roegiers F, Jan YN. 2004. Asymmetric cell division. Curr Opin Cell Biol 16:195-205.

Rubin EH, Gilliland DG. 2012. Drug development and clinical trials--the path to an approved cancer drug. Nat Rev Clin Oncol 9:215-222.

Ryder EF, Snyder EY, Cepko CL. 1990. Establishment and characterization of multipotent neural cell lines using retrovirus vector-mediated oncogene transfer. J Neurobiol 21:356-375.

Sakakibara S, Nakamura Y, Yoshida T, Shibata S, Koike M, Takano H, Ueda S, Uchiyama Y, Noda T, Okano H. 2002. RNA-binding protein Musashi family: roles for CNS stem cells and a subpopulation of ependymal cells revealed by targeted disruption and antisense ablation. Proc Natl Acad Sci U S A 99:15194-15199.

Sakakibara S, Okano H. 1997. Expression of neural RNA-binding proteins in the postnatal CNS: implications of their roles in neuronal and glial cell development. J Neurosci 17:8300-8312.

Sanes JR. 1989. Analysing cell lineage with a recombinant retrovirus. Trends Neurosci 12:21-28.

Sato T, Vries RG, Snippert HJ, van de Wetering M, Barker N, Stange DE, van Es JH, Abo A, Kujala P, Peters PJ, Clevers H. 2009. Single Lgr5 stem cells build crypt-villus structures in vitro without a mesenchymal niche. Nature 459:262-265.

Schnell U, Dijk F, Sjollema KA, Giepmans BN. 2012. Immunolabeling artifacts and the need for live-cell imaging. Nat Methods 9:152-158.

Schofield R. 1978. The relationship between the spleen colony-forming cell and the haemopoietic stem cell. Blood Cells 4:7-25.

Scotter EL, Narayan P, Glass M, Dragunow M. 2008. High throughput quantification of mutant huntingtin aggregates. J Neurosci Methods 171:174-179.

Seaberg RM, van der Kooy D. 2002. Adult rodent neurogenic regions: the ventricular subependyma contains neural stem cells, but the dentate gyrus contains restricted progenitors. J Neurosci 22:1784-1793.

Shen Q, Zhong W, Jan YN, Temple S. 2002. Asymmetric Numb distribution is critical for asymmetric cell division of mouse cerebral cortical stem cells and neuroblasts. Development 129:4843-4853.

Shimojo H, Ohtsuka T, Kageyama R. 2008. Oscillations in notch signaling regulate maintenance of neural progenitors. Neuron 58:52-64.

Singec I, Knoth R, Meyer RP, Maciaczyk J, Volk B, Nikkhah G, Frotscher M, Snyder EY. 2006. Defining the actual sensitivity and specificity of the neurosphere assay in stem cell biology. Nat Methods 3:801-806.

Singh SK, Clarke ID, Terasaki M, Bonn VE, Hawkins C, Squire J, Dirks PB. 2003. Identification of a cancer stem cell in human brain tumors. Cancer Res 63:5821-5828.

Singh SK, Hawkins C, Clarke ID, Squire JA, Bayani J, Hide T, Henkelman RM, Cusimano MD, Dirks PB. 2004. Identification of human brain tumour initiating cells. Nature 432:396-401.

Snyder EY, Daley GQ, Goodell M. 2004. Taking stock and planning for the next decade: realistic prospects for stem cell therapies for the nervous system. J Neurosci Res 76:157-168.

Snyder EY, Deitcher DL, Walsh C, Arnold-Aldea S, Hartwieg EA, Cepko CL. 1992. Multipotent neural cell lines can engraft and participate in development of mouse cerebellum. Cell 68:33-51.

Somorjai IM, Lohmann JU, Holstein TW, Zhao Z. 2012. Stem cells: a view from the roots. Biotechnol J 7:704-722.

Stephens DJ, Allan VJ. 2003. Light microscopy techniques for live cell imaging. Science 300:82-86.

Stolt CC, Lommes P, Sock E, Chaboissier MC, Schedl A, Wegner M. 2003. The Sox9 transcription factor determines glial fate choice in the developing spinal cord. Genes Dev 17:1677-1689.

Stuurman N, Swedlow JR. 2012. Software tools, data structures, and interfaces for microscope imaging. Cold Spring Harb Protoc 2012:50-61.

Sun Y, Goderie SK, Temple S. 2005. Asymmetric distribution of EGFR receptor during mitosis generates diverse CNS progenitor cells. Neuron 45:873-886.

Sunabori T, Tokunaga A, Nagai T, Sawamoto K, Okabe M, Miyawaki A, Matsuzaki Y, Miyata T, Okano H. 2008. Cell-cycle-specific nestin expression coordinates with morphological changes in embryonic cortical neural progenitors. J Cell Sci 121:1204-1212.

Takahashi K, Tanabe K, Ohnuki M, Narita M, Ichisaka T, Tomoda K, Yamanaka S. 2007. Induction of pluripotent stem cells from adult human fibroblasts by defined factors. Cell 131:861-872.

Takahashi K, Yamanaka S. 2006. Induction of pluripotent stem cells from mouse embryonic and adult fibroblast cultures by defined factors. Cell 126:663-676.

Taylor RM, Snyder EY. 1997. Widespread engraftment of neural progenitor and stem-like cells throughout the mouse brain. Transplant Proc 29:845-847.

Temple S. 1989. Division and differentiation of isolated CNS blast cells in microculture. Nature 340:471-473.

Tham M, Ramasamy S, Gan HT, Ramachandran A, Poonepalli A, Yu YH, Ahmed S. 2010. CSPG is a secreted factor that stimulates neural stem cell survival possibly by enhanced EGFR signaling. PLoS One 5:e15341.

Tlsty TD, Coussens LM. 2006. Tumor stroma and regulation of cancer development. Annu Rev Pathol 1:119-150.

Torii M, Matsuzaki F, Osumi N, Kaibuchi K, Nakamura S, Casarosa S, Guillemot F, Nakafuku M. 1999. Transcription factors Mash-1 and Prox-1 delineate early steps in differentiation of neural stem cells in the developing central nervous system. Development 126:443-456.

Tropepe V, Coles BL, Chiasson BJ, Horsford DJ, Elia AJ, McInnes RR, van der Kooy D. 2000. Retinal stem cells in the adult mammalian eye. Science 287:2032-2036.

Tropepe V, Sibilia M, Ciruna BG, Rossant J, Wagner EF, van der Kooy D. 1999. Distinct neural stem cells proliferate in response to EGF and FGF in the developing mouse telencephalon. Dev Biol 208:166-188.

Uchida N, Buck DW, He D, Reitsma MJ, Masek M, Phan TV, Tsukamoto AS, Gage FH, Weissman IL. 2000. Direct isolation of human central nervous system stem cells. Proc Natl Acad Sci U S A 97:14720-14725.

van Lohuizen M, Verbeek S, Scheijen B, Wientjens E, van der Gulden H, Berns A. 1991. Identification of cooperating oncogenes in E mu-myc transgenic mice by provirus tagging. Cell 65:737-752.

Verveer PJ, Swoger J, Pampaloni F, Greger K, Marcello M, Stelzer EH. 2007. High-resolution three-dimensional imaging of large specimens with light sheet-based microscopy. Nat Methods 4:311-313.

Vescovi AL, Snyder EY. 1999. Establishment and properties of neural stem cell clones: plasticity in vitro and in vivo. Brain Pathol 9:569-598.

von Holst A, Sirko S, Faissner A. 2006. The unique 473HD-Chondroitinsulfate epitope is expressed by radial glia and involved in neural precursor cell proliferation. J Neurosci 26:4082-4094.

Voog J, Jones DL. 2010. Stem cells and the niche: a dynamic duo. Cell Stem Cell 6:103-115.

Wagers AJ. 2012. The stem cell niche in regenerative medicine. Cell Stem Cell 10:362-369.

Wang TW, Stromberg GP, Whitney JT, Brower NW, Klymkowsky MW, Parent JM. 2006. Sox3 expression identifies neural progenitors in persistent neonatal and adult mouse forebrain germinative zones. J Comp Neurol 497:88-100.

Weaver VM, Petersen OW, Wang F, Larabell CA, Briand P, Damsky C, Bissell MJ. 1997. Reversion of the malignant phenotype of human breast cells in three-dimensional culture and in vivo by integrin blocking antibodies. J Cell Biol 137:231-245.

Weiss S, Dunne C, Hewson J, Wohl C, Wheatley M, Peterson AC, Reynolds BA. 1996. Multipotent CNS stem cells are present in the adult mammalian spinal cord and ventricular neuroaxis. J Neurosci 16:7599-7609.

Weissman IL, Anderson DJ, Gage F. 2001. Stem and progenitor cells: origins, phenotypes, lineage commitments, and transdifferentiations. Annu Rev Cell Dev Biol 17:387-403.

Wels J, Kaplan RN, Rafii S, Lyden D. 2008. Migratory neighbors and distant invaders: tumor-associated niche cells. Genes Dev 22:559-574.

Wernig M, Meissner A, Foreman R, Brambrink T, Ku M, Hochedlinger K, Bernstein BE, Jaenisch R. 2007. In vitro reprogramming of fibroblasts into a pluripotent ES-cell-like state. Nature 448:318-324.

Xia X, Wong ST. 2012. Concise review: a high-content screening approach to stem cell research and drug discovery. Stem Cells 30:1800-1807.

Xiong W, Chia SC, Lim JH, Shvetha S, Ahmed S. 2011. Detection of unstained living neurospheres from phase contrast images with very large illumination variations. Conf Proc IEEE Eng Med Biol Soc 2011:6154-6157.

Yan P, Zhou X, Shah M, Wong ST. 2008. Automatic segmentation of high-throughput RNAi fluorescent cellular images. IEEE Trans Inf Technol Biomed 12:109-117.

Yin AH, Miraglia S, Zanjani ED, Almeida-Porada G, Ogawa M, Leary AG, Olweus J, Kearney J, Buck DW. 1997. AC133, a novel marker for human hematopoietic stem and progenitor cells. Blood 90:5002-5012.

Yu W, Lee HK, Hariharan S, Bu W, Ahmed S. 2010. Evolving generalized Voronoi diagrams for accurate cellular image segmentation. Cytometry A 77:379-386.

Zencak D, Lingbeek M, Kostic C, Tekaya M, Tanger E, Hornfeld D, Jaquet M, Munier FL, Schorderet DF, van Lohuizen M, Arsenijevic Y. 2005. Bmi1 loss produces an increase in astroglial cells and a decrease in neural stem cell population and proliferation. J Neurosci 25:5774-5783.

Zhong W, Feder JN, Jiang MM, Jan LY, Jan YN. 1996. Asymmetric localization of a mammalian numb homolog during mouse cortical neurogenesis. Neuron 17:43-53.